Operando characterization of organic mixed ionic/electronic materials

Ruiheng Wu,[1] Micaela Matta,[2] Bryan D. Paulsen,[3] Jonathan Rivnay,[3,4*]

[1]Department of Chemistry, Northwestern University, Evanston, IL 60208, USA

[2]Department of Chemistry, University of Liverpool, Liverpool, L69 7ZD, United Kingdom

[3]Department of Biomedical Engineering, Northwestern University, Evanston, IL 60208, USA

[4]Simpson Querrey Institute, Northwestern University, Chicago, Illinois 60611, USA.

E-mail: jrivnay@northwestern.edu

Abstract

Operando characterization plays an important role in revealing the structure-property relationships of organic mixed ionic/electronic conductors (OMIECs), enabling the direct observation of dynamic changes during device operation and thus guiding the development of new materials. This review focuses on the application of different operando characterization techniques in the study of OMIECs, highlighting the time-dependent and bias-dependent structure, composition, and morphology information extracted from these techniques. We first illustrate the needs, requirements, and challenges of operando characterization, then provide an overview of relevant experimental techniques, including spectroscopy, scattering, microbalance, microprobe, and electron microscopy. We also compare different in silico methods and discuss the interplay of these computational methods with experimental techniques. Finally, we give an outlook on the future development of operando for OMIEC-based devices and look towards multimodal operando techniques for more comprehensive and accurate description of OMIECs.

Table of contents

1. Introduction

Organic mixed ionic–electronic conductors (OMIECs) are soft organic materials that solvate and transport ionic species as well as transport electronic charges, enabling extensive ionic-electronic coupling.[1] Due to their mixed conductivity and chemical tunability, OMIEC materials are attractive for many applications, such as energy storage,[2] neuromorphic computing,[3-7] biosensors,[8-11] bio actuators[12, 13] and drug delivery.[14, 15] OMIECs under operation are characterized by a time and voltage dependent chemical composition, environment, and morphology. The ionic/electronic charge density across their heterogeneous domains are a function of the applied potential and local chemical environment, and thus vary during device operation. Time resolved studies in device relevant conditions are therefore essential to capture these dynamic changes and establish meaningful structure properties relationships. The

systematic design and optimization of OMIECs is thus conditional on the widespread use and development of operando characterization techniques.

The complexity embodied in OMIEC materials and devices stems from both their intrinsic composition and their operation. OMIECs are most often polymeric and can be classified into different categories depending on the relationship between the ion conducting and electron conducting components.[1] As shown in **Figure 1b**, OMIEC materials can be homogenous, i.e. a single component transporting both ionic and electronic charge, or inherently heterogenous, such as block copolymers or blends of distinct ionic and electronic transporting components. Electronic transport generally occurs through extended π-conjugation, though radical polymers are a growing area of interest for OMIECs.[16] The ionic carriers populating OMIECs can be either extrinsic (i.e. sourced an electrolyte in contact with the material) or intrinsic (i.e. from component polyelectrolytes). Further, the moieties supporting ionic transport can be polyelectrolytes with repeating ionically charged groups and polymer electrolytes that, though neutral, solvate ions with coordinating groups (e.g. ether oxygens). Even though most OMIEC materials are polymeric, various small molecules[17] and liquid crystals[18] have been synthesized and used for mixed transport applications.

When incorporated into functioning devices, OMIEC materials undergo extensive compositional and structural changes that modulate materials properties and affect device performance. External bias induces transport and redistribution of charges (ions/electrons) in OMIECs. For OMIECs having intrinsic ions and operating without a contacting external electrolyte, ions and electrons in the material are redistributed by the applied electric field. In the presence of an external electrolyte, ions diffuse and/or drift into the OMIEC thin film and establish a dynamic equilibrium with the external environment. This causes mass transport across the electrolyte-OMIEC interface, which can induce film swelling and/or multi-scale structural changes. From the molecular to the macroscopic level, the structural changes may include modulation of polymer backbone planarity, π-stacking distances between molecules, spacing and segregation of aggregates, and changes in the ratio of crystalline to disordered domains. Because of the high compositional and structural complexity reflected in operation, small changes in molecular arrangement and morphology can lead to significant changes in OMIEC performance,[19-21] justifying the need for operando characterization.

In this review, we argue for the importance of operando characterization tools for OMIECs, showcase their unique structural insights, and discuss their implementation challenges. In doing so, this review surveys the existing applications of common characterization tools used to study OMIECs and highlights the most fruitful areas for future development. For existing operando characterization tools, we focus on the information that these tools can bring to the researcher and the potential improvements. For those operando techniques that have not yet been implemented or are not yet widely applied, this review emphasizes their corresponding ex situ and in situ experiments to analyze the specific difficulties in setup implementation. In addition, we briefly mention some commonly used tools that present critical issues hindering operando implementation, and discuss alternatives. Furthermore, we survey the application of molecular simulations to OMIEC materials, highlighting how these 'in silico operando experiments' can provide valuable insight that complements and even overcomes the limits of some experimental characterization tools.

2. Operando Characterization

2.1 The importance of operando characterization

In recent years, 'operando' characterization has become a hot topic in various fields.[22-27] The term 'operando', from Latin verb to operate or work, has come to mean in science as 'during operation', and operando characterization refers to a study performed in application relevant environments, conditions, and geometries. Shown in **Figure 1a**, these characterization techniques include spectroscopy, scattering, scanning probe techniques, gravimetric techniques, and computational methods. Together, these operando techniques establish application relevant structure-property relationships and guide further design and optimization of OMIEC materials. Due to their dynamic structure and composition in response to changes in the electrical potential and chemical environment, operando characterization of OMIECs is necessary. Characterizing different structural/compositional states is paramount to understanding charge transport, the ionic-electronic coupling and potential dependent structure-property relationships. Meanwhile, time-resolved operando experiments record the transient structural change and related charge population, which reveals intermediate states and charge transport mechanisms of operation. Time-resolved experiments generally involve electrical signals measured concurrently with

optical, mechanical, or other structural signals, during OMIEC operation, thus requiring signal synchronization for time-resolved data analysis. Non-time resolved experiments mostly probe steady state conditions and cannot reflect the dynamic changes in operation. In some kinetic sensitive applications such as supercapacitors, time-resolved experiments are required. Conversely, for light-emitting electrochemical cells (LEECs) or batteries steady state, non-time resolved experiments can be adequate.
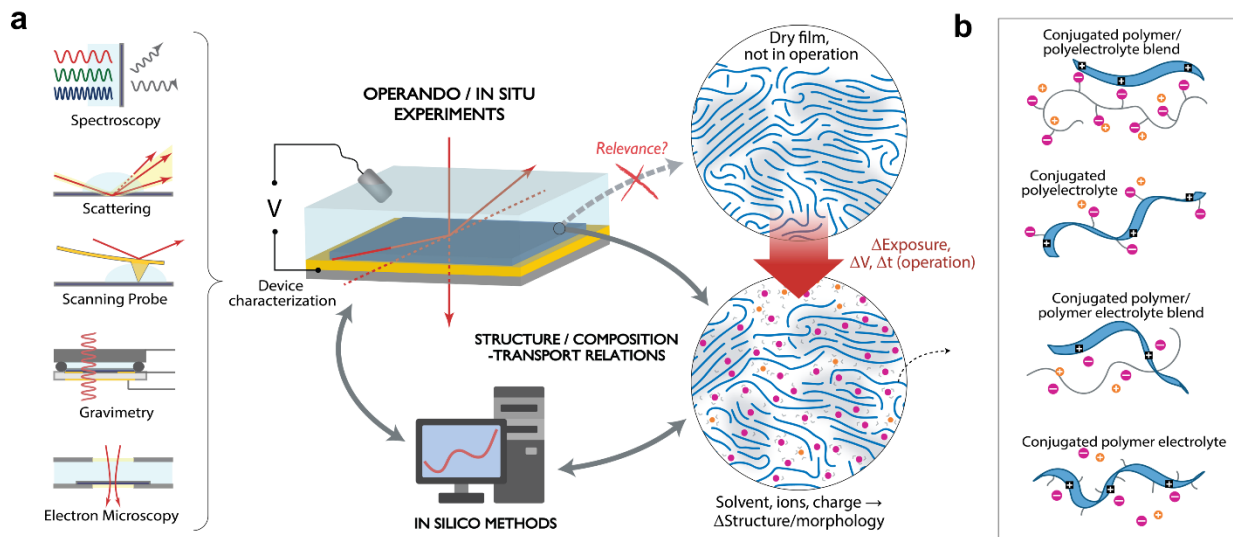
Figure 1 (a) Different operando characterization techniques reveal the structure-property relationships of OMIEC in application-relevant scenarios. (b) Different types of OMIEC materials.

Compared to ex situ studies ('off site', where characterization occurs in film conditions or environments other than working conditions), operando characterization reflects structural and compositional changes experienced in operation. Early 'ex situ' experiments dominated OMIEC characterization due to specific experimental settings being incompatible with operating conditions (e.g., vacuum, dry) and the difficulty of setting up real-time monitoring apparatus.[28-32] The mismatch between ex situ requirements and the operating environment points out the shortcomings of these ex situ techniques. First, the reversible changes during material operation cannot be captured after leaving the operating environment. For example, electrolyte immersion of OMIECs in some application scenarios alters the structure of the polymer film[33] and the distribution of internal charges/ions,[34] but these effects are lost when OMIECs are investigated in

a dry or vacuum experimental setup.[33] Also, optical and structural changes occurring with charging and discharging tend to relax back to an open circuit or ambient doping state after removing the external potential during ex situ investigations.[35, 36] Second, the structure, chemical composition, and mechanical properties of the films will change due to the additional steps in ex situ sample preparation. In many cases, it can prove difficult to distinguish between the behavior during operation and the spurious changes introduced by ex situ sample preparation. Lastly, the counts/signal intensity obtained from different ex situ samples (even for the same material) are more difficult to quantitatively compare, whereas counts/signal intensity within a single operando experiment are directly comparable. The fixed sample alignment and geometry during operando experiments eliminates the need for calibration or normalization to correct for sample-to-sample variation (thickness, structure, etc), changes to experimental setup or environmental factors across multiple ex situ experiments.

While similar, 'operando' is distinct from 'in situ'. In situ characterization, commonly understood to mean "on the site", has given many useful insights into OMIEC structure and properties, particularly during materials deposition and processing. One of the most prominent examples is the investigation of the structural evolution during film formation in solution-based casting techniques.[37, 38] The presence of solvents in the casting process of thin film materials makes the collection of structural signals difficult in a similar way to the presence of electrolytes. Additionally, in situ characterization of thermal annealing of organic polymer films has been extensively performed.[39, 40] For inhomogeneous polymer films, such as donor acceptor bulk heterojunctions, phase separation during thermal annealing has been of interest to researchers across multiple application areas.[41-43] However, in situ studies often target specific processing steps and can occur in artificial environments/geometries that do not reflect functioning devices. Depending on the ultimate device application, in situ experiments can often be accurately considered operando, such as the measurement of the steady-state properties of OMIECs under device relevant applied voltages and conditions. For instance, UV-Vis-NIR spectroelectrochemistry is an in situ technique, and in the case of OMIEC electrochromic applications is also a good example of an operando measurement. The technique captures the spectral information of the material while charging and discharging, to analyze the species transformation and chemical reactions inside the OMIEC material that would occur during device operation.

The challenges and requirements of operando characterization can be categorized under the following four aspects: chemical environment, device geometry, charge distribution, and device-related time scale. First, the chemical environment in operando experiments should be the same as the application scenario. Take the example of whether an additional external electrolyte is needed in operating conditions. For applications employing solvent free OMIECs with intrinsic ions, there is no requirement for external electrolyte and operando experiments can be performed under more controlled conditions, such as under high vacuum. This reduces the technical difficulty of operando experiments and broadens the choice of characterization methods. In OMIEC applications that require external electrolytes, ion and solvent uptake occurs during electrochemical doping/dedoping, and as a result OMIECs can swell 10-1000% compared to the dry state.[33, 44-46] For this reason, operando characterization must be carried out in a electrolyte immersed/contacted state, allowing solvated ions need to drift/diffuse into the material, thus significantly complicating its implementation.

The second requirement is the application-oriented device geometry, including parameters such as OMIEC film thickness, material anisotropy, electrode distances, electrode area, and device substrate, etc. For example, thick/bulk OMIEC samples should not be presumed to represent the thin film structure or properties found in an actual device (unless explicitly confirmed). Also, different casting methods can induce or modify film anisotropy in conjugated polymers.[47, 48] This requires consistent sample preparation for operando experiments to mirror real devices to accurately reflect the ion and electron transport conditions and film morphology. The substrate and electrode geometry influence charge transport kinetics and may even change the rate-determining step (RDS) in the transport mechanism.[49, 50]

Closely related to device geometry, the third requirement for operando characterization is the need to reflect device relevant potential profiles as well as the resulting electronic and ionic distributions/gradients occurring under operating conditions. Thus, not simply applied potentials, but induced electric fields must be considered: a few volts applied laterally across a mm-scale thin film are not equivalent to a few volts applied vertically through a 10-100 nm thin film. In addition, accurate chemical environment and sample geometry is important to establish device relevant concentration gradients and electric fields. For example, OECTs need to be exposed to

electrolyte and require ion uptake to induce charge heterogeneity, but LEECs operate in dry conditions to establish internal charge gradients.[51]

The last aspect is the device-relevant timescale, which needs to be compatible with the operating dynamics of the device. The temporal resolution of an operando experiment needs to be able to capture the kinetics of the structural and electronic properties as they change from non-equilibrium to equilibrium states. This is regulated by the device RC time constant, equivalent to the characteristic cell time constant in traditional electrochemistry,[52] where R is resistance and C is capacitance, both of which represent the summation of many physical processes. Finally, the temporal resolution required to capture individual physical processes is a more demanding requirement. For example, while the charging/discharging time scale or ionic to electronic signal transduction for bioelectronic signal recording may require ms level time resolution, individual electronic and ionic charge transfer/transport/hopping events may demand ns resolution.[53]

2.2 Applications specific environments and operando challenges

In general, there are common difficulties that need to be overcome to implement operando OMIEC characterization. For instance, the chemical environment may introduce competing signals that undermine the measurement of desired phenomena. Depending on the device setup, specially designed electrochemical cells may be required. In addition, a long integration time (data collection time) is used in many characterization tools, such as X-ray scattering, Infra-red and Nuclear Magnetic Resonance spectroscopy. The long integration time needed for high resolution, low noise data is at odds with the time resolution required for kinetics studies, requiring a compromise between data quality and device relevant timescale.

The applications of OMIECs and their corresponding operating environments can also create hurdles to operando characterization. Operating devices can necessitate OMIECs that are dry, hydrated, solvent swollen, or electrolyte immersed. Dry OMIEC (containing no solvent or liquid electrolyte) integrated in solid state devices (light emitting electrochemical cells, solid state organic electrochemical transistors, solid state neuromorphic devices, etc.) present the fewest hurdles to operando characterization. Aside from geometric considerations, the substrate may present absorption and scattering that overlap or attenuate desired signals from the OMIECs. Additionally, the OMIEC in functioning devices may be present as a thin film underneath several

overlayers (i.e. electrodes, dielectrics) or encapsulation. These considerations are potentially relevant to all OMIEC application environments. Being solid-state, applications with dry OMIEC films are broadly compatible with high vacuum systems common in characterization techniques such as traditional X-Ray Photoelectron Spectroscopy and Electron Microscopes. However, some dry films contain moderately volatile components such as dopants, surfactants, and additives that while stable in ambient conditions, are incompatible with high vacuum characterization environments.

Hydrated or solvent swollen OMIECs are similarly incompatible with high vacuum characterization environments, and generally require environmental controls to maintain a high relative humidity or solvent vapor saturated environment during characterization. These saturated vapor atmospheres introduce additional absorption and scattering that interfere with operando characterization, hindering data analysis/interpretation. OMIECs integrating ionic liquids are unique in that ionic liquids display negligible vapor pressure and can be incorporated into high vacuum systems as if they were solid state.[54]

Liquid electrolyte immersed OMIEC applications present more obstacles to operando characterization with respect to their dry counterparts. Especially for OMIEC thin films, unwanted absorption and scattering from water or other solvents can make the desired signals undetectable. Additionally, some electrostatic techniques, such as scanning kelvin probe microscopy, cannot function when immersed in an ionic conducting media which screens the electrostatic effects upon which the technique is based. Altogether, it becomes apparent that certain applications are more or less compatible with certain characterization techniques, the details of which we will discuss below as each technique is introduced.

3. OMIEC in operation

3.1 Ionic and electronic processes in OMIECs

Targeted physical responses in OMIEC devices in response to external bias include optical changes, charge storage, signal transduction and mechanical modulation. All these responses require mixed ionic-electronic transport and coupling, which are key to OMIEC performance and applications.[1] There are several basic processes involved: ionic transport, electronic charge

carrier injection/collection, electronic transport, and electronic charge stabilization (ionic-electronic coupling). Among these processes, electronic injection/collection is largely associated with electrode selection and work function modification,[55-57] which is often discounted in the optimization of OMIEC materials.[57-61] The electronic charge stabilization, manifest as counter ion doping, arises from ionic-electronic coupling, leading to a delocalization effect of the holes/electrons in the conjugated system. Aside from charge injection/collection, these processes require a dedicated discussion due to their complexity.[62-65]

Ionic transport occurs through a variety of mechanisms depending on material morphology, environment, and application, see ref [[66]] in detail. For polymeric OMIECs working in dry conditions, ion solvation occurs by coordination to polar or charged groups.[67, 68] Often in dry polymer electrolyte based OMIECs, only the cation or anion is coordinated, while the other resides in inter-chain voids. In dry polyelectrolyte based OMIECs, only the counter ions are mobile and are coordinated in ion clusters. Ion transport from one coordination site or void to another is a thermally active process depending on chain motion in dry film and is heavily influenced by chain flexibility. When OMIECs are subjected to limited electrolyte swelling, the dependence of ion transport on polymer chain motion is still crucial. However, chain motion is enhanced through the plasticizing effect of solvent molecules, and the ion coordination to OMIECs is weakened as solvent molecules contribute to ion coordination. In the case of substantially electrolyte swollen or hydrogel OMIECs, vehicle transport of an ion and its solvation shell as a single unit is the dominant mechanism. While vehicle transport can require chain reorganization, in the limit of a hydrogel-like morphology, solvated ions move rapidly through continuous solvent channels in the heterogeneous bulk morphology[69] and are decoupled from the polymer chain motion. During the operation of these OMIECs, it is apparent that moderate swelling of the electrolyte facilitates ion uptake and transport.[70-72] In addition, the type of ions in the OMIEC also affects the way they are transported. For instance, high proton conductivity with low activation barriers is possible in OMIECs through the Grotthuss mechanism,[73, 74] which rapidly transfers protons through a hydrogen bonding network. In addition, the size and the hardness of ions influence their solvation shell and thus affect ion-material interactions and ionic transport.[75, 76] On the macroscopic scale, the above ionic transport processes occur in response to both electric field (drift) and concentration gradients

(diffusion) that can be described with the combination of Ohm's law and Fick's law, respectively.[77, 78]

As often is the case with ionic species, electronic carrier transport in OMIECs is also thermally activated. The static disorder in the polymer due to the conformational (i.e. kinks, chain ends) and electrostatic (ions) disorder translates in a broadening of the tail edge of the density of states that localizes electronic carriers.[79] Thermal energy allows charge carriers to hop into more delocalized energy levels that are located deeper within the conduction band.[80] Electrons or holes move between delocalized electronic states either through intra- or inter-chain hopping.[81] The degree of crystallinity and short range order affect the size of domains where rapid and facile charge transport can occur. Generally, the morphology of OMIEC materials lies between two extremes: on the one hand, some rigid polymers show little long range order, but efficient intra-chain electronic transport down the polymer backbone.[82] On the other hand, in highly crystalline OMIECs (e.g. low molecular weight or small molecule OMIECs), inter-molecular transport through extended ordered domains dominates, but is impeded at grain boundaries.[83] Most OMIECs represent an intermediate case where interdomain connectivity is requires the presence of sufficiently long tie-chains that act as a bridge between ordered domains, enabling charge percolation across the entire film morphology.[84] Besides these chemical and structural factors, the applied electric field and carrier concentration also affect electronic charge transport. Carrier concentration is directly dependent on doping (ionic-electronic coupling described below). At low doping levels ions serve as traps diminishing electronic carrier mobility, and at moderate to high doping, electronic mobility increases many orders of magnitude.[66] Finally at extreme doping levels, induced disorder or band filling suppress electronic charge carrier mobility.[85] In operating devices, electric fields can lead to large variations of charge density (and thus electronic mobility) across the device.[86] Thus, this picture of electronic charge transport is altered by the changes in morphology and electrostatic potential associated with OMIEC operation. In particular, for heavily doped OMIECs operating in dry conditions, the high ionic concentration alters the potential surface of the electron transport pathway, thus leading to a band-like charge transport mechanism.[87, 88] In the case of hydrated or solvent swollen OMIECs, swelling affects mainly the amorphous domains, and can disrupt the connecting tie chains between crystallites or aggregates. This hinders the percolation of electronic charges while at the same time enhancing ion diffusion.[83]

Ionic-electronic coupling requires intimate proximity of polymer chains and ions. Due to the ability of electrolyte to percolate throughout the entire volume of the OMIEC film, the capacitive coupling between ions and organic material is volumetric rather than limited to the film surface or film/electrolyte interface. At the molecular level, ions are thought to stabilize the nearby electronic charges on the polymer backbone (e.g. polythiophene) through electrostatic interaction. This mechanism differs from the direct charge transfer from ions to polymers that can occur in systems such as polypyrrole, which can undergo direct protonation.[89, 90] The ionic-electronic coupling efficiency is sensitive to the applied potential.[44] The potential dependent coupling modulates macroscopic physical responses in operation and is pivotal to various application scenarios of OMIECs. These physical responses include film swelling, optical changes, electronic conductivity changes, charge accumulation/depletion (energy storage and ion pumps) and ion-to-electron signal transduction.

3.2 Electrical and electrochemical characterization of mixed transport

When considering mixed transport some quantities of interest are the concentrations of ionic species (anions and cations) and electronic species (electrons and holes), as well as the electric field and concentration gradient dependent velocities of these species (mobilities and diffusivities respectively).[66] In the case of electronic carriers, the concentration is dependent on the concentration of excess ions acting as dopants, and the electronic mobilities are themselves dependent on the resulting electronic carrier concentrations.[85, 87, 91, 92] The conductivities of individual species σ_i are the product of their charge q_i, mobility μ_i, and concentration c_i, shown in Equation 1:

$$\sigma_{Total} = \sum_i \sigma_i = \sum_i q_i c_i \mu_i \quad (1) = \sum_i q_i c_i \mu_i \quad (1)$$

However, due to practical considerations, conductivities are often reported as summed total ionic and/or electronic conductivity. Ionic and electronic conductivities can vary greatly (as much as 10 orders of magnitude) depending on OMIEC type and operating conditions, with optimized ionic and electronic conductivities exceeding 0.1 and 1000 S cm^{-1}, respectively. For an expanded review of the interplay of ionic and electronic transport in OMIECs and their dependence on operating conditions see ref[66]. In the case of electronic conductivity, electrons and holes are

singly charged species and transport is generally single carrier as electrons and holes in close proximity tend to recombine. However, anions and cations can coexist and can be mono- or multivalent; therefore total ionic conductivity alone cannot completely describe the underlying picture.[77, 78] However, if ionic and electronic conductivities are of a similar order of magnitude it can become exceedingly difficult to isolate the ionic and electronic contributions and a simple total conductivity is sometimes reported.

Ionic and electronic transport in OMIECs is generally assessed through electrical characterization, particularly current-voltage measurements and electrochemical techniques (vide infra). In the simplest current-voltage (J-V) setup, the OMIEC is connected between two noble metal (ion blocking) electrodes, shown in **Figure 2a**. Polarization results in a transient ion transport leading to ion accumulation/depletion at the electrodes.[51, 93-96] Steady-state two terminal J-V measurements should give only electronic transport component, but the fixed total ion composition complicates matters. The aforementioned ion migration and accumulation produces a non-uniform potential profile, and since excess ions serve as dopants, this results in a non-uniform electronic mobility across the sample. Four probe measurements can mitigate these problems.[87] Stepped voltage current transients and impedance spectroscopy can separate ionic and electronic components,[21, 97, 98] especially when one type of transport (often ionic) is much slower than the other. Generally, this geometry is limited to determining a single conductivity (a total conductivity, or ionic or electronic if one predominates).

Alternatively, traditional electrochemical techniques feature an OMIEC in contact with an ion-blocking working electrode and an electron-blocking electrolyte interface, shown in **Figure 2b**. When characterizing mixed transport, it is favorable to choose a potential range and ambient environment that minimizes faradaic reactions (oxidation or reduction of the solvent, ions, or dissolved species) at the electron blocking interfaces OMIEC/electrolyte interface. J-V measurements in this geometry can be collected during linear potential sweeps, at fixed potentials with a superimposed small variable frequency sinusoidal potential, or during stepped potentials. The most common technique using linear potential sweeps is cyclic voltammetry (CV). In OMIEC CV, redox peaks reveal the pseudocapacitive charging, which reflects the potential dependent volumetric capacitance (C^*) of the OMIEC.[99-102] CV also determines the potential ranges of stable hole and electron accumulation (oxidation and reduction, respectively).

When the transport of one species represents the rate limiting step, diffusivity can be extracted from the sweep rate dependence.

Electrochemical impedance spectroscopy (EIS) varies the frequency of applied potential to extract the real and imaginary components of the complex impedance. A strength of EIS is the separation of physical processes by timescale (frequency). In the simplest case the frequency dependent complex impedance can be modelled with a Randles equivalent circuit, consisting of a resistor (R_s) in series with a parallel resistor (R_p) and capacitor (C).[103] The importance of these equivalent circuit elements are the physical processes they capture. R_s manifests as a high frequency impedance plateaued minimum, and is the summation of all the series resistances arising from the lead wires and traces, the electrical out-of-plane resistance of the OMIEC film, an effective resistance to out-of-plane ion transport in the OMIEC film, and the bulk electrolyte resistance. R_p manifests as a low frequency impedance plateaued maximum, and captures the direct electron transfer process occurring between the electrolyte and the OMIEC and the electrolyte and the buried electrode. C manifests as a mid frequency impedance decrease with increasing frequency, and is a conflation of the 2-D capacitances at the electrolyte-OMIEC and buried electrode interface, and the 3-D C* of the bulk of the OMIEC. Impedance data deviating from simple Randles-like behavior require complicated equivalent circuit models[104, 105] which can give additional insight into ionic diffusion coefficients,[106-109] electronic mobilities,[110] and electronic density of states.[111]

Coulometry, measuring the current over time during potential steps, is closely related (by a Laplace transform) to EIS and gives similar information. As with EIS, the results are fit with equivalent circuit models. While EIS uses a small potential oscillation about a constant potential offset it is safe to assume the structure and properties of the OMIEC are relatively constant. Conversely, coulometry employs large potential steps across which there are often large structural and property changes of the OMIEC. This can significantly complicate model interpretation. It must be noted that it is difficult to isolate ionic transport in the OMIEC with coulometric measurements. While it is common in the literature to extract diffusivities from current decays using the Cottrell equation, these reports rarely account for the effect of RC charging (which are quite massive in CPs and OMIECs), which the Cottrell equation assumes are

negligible. This indiscriminate misapplication of the Cottrell equation unfortunately yields untrustworthy diffusivity values.

On the whole, these techniques (CV, EIS, coulometry) are best equipped to measure stored charge (C*, charge storage capacity, energy density, etc), and the potential dependence thereof (potential dependent C*, equivalent to the electrochemical density of states). In particular cases they can also give diffusivities/mobilities of individual ionic and electronic species.

Combining the above characterization schemes (dual ion-blocking interface, and one ion blocking and one electron blocking interface) produces an electrochemical test bed with an in situ electrical conductivity measurement, now more commonly known as an organic electrochemical transistor (OECT, shown in **Figure 2c**).[112, 113] The general structure of OECTs involves an OMIEC channel separating a source and drain electrode (which combined function as the working electrode) coupled to a gate electrode (serving as the counter and reference electrode) through an electrolyte. OECTs isolate electronic conduction without fixing ionic concentrations, avoiding the ion accumulation/depletion at electrode interfaces that occurs in a two-terminal measurement with fixed total composition. The source-drain current captures electronic transport, while the gate current captures ionic transport.[85, 114] The OECT testbed gives electronic mobility with high confidence. The extracted threshold voltage (a measure of the potential at which the OMIEC conductance "turns on") relates the potential dependent charging with the onset of electronic transport. The gate transconductance (dI_d/dV_g), normalized by the applied gate voltage beyond the threshold voltage and channel dimensions, conveys the product of electronic mobility and volumetric capacitance (μC^*) which is a particularly useful OMIEC material figure of merit.[103] As with the above current voltage test beds, OECTs do not effectively capture ionic conductivity or ion diffusivities/mobilities.

While OECTs work well at isolating electronic transport, iontronic (or ionotronic) devices (which accomplish the basic effects of traditional electronic devices, such as diodes and transistors, but with ionic currents) can similarly isolate and quantify ionic transport (**Figure 2d**).[115-117] In the most basic structure, coating the metal electrodes of a two-terminal set up with electrically insulating ionically conducting polymer electrolytes or polyelectrolytes allows the isolation of ionic conductivity. More complicated assemblies produce ion transistors and

diodes[118-120] enabling the isolation of anion or cation transport to extract diffusivities/mobilities of specific species. Replacing the ion-blocking contacts of an OECT with individual electrolyte interfaces transforms the OMIEC into an iontronic device. As often is the case, these electrical and electrochemical testbeds are themselves the devices of interest for in situ and operando OMIEC characterization.
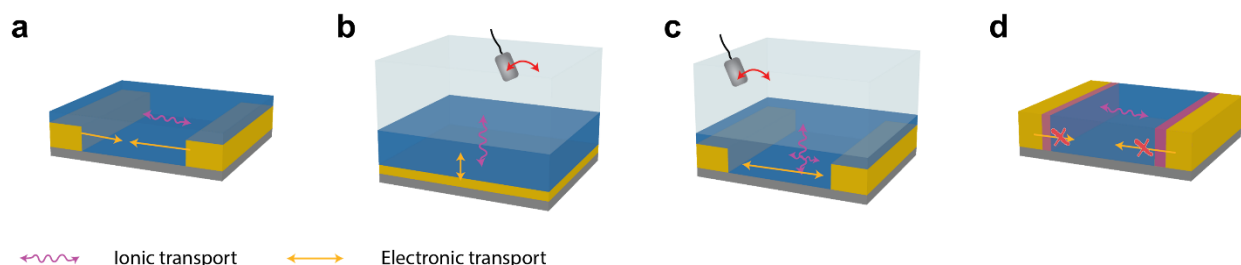
Figure 2. Different geometries based on the direction of ionic drift/diffusion and electronic transport in operando characterization: (a) OMIEC connected between two noble metal electrodes; (b) OMIEC in contact with an ion-blocking working electrode and an electron-blocking electrolyte interface; (c) Organic electrochemical transistor (OECT); (d) Iontronic devices.

4. Optical Spectroelectrochemistry

Spectroelectrochemistry refers to a series of in situ analytical techniques that incorporate electrochemistry and spectroscopy simultaneously and has been widely applied in OMIEC characterization. Depending on the similarity of conditions between the electrochemical technique (coulometry, EIS and CV) and OMIEC device operation, spectroelectrochemistry can at times be considered an operando technique. Steady-state and slow to moderate sweep rate spectroelectrochemical techniques can accommodate long integration times, while transient measurements require sub second level temporal resolution. Optical techniques in this section include UV-Vis-NIR spectroscopy, Infrared (IR) spectroscopy, Terahertz (THz) spectroscopy, and Raman spectroscopy. The electromagnetic range used in these techniques corresponds to different types of electronic and vibrational transitions in molecules, enabling to characterize a range of energy levels of OMIEC materials. This information, particularly when combined with theoretical models, gives insight into the material structure and ion environment.

1 Pump-probe techniques such as transient absorption and ultrafast spectroscopy enable the study

2 of excited states decay dynamics (UV-Vis-NIR) as well as ionic mobility (THz). The information

3 that can be obtained by different techniques is briefly organized in **Table 1**. In **4.1**, operando

4 spectroscopy in the UV-Vis-NIR band is discussed, including absorption spectroscopy, transient

5 absorption, photoluminescence and ellipsometry; in **4.2**, the characterization of OMIECs with IR

6 and THz absorption techniques will be discussed; and in **4.3**, in situ/operando Raman

7 spectroscopy as a complementary technique to IR spectroscopy for detecting molecular

8 vibrations will be addressed.

9 **Table 1.** Summary of optical spectroscopic techniques employed in operando study of
10 OMIECs.
11

Method	Description	Electronic carrier Information	Ionic carrier Information	Structural & Morphology Information	Representative operando/ in situ example(s)	Implementation barriers
UV-Vis-NIR Absorption	Measure optical absorption in UV-Vis-NIR range (200-2500 nm)	Neutral/charged subpopulations, optical band gap	-	Degree of aggregation/ packing	Polythiophenes[19, 72, 121-123] C60 Derivatives[124] pgNaN[125] BBLs[126] NDI-T2[127]	-
PL	Measure fluorescence emitted by excited species	Emissive species population, excitation energy	Concentration, environment	Degree of aggregation/ packing	iTMC[128] PPV[129-131]	-
Spectroscopic Ellipsometry	Measures the reflected elliptically polarized light from the sample and sample-substrate interface	Conductivity, optical constants, neutral/charged subpopulations, optical band gap	Chemical composition	Thickness, degree of aggregation/ packing	PEDOT:PSS[132]	-
IR absorption	Measure optical absorption in IR range (700 nm -10 μm)	Absorption of low energy carriers, vibrational signatures of neutral/charged species	Molecular ion environment	-	P3HT[133-135] BBL[136]	Broad water absorption
THz Spectroscopy	Measure optical absorption in THz range	Mobility	-	-	P3HT:PCBM[137]	Complex setup, few THz transparent cells/substrates

|	(10 μm -1 mm)					
Raman	Measure Raman scattering from the sample	Neutral/charge subpopulations and domain distributions, vibrational signatures of neutral/charged species	Molecular ion environment	Vibrational signatures of ordered/amorphous domains	Polythiophenes[138-146] NDI-T2[147]	Weak signal, limited choice of excitation wavelengths

1

4.1 UV-Vis-NIR spectroelectrochemistry

UV-Vis-NIR spectroelectrochemistry (operando UV-Vis-NIR spectroscopy) covers the 200-2500 nm spectral range and is popular in OMIEC characterization. The technique provides information on the transition of electrons in the frontier orbitals (HOMO and LUMO) of molecules (using PEDOT, a p-type OMIEC material for example, shown in **Figure 3a**). The spectrum (**Figure 3b**) mainly reflects absorption resulting from excitations of π-π* transitions (**Figure 3c**) and charged species (polarons and bipolarons, **Figure 3d**) in conjugated polymers. The optical properties of organic conjugated materials are not only related to the conformational and charged status on the molecular backbone, but also intermolecular aggregation (**Figure 3c**, left).[148-150] It is an important operando technique due to its ability to capture the intermediate states and kinetics of OMIEC material during electrochemical doping/dedoping.

The polaron and bipolaron model of conjugated polymers is generally used to describe the charged species of OMIEC material after electrochemical doping.[151-153] Polaron refers to the individual electrons accompanying local vibrational mode deformation, and bipolaron refers to the paired electrons in local vibrational mode deformation that has different mobility and effective mass than the free carriers. While many researchers regard polarons as stabilized radical cations/anions and bipolarons as dications/dianions in doped CPs,[64, 154-157] it has been reported that the formation of polarons arises from the symmetry breaking in the electron density distribution of radical cations/anions.[158] There have been different interpretations of the visible-near-infrared spectral bands of polarons and bipolarons, as shown in **Figure 3d**. In the early literature, the absorption band of polaron lies from the red end of the visible spectrum to the near-infrared band, while the absorption band of bipolarons lies into further infrared band.[151, 159]

According to recent DFT calculations, Zozoulenko et al. show a partial overlap of the absorption bands of polarons and bipolarons, i.e., the absorption bands of bipolarons are also present in the absorption bands originally considered to be polarons.[160] It is worth noting that the polaron and bipolaron model is a simplification of real OMIEC operation. The polaron/bipolaron model neglects multiple charged species in particular oligomer lengths, instead assuming a simple increase in polaron/bipolaron concentration.[160] According to the DFT calculation, such a treatment changes the band energy as well as the singlet/triplet states.[160]
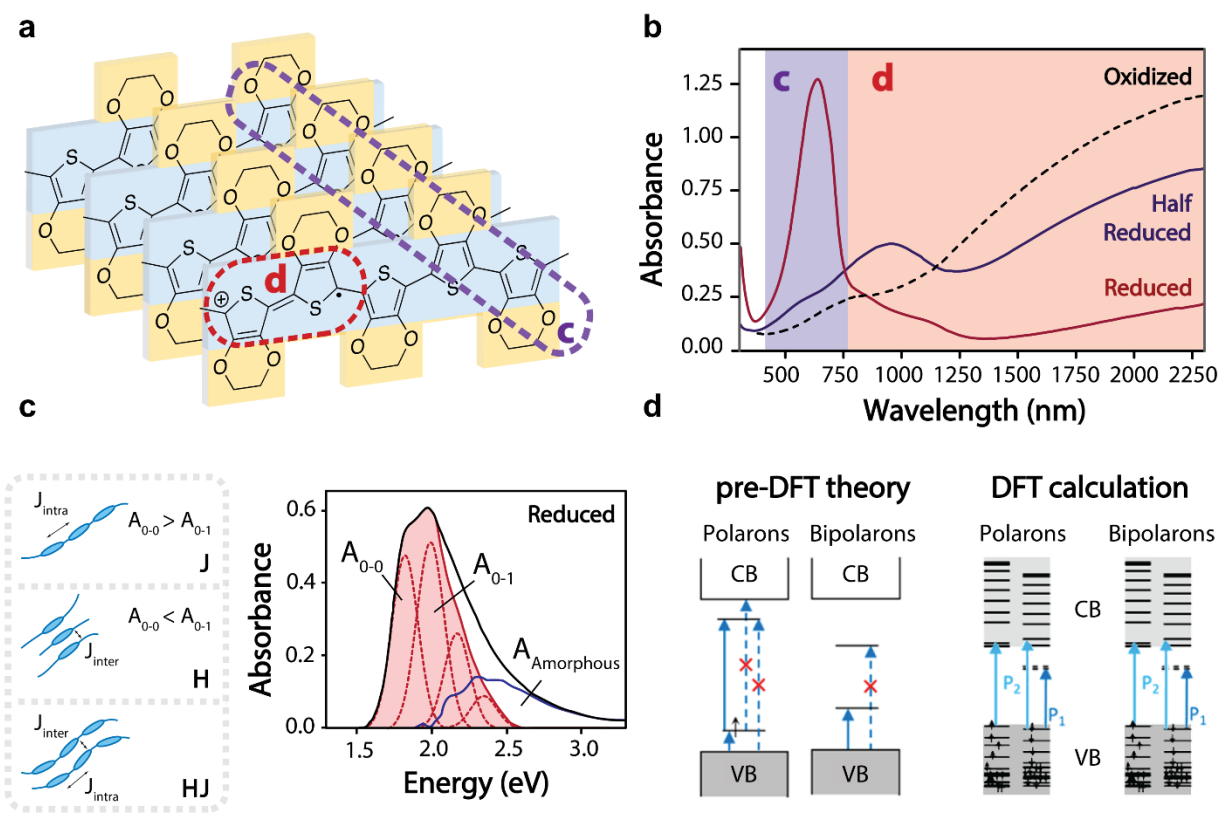
Figure 3. (a) The molecular stacking of a typical OMIEC material PEDOT (b) Experimental UV–vis–NIR absorbance spectra of oxidized (black dash) , half-reduced (blue) and reduced (red) PEDOT:PSS. The neutral aggregation (purple) and charged state (red) are shaded in the spectrum. Reproduced with permission from [[156]]. Copyright 2014 Royal Society of Chemistry. From UV–vis–NIR absorption spectra, the following information can be extracted: (c) Left: J-aggregate (up), H-aggregate (middle) and HJ-aggregate (down) from Spano model; right: experimental absorbance spectrum of electrochemically reduced PEDOT:PSS (with 50 vol%

EG) films with 0-0, 0-1 and higher order peak (red dash) from molecular aggregate and the residual absorbance contribution (blue) from amorphous domain. Adapted with permission from [161]. Copyright 2016 Royal Society of Chemistry. (d) Polaron and bipolaron band diagram; reported with permission from [160]. Copyright 2019 American Chemical Society.

Unlike in small molecule chromophores, conjugated polymers present intra-chain and inter-chain chromophore interactions. These π-stacking and dipole interactions between aromatic rings in OMIECs affect their density of states and consequently their spectral signature. The photophysics of semicrystalline conjugated polymers such as polythiophenes has been explained by Spano et al.[148, 162, 163] starting from Kasha's theory of H and J aggregates (see **Figure 3c**, left). J aggregates stem from the head-to-tail arrangement of chromophores, akin to the interactions between neighboring repeating units in a polymer chain. H aggregates arise instead from the side-by-side stacking of chromophores, corresponding to the lamellar π-stacking between different polymer chains. In J aggregates, the $S_0 \rightarrow S_1$ absorption shows a red shift due to the optically allowed transition being at the bottom of the exciton band, while in H aggregates we observe a blue shift of the absorption peak with the allowed transition falling at the top of the exciton band. This difference results in a strongly allowed 0-0 emission in the vibronic structure of J aggregates, while the same transition is thermally activated for H aggregates. A single conjugated polymer chain can be viewed as a J aggregate, where each conjugated monomer is electronically coupled to its neighbors. The H aggregate model is instead more suitable to describe polymers with short backbone or low backbone planarity, where interchain π-stacking dominates.[164] where interchain π-stacking dominates. In order to describe the range of behaviors observed across conjugated polymers, Yamagata and Spano developed a two-dimensional HJ aggregation model in which the spectral features depend on the relative magnitudes of the intrachain and interchain exciton bandwidths.[149] The ratio between the relative intensities of the 0-0 and 0-1 vibronic peaks (**Figure 3c**, right) can be used to quantify the degree of J or H character of the polymer and thus provide information on the degree of aggregation and disorder. This model was applied to monitor the structural effects of ion doping on different domains of P3HT[165, 166] and PEDOT.[161] Finally, the shorter wavelength region of the UV-Vis spectrum not captured by the Spano model is associated to amorphous domains, including small molecular weight fragments that present an oligomer-like behavior.[162, 167-169]

4.1.1 Subtypes of UV-Vis-NIR spectroelectrochemistry

Basic UV-Vis-NIR spectroelectrochemistry can be divided into two modes: the transmission mode and the reflection mode. The transmission mode is achieved by casting the sample on an electrically conductive UV-Vis-NIR transparent working electrode (for example ITO glass), shown in **Figure 4a**. The chosen substrate should be suitably conductive to ensure a uniform and stable voltage on the whole sample. Since water and most organic electrolytes do not absorb strongly in UV-Vis-NIR wavelengths, beam attenuation is minimal and the signal-to-noise ratio is high. It is worth noting that the absorption of aqueous electrolyte gradually increases in the infrared band above 1300 nm and shows a broad background absorption, while the background of most organic solvent is weak and narrow.[170] Another approach is to collect reflectance UV-Vis-NIR absorption spectroscopy, including the diffuse reflection spectroscopy (DRS) and attenuated total reflection (ATR) spectroscopy. DRS is suitable for thick or surface inhomogeneous samples (e.g., drop-cast OMIEC samples) where UV-Vis-NIR light is difficult to transmit, and has been reported for ex situ characterization of conjugated polymers[171-173] as well as in situ characterization of solid-state reactions.[174-176] DRS can be combined with different characterization tools (e.g. EQCM, X-ray diffraction, etc.), enabling simultaneous multi-modal measurements of the same sample in real time. ATR spectroscopy employs a crystal in contact with the sample, light passing through the ATR crystal undergoes total internal reflection at the crystal-sample interface. The evanescent wave generated by total reflection is subject to the wavelength dependent absorption of the sample, producing a spectral signal. The penetration depth of evanescent wave varies from hundreds of nm to several μm depending on incident angle and wavelength.[177] A typical setup for operando ATR UV-Vis-NIR absorption measurement is shown in **Figure 4d**. This setup avoids the passage of the beam through the bulk solvent, making it capable of circumventing solvent absorption background, and isolating optical absorption near the sample surface.

Derivative UV-Vis-NIR spectroelectrochemistry techniques can be achieved by changing the instrumental geometry, the incident light source, or the outgoing beam collection from absorption spectra. Experiments monitoring electrochromic "moving fronts" in OMIECS arising from lateral ionic and electronic transport in OMIEC thin films allow the estimation of ion mobilities.[69, 161, 178] Transient absorption spectroscopy (TAS) uses an optical pump pulse to

1 excite the sample to its excited state, followed by a white light probe pulse to monitor the

2 relaxation processes. Spectroscopic ellipsometry applies polarized light as the incident beam to

3 deduce a materials complex dielectric constant and conductivity. Photoluminescence (PL)

4 collects the outgoing fluorescence perpendicular to the beam path when working in transmission

5 mode and gives information on molecular energy levels. The operando application of TAS, PL

6 and spectroscopic ellipsometry in OMIEC characterization will be discussed in the following

7 sections.
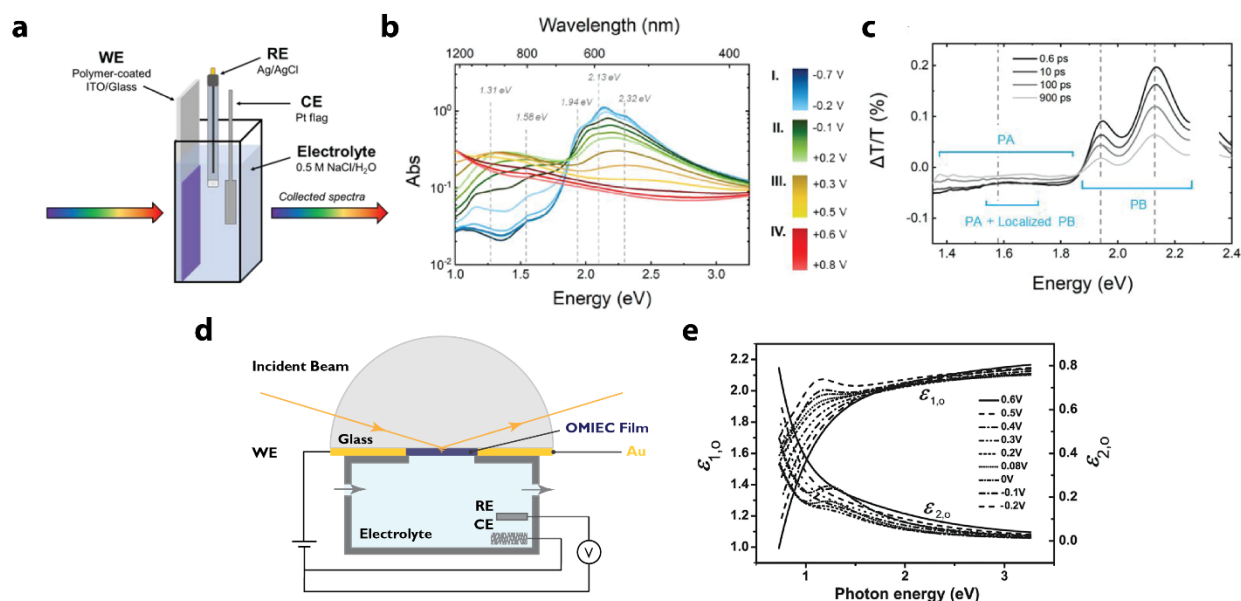
8

9 **Figure 4** (a) Operando UV-Vis-NIR spectroscopy setup in transmission mode. (b) The external

10 voltage dependent UV-Vis-NIR spectra and (c) transient absorption measurement for

11 ProDOT(OE$_3$)-DMP in transmission mode. (a)-(c) are adapted with permission from [123].

12 Copyright 2021 American Chemical Society. (d) Operando UV-Vis-NIR spectroscopy setup in

13 reflection (ATR) mode, named as Kretschmann cell. (e) Real (ε_1) and imaginary (ε_2) part of the

14 ordinary dielectric functions of the PEDOT:PSS film obtained by operando UV-Vis-NIR

15 ellipsometry in reflection mode. Adapted with permission from [132]. Copyright 2018 Elsevier.

16 4.1.2 UV-Vis-NIR absorption spectroelectrochemistry

17 Steady-state UV-Vis-NIR absorption spectroelectrochemistry is extremely widespread and

18 foundational technique, employed in conjugated polymer research to understand potential

dependent intermolecular aggregation, charge transfer states and charged species populations. To date, various OMIEC materials with high conductivity and stability have been characterized by the technique. In addition to PEDOT,[179, 180] a large group of newly synthesized p-type semiconductor OMIEC materials have been characterized by operando UV-Vis to follow the formation of polaron/bipolaron under different charging voltages.[72, 181-184] Undoped p-type polythiophene based OMIECs exhibit absorption peaks at approximately 600 nm due to H-aggregation and tend to show well-characterized 0-0 and 0-1 vibrational peaks, thus indicating extensive molecular ordering in the solid state.[19, 72, 121] For donor-acceptor materials like diketopyrrolopyrroles (DPPs), the neutral aggregation absorption peak is red-shifted to near infrared region due to the narrowing of the band gap of HOMO/LUMO and broadened by the reduced molecular stacking order.[182, 185] During electrochemical doping, the polymer is oxidized and shows a bleaching of neutral π-π^* peak as well as the growth of peaks corresponding to charge carrier populations (i.e. polarons and bipolarons). Steady-state spectroelectrochemistry UV-Vis-NIR spectroscopy is also important in charged species quantification and understanding stability of n-type OMIECs, and has been applied to fullerenes,[124] electron-rich polymers,[125, 126] and NDI based donor-acceptor materials.[127]

In addition to steady-state spectroscopic studies at different applied voltages, time-resolved UV-Vis-NIR spectroelectrochemistry provides a wealth of valuable information about material stability and charge/discharge reversibility. The durability of the oxidized/reduced state at open circuit voltage is tracked with materials exposed to air after oxidation/reduction,[185, 186] showing particularly importance in the study of neuromorphic/memory materials.[7] On the other hand, operando UV-Vis-NIR spectroscopy provides extra kinetic information, including mechanism of charged species formation and ion injection/migration rates, as voltage is applied. The dominant time constant of neutral-polaron kinetics can be extracted by exponential fitting of absorption changes.[122, 124, 187] It is worth noting that simulations of spectral kinetics often require simple (i.e. monoexponential for single species) decay curves, however more complex models for overlapping spectral features can be warranted. Combining the time constants obtained from spectral kinetics fittings with information from other operando experiments or theoretical calculations results in richer assessments of structure-property information relevant to swelling and ion injection.[122]

1   4.1.3 Transient Absorption

2   Transient absorption spectroscopy (TAS) is a common ultrafast laser pump-probe technique and

3   has been recently applied in OMIEC operando experiments. The technique is attractive to

4   OMIEC systems as it directly probes the excited states and yields information on their decay

5   kinetics, which relate to excited state lifetime as well as carrier mobility.[188] A laser beam is split

6   into two pulses: pump and probe. After the system is excited by the pump pulse, the weaker

7   probe pulse is used to monitor excited state dynamics.[189] The femtosecond time resolution[190-193]

8   is determined by the bandwidth of the laser, which is around 0.5-1 THz. The technique has been

9   applied to distinguish between free and bound carriers in bulk heterojunctions (BHJ).[194] In

10   addition to excited electron decay kinetics, a recent study of self-doped conjugated

11   polyelectrolytes by TAS reveals the strong electronic coupling between the polaron site and

12   nearby neutral sites, and demonstrated the photophysics of polarons and their interaction with the

13   surrounding environment.[195] Operando TAS on OMIEC material has been reported by Bargigia

14   et al. to investigate the electronic states of individual UV-Vis absorption peaks under different

15   external voltages.[123] Using ProDOT as a model material (spectroelectrochemistry in **Figure 4b**),

16   the charge transfer (CT) state was successfully identified prior to redox current and polaron

17   formation. As shown in **Figure 4c**, further studies of the photobleaching (PB) process reveal the

18   stability of the intermediate state in different electrolytes, with much faster quench kinetics

19   observed in aprotic organic electrolytes than in aqueous electrolytes. In general, it is possible for

20   operando TAS to identify intermediate doping states (informing reaction mechanism), the

21   coupling between different electronic states, and the interaction of charged species with the

22   environment in operating conditions.

23   4.1.4 Photoluminescence

24   Photoluminescence (PL) or fluorescence spectroscopy, which detects the photons emitted by an

25   excited species returning to the ground state, has been applied early on for ex situ,[196, 197] in situ[129]

26   and operando characterization[128] of conjugated polymers. The technique works as a complement

27   to absorption spectroscopy and gives additional information about molecular ordering and ionic

28   species population in OMIEC materials. As described in **Section 4.1**, the 0-0 fluorescence peak

29   of the material completely disappears in the ideal H aggregate, which is fully ordered in Spano

model. Therefore, the ratio of 0-0/0-1 fluorescence peak can be used to describe the degrees of molecular ordering.[150] In addition, the population and transport dynamics of ionic dopants in OMIEC can be detected by time-resolved photoluminescence spectroscopy measuring the bleaching time of fluorescence. According to the molecular line theory proposed by Zhou and Swager, the single state exciton generated upon absorption of light migrates rapidly along the polymer backbone[198] by hopping between chromophores.[199] The exciton will be quenched when it reaches the site occupied by exciton quencher[198, 200] or domain/phase interface in heterojunction.[201-204] High-valence ions, such as calcium ions,[205] charged proteins[206] and nucleic acids[207] are often good exciton quenchers, which makes this technique suitable for the analysis of ionic species. Lastly, photoluminescence spectroscopy provides the information on polaron concentrations. The electron transfer from excitons to polarons leads to the fluorescence quenching,[208] and polaron absorption of fluorescence further reduce the emission efficiency.[209] The florescence quenching from polarons is reversible, such that molecular florescence recovers after the elimination of polarons. This phenomenon has been reported in molecular doping[210] and photo induced polaron formation[211, 212] of conjugated polymers.

In situ PL spectroscopy has been used for film formation studies of organic polymers during spin-coating, which measures both absorption and PL spectra during the solution processing of the studied films.[37, 213] By continuously tracking the changes in the absorption and PL spectra of P3HT, the investigators revealed the film formation kinetics.[37] This approach to incorporate in situ PL and absorbance measurements can be easily extended to operando measurements on OMIEC materials to understand the dependence of local microstructure and macroscopic optoelectronic properties on deposition method, film post-processing, and electrical operation. There are no exceptional hurdles to in situ/operando implementation that are particular to PL compared to in situ/operando UV-Vis absorption spectroscopy.

In organic light-emitting devices, operando PL spectroscopy has been applied to reveal ionic species population and lattice defects through the PL monitoring of exciton quenchers. The technique was used to study temperature and operating time dependent ion doping in polymeric light-emitting electrochemical cells (LEECs).[128, 129] In the operation of LEECs, a hetero junction is formed by the p- and n-type electrochemical ionic doping, creating recombination zones where light emission occurs. Continuous operation of the device over long time causes the charge

carriers to be compensated by opposite ionic charge, leading to electrochemically doped

molecules that block exciton hopping and trigger fluorescence quenching. The degree of PL

recovery after turning off the external bias indicates the reversibility (versus permanent material

degradation) of the LEEC material after long time (12-72h) operation.[128] Fluorescence

spectroscopy can also distinguish between p and n doped regions due to different ionic doping

levels and assist electrical probes in measuring local potential and conductivity in LEEC

channel.[130] In the field of OLEDs, time-resolved PL spectroscopy has been applied to study the

defect states (quenchers) caused by both electric field induction and chemical doping.[131] Looking

forward, the sensitivity of PL spectra to these charged dopant ions should enable the

development and characterization of OMIEC materials sensitive to the binding of small

molecule/ions during biosensing.

4.1.5 Spectroscopic Ellipsometry

Spectroscopic ellipsometry uses incident high-precision linear polarized light and measures the

reflected elliptically polarized light from the sample and sample-substrate interface. The

dielectric constant in each direction of the film, the film thickness of different layers, and the

surface morphology can be modelled using Fresnel theory. This information is helpful in

elucidating the swelling and vertical film structure/morphology of OMIEC materials. The

technique has also been applied to quantitatively analyze the chemical composition of polymer

thin films from optical and thickness data.[214] In addition, the technique gives complex optical

constants at different wavelengths. The real part of the constants is the refractive index of the

sample, and the imaginary part is the extinction coefficient related to the absorption.[215] Thus,

spectroscopic ellipsometry provides UV-Vis-NIR spectroscopy and associated information on

molecular packing.

In situ studies employing this technique have focused on real-time monitoring the swelling of

insulating polymer films subjected to solvent vapor treatment.[216] Operando UV-Vis-NIR

spectroscopic ellipsometry has been implemented in recent years[217] and used to measure the

electrochemical doping and dedoping processes of a prototypical OMIEC material, PEDOT:PSS,

operating in an aqueous environment.[132] Within the Tauc-Lorentz-Drude (TLD) model,[218, 219] the

technique gives optical constants and provide the information on complex dielectric constant as

well as potential dependent electronic conductivity.[132] The potential dependent local conductivity can be understood with respect to a 'threshold voltage', representing field effect dominance (surface charged) below the 'threshold voltage' and ion injection dominance (bulk charged) once the 'thereshold voltage' is reached.[132] It is worth mentioning that the Kretschmann cell configuration (**Figure 4d**) used in this study effectively prevents the optical path from passing through the aqueous electrolyte, which effectively reduces the absorption of NIR light by water molecules, thus allowing the effective range of the spectrum to be extended and distinguishing the contribution of free charge carriers to the total absorption in the NIR range.

In summary, UV-Vis-NIR spectroelectrochemistry techniques are a popular tool for the characterization of OMIEC materials, as they enable non-invasive operando measurements with a high signal-to-noise ratio, even in aqueous or organic electrolytes. These methods enable the time resolved analysis of OMIECs during operation; in particular, structure and morphology dynamics of thin films can be correlated to changes in electrical properties such as current and voltage.

Further insight into structure-property relationships for OMIECs in operation can be obtained by coupling spectroelectrochemical measurements with additional characterization techniques. In particular, optical techniques are being leveraged for the operando imaging of OMIEC materials. Recently, operando interferometric scattering microscopy (iSCAT) has been used to image ionic diffusion in battery materials.[220] The insight of iSCAT into nanoscale composition and structure provides the possibility to observe ion transport and domain changes in OMIEC materials in operation.

4.2 IR and THz Absorption

4.2.1 Fourier-transform infrared spectroscopy

In contrast to the commonly used operando UV-Vis-NIR spectroscopy, operando infrared (IR) and terahertz (THz) spectroscopies are relatively underreported in operando OMIEC characterization. Fourier-transform infrared spectroscopy (FTIR) is capable of distinguishing and identifying functional groups, shedding light on the charge density and local environment of

organic materials. In OMIECs and in the wider category of conjugated polymers, polaron

formation results in a change in bond length alternation that is reflected in the polymer's IR

signature. Due to its ability to capture the population of different charged species and their

molecular environment, the technique is appealing for operando OMIEC characterization.

Attenuated Total Reflection (ATR) mode is the most common technique current used in FTIR

for its convenience and robustness. To enhance the IR absorption signal, the incident IR beam

can be reflected several times at the crystal-sample interface, termed multi-bounce or multi-

reflection ATR, **Figure 5a**. The technique is broadly applied to probe the vibrational modes of

molecular dopants in conjugated polymers[221] and small molecule organic semiconductors,[222] to

reveal different oxidation species as well as the interaction between charged molecular dopants

and charged organic molecules. Most OMIEC relevant in situ IR experiments have been carried

out on CPs or small molecules using acetonitrile or PEO as the solvent/mediums, including

during electropolymerization[223] as well as electrochemical cycling (doping/dedoping) of p-

type[133] and n-type semiconductors.[136] In situ/operando IR spectroscopy is rarely implemented in

aqueous electrolyte due to the strong absorption of water molecules over mid infrared bands. For

OMIEC materials, in situ ATR-FTIR directly detects the absorption of polarons and bipolarons

dependent with oxidation voltage.[133] In situ ATR-FTIR covers a wider range of infrared

wavelengths than operando NIR spectroscopy, resulting in complete absorption peaks of polaron

and bipolarons. In CP films in contact with $LiClO_4$/PEO solid polymer electrolyte, reports

revealed the ion uptake kinetics during electronic charging and discharging by tracking the

polaron IR absorption.[134, 135] The time integration of the polaron broad peak shows the kinetic

asymmetry of the film between charging and discharging (**Figure 5c-e**). In addition, the channel

length has no effect on charging kinetics but a small effect on discharging kinetics, indicating a

small amount of charge trapping in the system. Importantly, the independence of electrolyte

thickness on the CP film discharge indicates that the electronic doping kinetic in this system is

limited by the anion uptake, as shown in **Figure 5b**. The subsequent fitting of the kinetic curves

with a diffusion model showed a strong correlation between the anion diffusion constant and the

applied voltage.
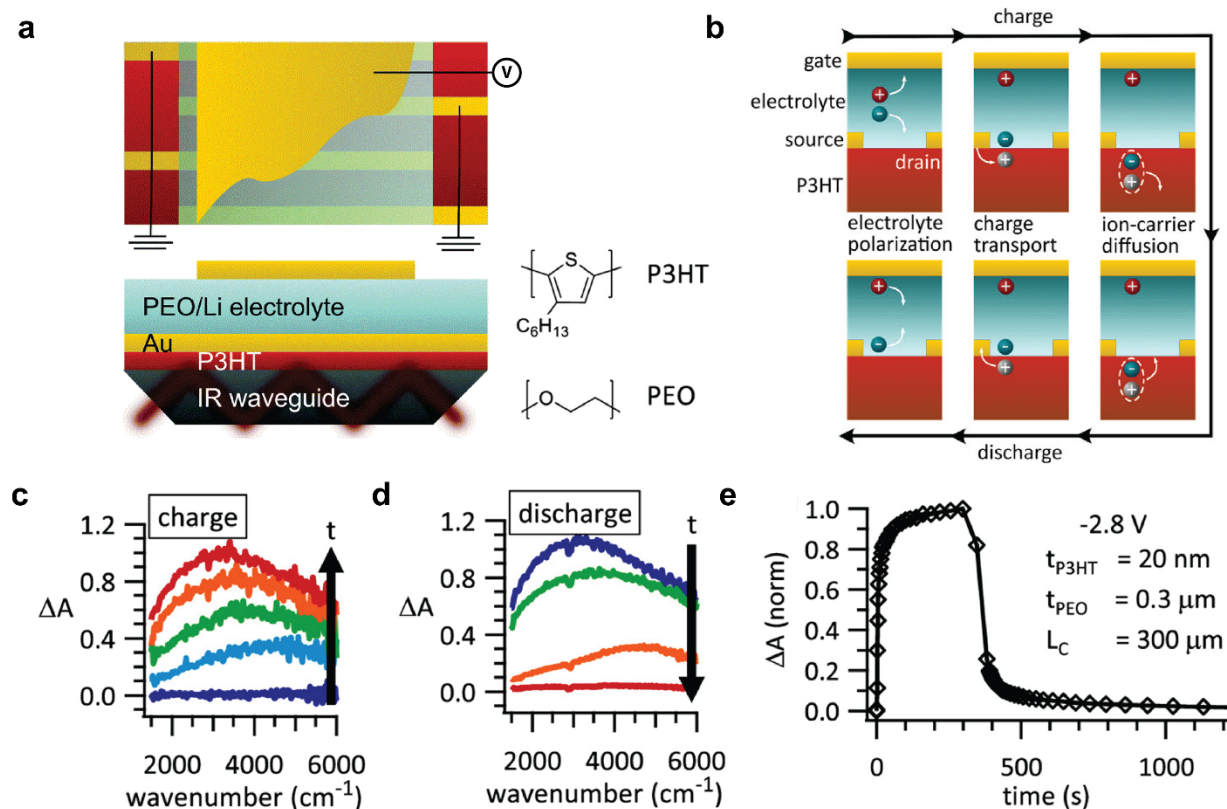
Figure 5 (a) Operando FTIR setup in ATR mode. Multiple reflections at the interface are designed to increase the signal intensity. Adapted with permission form [134]. Copyright 2019 Royal Society of Chemistry. (b) Proposed progression of charging and discharging in OMIEC active layer,[135] based on time-resolved infrared spectra during (c) device charging and (d) device discharging. (e) Integrated absorbance from (c) and (d) plotted vs. time. The gate voltage was -2.8V, and the voltage is set to 0 V at t=400s for discharging. (b)-(e) are adapted with permission from [135]. Copyright 2021 American Chemical Society.

The development of future operando IR spectroscopy for OMIEC materials needs to overcome the following difficulties: First, ATR-IR, even using multibounce mode, requires the averaging of multiple measurements, which limits the time resolution far above the timescales changes in OMIEC materials in operating conditions. For ultrafast kinetics, such as polaron formation and decay, time-resolved IR spectroscopy based on pump-probe techniques has been reported on melanin.[224] Second, special methods and cell designs for circumventing the water absorption are necessary when investigating OMIECs in aqueous electrolyte. A potential substitute solvent is heavy water, which exhibits low background absorption between 1300 cm^{-1} and 1900 cm^{-1}.[224]

The combination of operando IR with other absorption spectroscopy techniques is also a foreseeable trend. A measurement platform combining three fiber optic probes for operando ATR-IR, Raman and UV-Vis-NIR spectroscopy, has been implemented in the study of homogeneous catalytic systems.[225] Such a platform could be adapted to multimodal optical characterization of OMIEC materials in real time.

4.2.2 Terahertz Spectroscopy

In conjugated polymers, terahertz (THz) spectroscopy is mainly applied to detect short-range charge transport and transient photoconductivity in a material. THz pulses are generated via different methods, including nonlinear optical processes, semiconductor photoconductivity and free electron lasers.[226, 227] The transmitted light is collected by THz detector and the entire setup is purged by dry nitrogen or helium to prevent atmospheric water absorption. The technique has not been applied in operando measurement of OMIEC materials, but could be readily employed for the direct determination of potential dependent charge carrier mobility by probing THz dielectric response of charge species, including free carriers, polarons and excitons.[226] THz absorption spectroscopy (both pump-probe and non-pump-probe) has been reported to characterize the voltage-dependent response of conjugated polymer-based THz wave modulators.[226, 228-230] In pump-THz probe experiments, the electric field of the THz pulse is recorded after absorption by the excited sample. By varying the delay time of the pump-probe setup, the time-dependent photoconductivity can be obtained and Fourier-transformed to obtain the complex frequency-dependent photoconductivity.[226] The Drude-Smith model is used to relate optical conductivity to the interband transition, the electron lifetime, and the transport relaxation time.[231] This model has been adapted for the determination of carrier lifetime and mobility in solar cell materials,[232, 233] as well as the elucidation of charge injection[234] and hopping processes in conjugated polymers.[235] In situ studies of printed electronic devices by pump-probe THz spectroscopy have shown to produce reliable surface conductivity mapping in comparison to conventional methods such as AFM and four-point probe techniques.[236] The absorption of the THz beam by the electrolyte and cell material is the biggest obstacle to the operando THz application in the presence of liquid electrolyte. Currently, operando implementation of THz for OMIECs is practically achievable using a THz transparent electrochemical cell.[237]

1   4.3 Raman Spectroscopy

2   Raman spectroscopy determines molecular vibrational modes and is well-suited for operando

3   OMIEC characterization. By decoupling different components through exciting wavelength

4   choice and multiple peak fitting, the technique provides insight into the relative neutral/charge

5   subpopulations, including polaron and charge transfer character, and their distributions across

6   different microstructural environments. This is important due to the sensitivity of relative charge

7   populations to electrochemical potential and local chemical environment which can be radically

8   different between ex situ and operando settings. The sensitivity of Raman spectroscopy to

9   changes in molecular polarization differentiate it from traditional IR spectroscopy, which

10   captures the dipole moment variation. Because of the different selection rules, Raman

11   spectroscopy provides information on π-conjugated bonds that can be easily polarized, and even

12   side chain vibrations that are in the dense fingerprint region of IR spectroscopy. The insensitivity

13   to water between 1000-2000 cm^{-1} (where the C=C and C=O stretching peaks are located) makes

14   the technique helpful in the study of OMIEC materials that require operation in aqueous

15   electrolytes.[238, 239]

16   Despite some simple strategies to assign Raman peaks in simple molecules, the interpretation of

17   Raman spectra in complex conjugated polymers requires the support of DFT calculations, which

18   give the corresponding Raman spectral lines for the individual canonical vibrational modes of a

19   particular molecule. For highly conjugated OMIEC molecules, a small number of vibrational

20   peaks located in the 1300 cm^{-1} - 1600 cm^{-1}, which correspond to the C-C and C=C bond

21   stretching on conjugated backbone, are of significant interest in Raman spectroscopy.[138, 240-242]

22   These peak centers shift with the bond force constant related to excitation wavelength, electronic

23   density, and effective conjugation length. Due to their computational cost, most DFT

24   calculations are performed on isolated oligomers; the surrounding environment is only indirectly

25   accounted for by mean field models (see also **Section 10**).[146, 243, 244]

26   Operando Resonance Raman spectroscopy exploits the intensity enhancement generated when

27   the wavelength of the incident laser pump corresponds to an electronic transition of the material.

28   When applied to OMIECs, the technique provide insight on the aggregation and charge state as a

29   function of external potential. While OMIEC materials are often semicrystalline and a contain

significant disordered fraction, information on the charging state within the disordered domain is difficult to ascertain. However, by choosing a Raman excitation wavelength consistent with different electron transition energies obtained from UV-Vis-NIR spectroelectrochemistry, the electrons will be pumped to a real excited electronic state instead of a virtual state. As the resonant scattering intensity is much stronger than the non-resonant scattering, selectivity is obtained between different domains with different intrinsic transition wavelengths.[245] Multiple sets of vibrational mode peaks at varied excitation wavelengths will have different ratios and peak shapes, which reflect the molecular ordering and configuration of different domains. Specifically, neutral and charged species in ordered and disordered domains can be separately deconvoluted. In electrochemical steady state, the ability of resonance Raman spectroscopy to simultaneously discriminate between different charged species and crystalline/amorphous domains is exploited to the maximum extent.[246]

Currently, the electrochemical doping characterization of OMIEC materials using in situ/operando Raman techniques has been reported.[138, 139, 141, 142, 147] In situ/operando Raman cell design requires one light-transmitting window and the requisite electrical connections, and the device geometry under study determines whether the material is coated on a conductive or insulating substrate. As shown in **Figure 6a**, the laser beam passing through the substrate (or electrolyte for inverse setup) is carefully focused on the polymer film, and the back scattered light is collected by an objective lens to the detector. The technique has also been employed to track the molecular ordering during a thermal annealing process,[247, 248] and to monitor the charged species during $FeCl_3$ vapor doping.[139, 249]
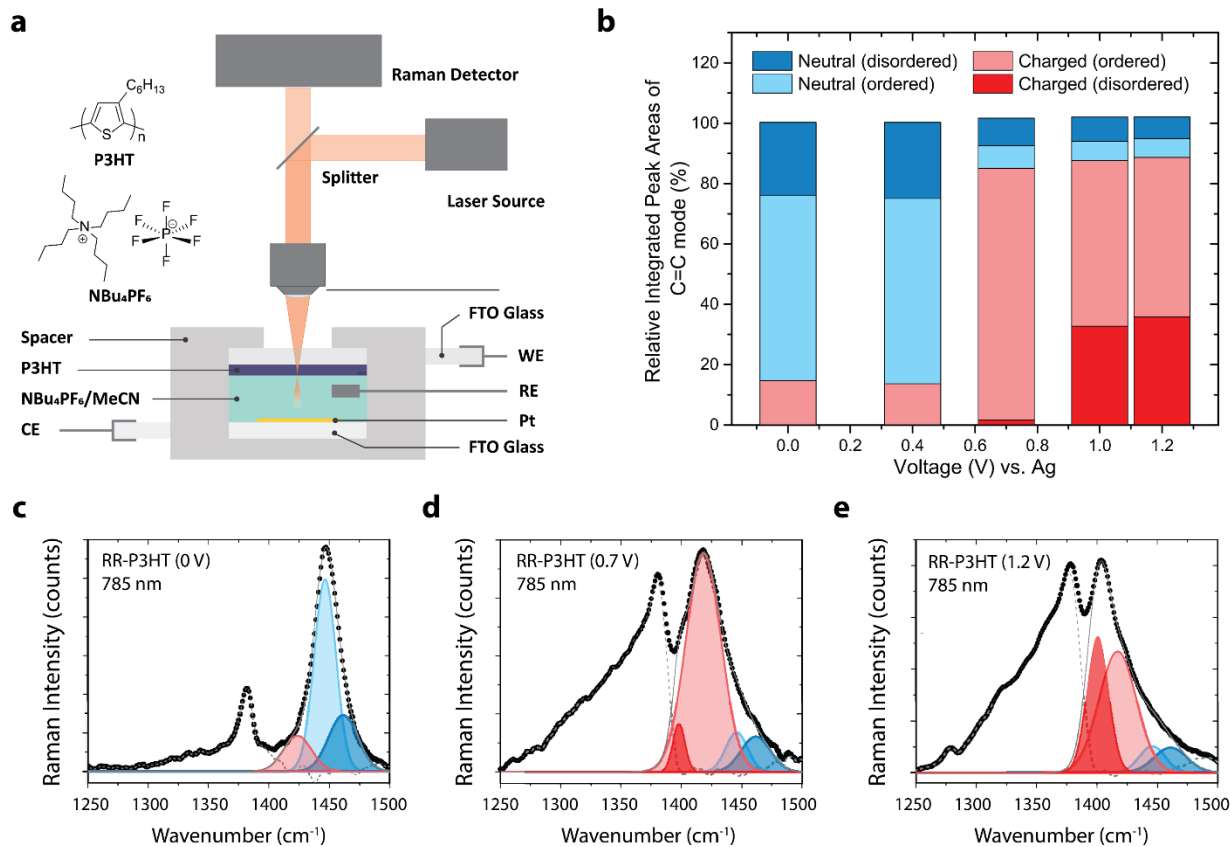
Figure 6 (a) A typical operando Raman cell in which the sample is held upside down on the electrolyte. Note that setups employing an electrolyte on top of the sample are also available. Reproduced with permission from [143]. Copyright 2018 American Chemical Society. (b) Voltage dependent relative integrated peak areas of C=C mode (%) for neat RR-P3HT. Representative Raman spectrum of RR-P3HT under 785 nm excitation during (c) 0 , (d) 0.7 , and (e) 1.2 V applied with Gaussian fits. In situ/operando Raman delineated potential dependent charge fraction across ordered and disordered domains: neutral disordered phase (dark blue, centered at 1462 cm^{-1}), neutral ordered phase (light blue, centered at 1446 cm^{-1}), charged ordered phase (light red, centered at 1425 cm^{-1}) and charged disordered phase (dark red, centered at 1405 cm^{-1}). (b)-(e) are adapted with permission from [143]. Copyright 2018 American Chemical Society.

A prime example of the power of Raman techniques is reported by Nightingale et al.,[143] the conformational changes and molecular ordering of regioregular (RR) P3HT were tracked in situ with resonance Raman spectroscopy during electrochemical biasing. 488 and 785 nm lasers were

selected to resonantly excite neutral and charged species, respectively. In situ Raman spectroscopy of fully amorphous regiorandom (RRa) P3HT was measured to obtain the peak position representing amorphous phase, which is difficult to attain by ab initio calculations directly. The charge distribution across ordered and disordered domains by electrochemical doping from the thiophene ring C=C stretching peak is shown in **Figure 6c-e**. With increasing oxidation voltage, direct spectroscopic evidence clearly reveals the transition from mostly neutral semicrystalline films with excess charge in the ordered phase, to an intermediate charged state where most charge resides in the ordered phase, and finally to a highly oxidized state with significant charge in the disordered phase, as shown in **Figure 6b**. This series of changes is manifested in the Raman spectrum as an overall redshift of the thiophene ring C=C vibrational peak with increasing oxidation voltage. Similar in situ Raman spectroscopic tracing of potential dependent hole concentration in blends of P3HT and solid state ionic liquids was reported by Stewart et al.[144]

The first operando Raman measurements in a n-type OMIEC material were performed by Ohayon et al. to reveal the redox reaction of NDI-T2 during glucose sensing and prove the existence of an interface between the glucose oxidase and the polymer.[147] The voltage dependent Raman spectra of NDI-T2 were measured and compared with the Raman spectrum during glucose sensing. With increasing external potential over 0.7 V vs Ag/AgCl, the spectra showed the successful electrochemical doping of both NDI and T2 units. Upon adding both glucose and glucose oxidase at 0.7 V, the spectra revealed an efficient electronic communication between the enzyme active site and the NDI unit of the conjugated copolymer. It is worth noting that this mechanism could not be assessed with ex situ experiments, but required a contacting liquid electrolyte and applied electrochemical potential.
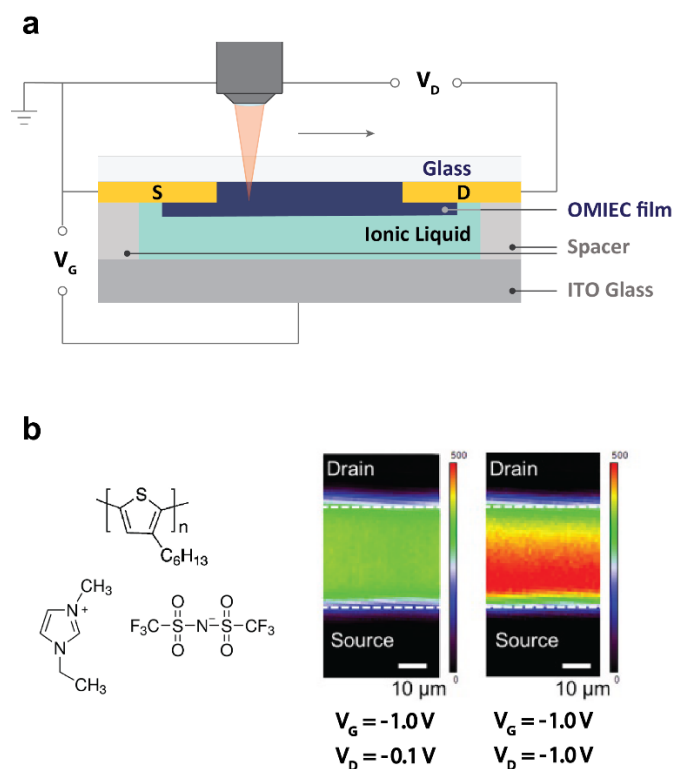
Figure 7 (a) A typical operando Raman cell for mapping polaron concentration in a transistor channel. Reproduced with permission from [140]. Copyright 2018 Elsevier. (b) Raman images of the channel region of a transistor at $V_G = -1.0$ V with excitation wavelength of 785 nm. The channel material is P3HT and the electrolyte is [EMIM][TFSI]. Adapted with permission from [140]. Copyright 2018 Elsevier.

Steady state characterization of devices made of OMIEC materials in operating condition is an important topic in operando experiments. For example, in OECTs the Raman mapping of polaronic vibrations across the channel have visualized the carrier distribution within the channels of working transistors with submicron resolution, shown in **Figure 7**.[140, 146] While these works focused on ionic liquid gated transistors, such spatial charge density mapping is applicable to other thin film OMIEC based devices. Due to the long times needed for Raman mapping, electrolyte choice and cell design should avoid electrolyte solvent evaporation and maintain a stable focal plane. The non-uniform voltage drop across the OMIEC channel may complicate the application of Raman mapping to devices. Another example is the implementation of resonant Raman characterization of OECTs in biomolecular sensing to measure the presence of glucose

from changes in the PEDOT:PSS Raman spectra.[145] A strength of operando Raman is that the technique gives unique spectral features for particular electroactive species, providing insights beyond the current-voltage measurement.[145]

To apply Raman spectroscopy to operando characterization for time-resolved kinetic studies of OMIEC materials, several issues must be addressed. First, as many OMIEC materials are implemented in the aqueous environments, evolved gases from additional electrochemical reactions or solvent volatilization can change the focal plane of the laser beam, thus affecting the stability of the signal. This problem could be solved by using a cover glass and requiring glass corrected lenses that adjusted for the change in refractive index change. Second, the inelastic scattering signal in Raman spectroscopy is weak, which makes it difficult to shorten the integration time and collect the signal that can be effectively fitted. Further, for resonant Raman spectroscopy, there is strong molecular florescence background under certain wavelengths, which adds to the baseline of the Raman spectrum further reducing the signal-to-noise ratio.[250] Increasing the integration time or beam intensity raises the risk of beam damage to the OMIEC sample of interest.

In spite of these hurdles, sub-second time-resolved operando Raman spectroscopy should be achievable, and has the potential to provide important kinetic information. The separate OMIEC backbone and side chain kinetics during operation can be obtained by tracing their corresponding vibrational modes. The kinetics of potential dependent charge distribution and structural changes in different domains should likewise be accessible as well. Finally, the dearth of commercially available laser wavelengths (which limits the specificity of excitable OMIEC resonance transitions) can be overcome with differential frequency generation (DFG) which occurs in nonlinear crystal materials, but an optical parametric amplifier (OPA) and ultra-fast laser source are required.[251] On the whole, Raman is an excellent tool for steady state operando characterization, and holds great promise for time-resolved studies of OMIEC systems.

5. Magnetic Resonance

Magnetic resonance techniques include electron paramagnetic resonance (EPR) and nuclear magnetic resonance (NMR), distinguished by the subatomic particles they probe. EPR has been applied to the in situ and operando detection of OMIEC materials as a method to directly detect

electron spins, which is described in **Section 5.1**. NMR has recently been reported to be applied to OMIEC materials[252] but has not yet been widely applied due to challenges in experimental implementation. In **5.2**, we will focus on the information that in situ/operando NMR has the potential to bring to the field. A brief technical comparison information is presented in **Table 2**.

Table 2. Summary of magnetic techniques employed in operando study of OMIECs.

Method	Description	Electronic carrier Information	Ionic carrier Information	Structural & Morphology Information	Representative operando/ in situ example	Implementation barriers
ESR	Measure the paramagnetism of single electrons	Concentration, spin state	-	-	PEDOT:PSS[25,3-255] PPy[256] pBTTT[257]	Sensitive to oxygen/radical
NMR	Measure the chemical shifts of targeted element nucleus	-	Diffusivity, type/ concentration, coordination	Coordination, chemical structure, local packing	PEDOT:PSS[25,2]	Weak signal, requires thick sample

5.1 Electron Paramagnetic Resonance

In situ/operando Electron Paramagnetic Resonance (EPR, or electron spin resonance, ESR, setup in **Figure 8a**) detects the paramagnetism of single electrons (or electronic doublet states). This enables the direct probing of potential dependent polaron/bipolaron population as a compliment to the spectroscopic evidence, and thus has found extensive use in CP and OMIEC materials. EPR samples are very sensitive to the local environment, thereby provide information about the molecular structure in the vicinity of unpaired electrons. Briefly, the energy level of a single electron splits under the magnetic field, and the incident microwave can be resonantly absorbed when its energy matches the Zeeman splitting. In the conventional interpretation (shown in **Figure 8b**), the electrons of a bipolaron are perfectly paired (S=0, singlet), while the polaron has a strong signal in the EPR due to the presence of a single electron (S=1/2, doublet). Recently, calculations by Zozoulenko et al. have supplied a new interpretation of the bipolaronic signal,[160] shown in **Figure 8c**. The +2 valence bipolaron is in triplet state with EPR signal, and the higher valence (+4, +6…) bipolaron presents the same singlet state as the conventional theory without EPR signal.
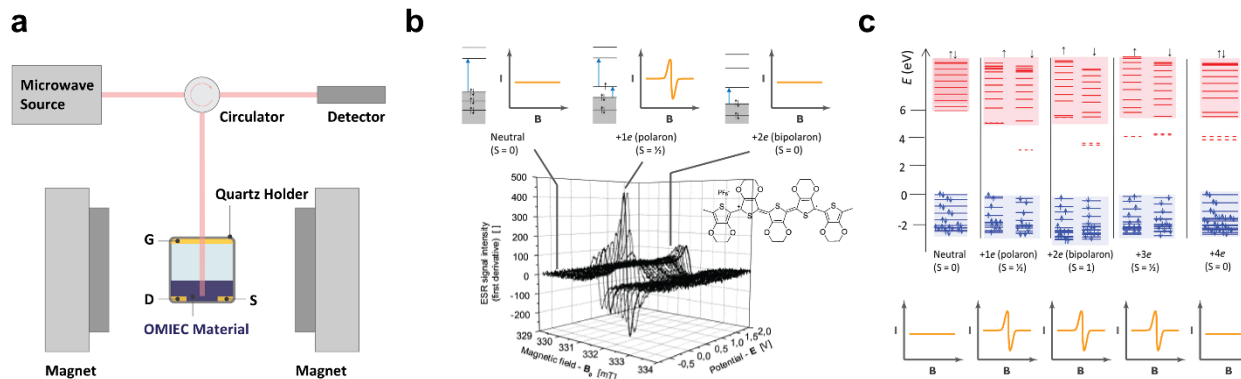
Figure 8 (a) In situ/operando EPR setup. (b) In situ EPR for PEDOT electrochemical doping in NaCl electrolyte illustrating the transition from neutral species to polaron and then to bipolaron. Reproduced with permission from [254]. Copyright 2005 Elsevier. (c) New interpretation of in situ EPR results after the introduction of highly charged polaritons. Adapted with permission from [160]. Copyright 2019 American Chemical Society.

Similar to the case of IR absorption spectroscopy, most in situ/operando experiments on conjugated polymers are currently performed at steady state in acetonitrile[253-256] or ionic liquids;[257] currently no time-resolved operando EPR experiments have been reported. For different polythiophenes, the paramagnetic signal of EPR first increases and then decreases with increasing oxidation voltage, implying that the paramagnetic polaron is generated at lower oxidation voltages and subsequently transforms to the non-magnetic bipolaron. The obtained EPR spectra can be fitted by a weighted combination of Gaussian and Lorentzian peaks after deconvolution, where the Gaussian term represents the defects fixed on the polymer backbone and the radicals trapped at the chain ends, and the Lorentzian term represents the polarons after doping.[254] A competing and more prevailing explanation is that the Gaussian term represents the paramagnetic polaron in the crystalline phase of the polymer, while the Lorentzian term represents the paramagnetic polaron in the amorphous phase, which arises at higher oxidation potentials.[255, 258] A recent report also studies the relationship between the electron spin relaxation and polymer structure in conjugated polymers.[259] EPR spectra combined with DFT calculations found that conjugated polymers with near-planar backbone conformation and high crystallinity were characterized by long spin relaxation times at room temperature.

Both in situ and operando EPR measurements are complicated in aqueous environments, as electrolyte side reactions can produce oxygen-containing radicals or paramagnetic oxygen molecules. Currently, studies of the electrochemical oxidation of PEDOT in aqueous solutions have been reported, in which the researchers used a strongly acidic electrolyte (H_2SO_4, pH = 0.3) to suppress the side reactions.[260] The authors compared the relative concentration changes of polarons and bipolarons extracted in EPR with the conductivity measured at different voltages, demonstrating that bipolarons are also carriers in OMIEC materials. All these studies lay the foundation for future time-resolved operando EPR spectroscopy of OMIEC materials in various working environments.

5.2 Nuclear Magnetic Resonance

By measuring the chemical shifts of targeted element, Nuclear Magnetic Resonance (NMR) gives crucial molecular and ionic information in OMIEC materials, including their population, environment, and dynamics, as displayed in **Figure 9a**. The technique has been implemented in operando OMIEC characterization recently[252] and its implementation is the subject of further development. While NMR is most often used to confirm the chemical structure of molecules in solution, most pertinent to OMIECs is solid-state NMR (ssNMR), which mainly provides information on atomic/ionic chemical environment and composition. Chemical shifts reveal the electron cloud density at the periphery of the atom, thus effectively distinguishing atoms of the same element that are in different chemical environments. The integration of different peaks in an NMR spectrum directly provides the ratio of these atoms and gives compositional information. Using conventional 1D and 2D H-1/C-13 ssNMR techniques, the amorphous phase composition, crystal stacking structures and molecular doping level of CP semiconductors have been well characterized.[261] Probing other elements can effectively open NMR for fruitful operando studies, by quantifying the ionic/molecular environment, population, and dynamics in OMIEC operation, as illustrated below.

As a technique sensitive to different chemical bonds, ssNMR is helpful to track chemical reactions and quantify the population of molecular/ionic species involved. For instance, the degradation of lithium battery materials has been studied by tracing lithium-containing small molecules[262, 263] and oligomers[264] in the solid electrolyte interphase. Similar OMIEC stability

experiments should be possible, offering the possibility to directly identify degradation products. In addition, ssNMR has been used to confirm the carbonyl lithiation of polymers in organic lithium-ion battery electrodes.[265, 266] When the doping cation is the proton, ssNMR can directly measure the degree of protonation and its binding sites in different CP materials,[267] which when extended to OMIECs should further elucidate proton conduction in acidic conditions. Extending ssNMR to other commonly used elements (H, C, F), the technique is one of the few methods for identifying specific species and local ion coordination in conjugated polymers without needing known calibration standards for comparison.

Operando NMR has already been carried out in polymer electrolyte systems analogous to OMIECs. In Li-7 ssNMR studies of lithium salts dissolved in poly(ethylene oxide) (PEO) show a sharp peak at -1.3 ppm,[268] which corresponds to the fast transport of lithium ions resulting from the segmental motion of PEO chains shown in **Figure 9c**.[269, 270] The narrow, sharp peak can be clearly discriminated from other Li ion peaks, such as static Li^+ in close proximity to PEO chains[268] or crystalline Li salts.[270] Despite the weaker signal intensity of Na comparing to Li,[271] ssNMR studies of Na^+ have been successful and exhibit similar results.[272] ssNMR has also been used to differentiate ions absorbed on carbon nanotubes and free ions, based on the strong chemical shift affected by the aromatic ring current.[273] In OMIEC materials, this can be used to differentiate the ions present adjacent to the conjugated backbone from those on the sides. Distinguishing elements from different environments allows one to track the transport of these elements in OMIECs. Jin et al has reported operando NMR in electrolyte gated PEDOT:PSS (setup shown in **Figure 9b**) and reveal the ion/solvent injection/extraction during electrochemical cycling.[252] Using PSS-Na as well as aqueous NaCl solutions as standards, Na^+ in PEDOT:PSS in PEDOT-rich domains and PSS-rich domains were identified separately by Na-23 NMR. Through H-NMR shown in **Figure 9d**, the free water molecules present in the electrolyte can be distinguished from the water molecules bound to the polymer. By integrating the NMR signals of these molecules/ions in different environments, ion transport and distribution can be obtained.

In addition, operando NMR is able to track ionic transport dynamics. The diffusion coefficients of different ions can be extracted from the intensity decay of NMR echo signal,[274, 275] and thus allows for calculation of the transference numbers of anions and cations.[276, 277] Operando pulsed-
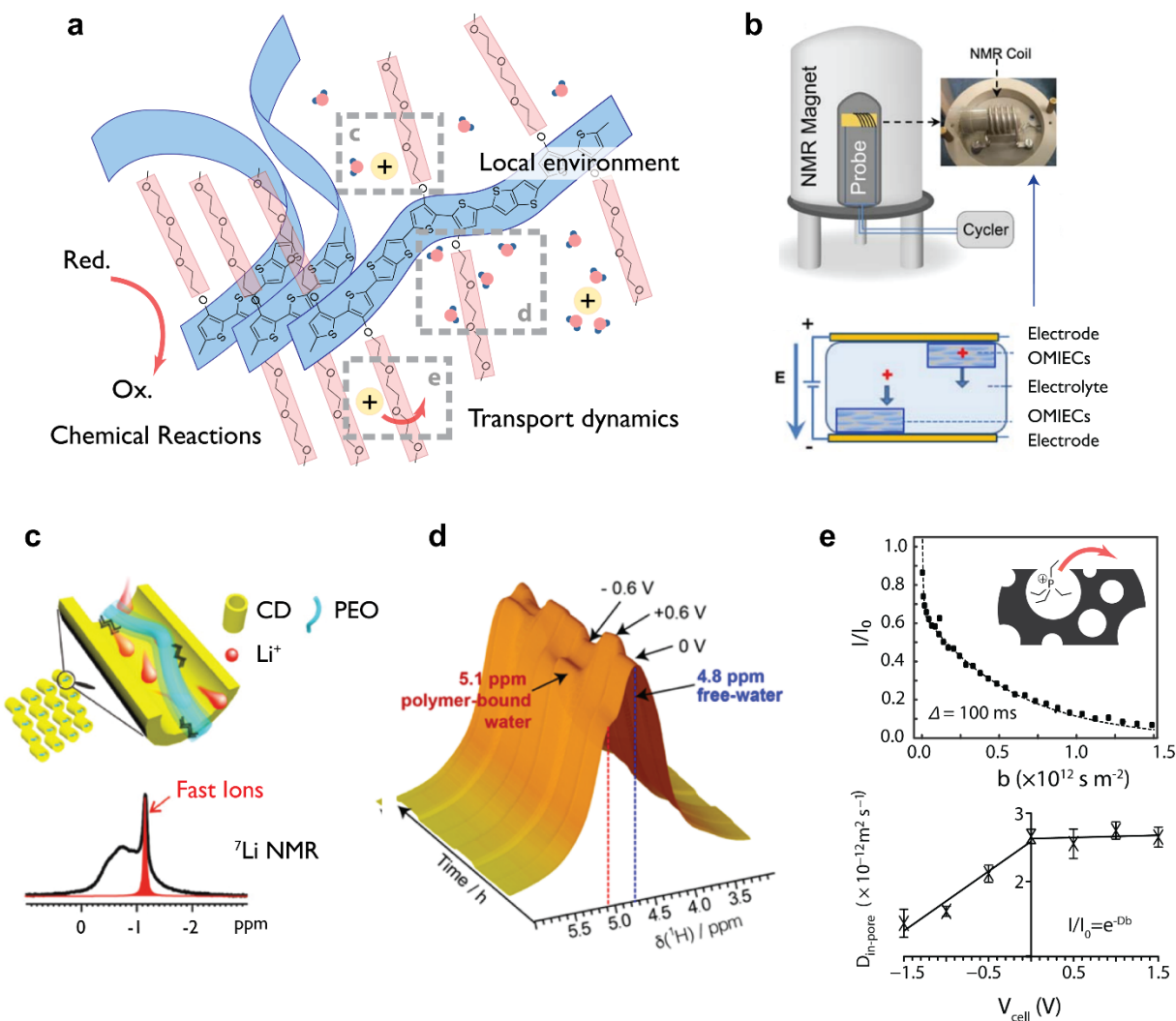
field gradient NMR (PFG-NMR), based on the displacement of ions in the length range of 10-100 μm, has been used for the direct observation of ion dynamics in supercapacitor electrodes,[278] as shown in **Figure 9e**. This technique shows a temporal resolution of milliseconds, which is sufficient for application in the study of ion diffusion and interaction in CP semiconductors.[279] By changing the magnetic field gradient, the diffusion coefficient D is readily fitted from the curve between normalized NMR peak intensity $\frac{I}{I_0}$ and b factor, shown in Equation 2:

$$\frac{I}{I_0} = e^{-Db} \quad (2)$$

Where b factor is a function related to the strength magnetic field gradient, the measured nuclei and the pulse pattern, defined by Equation 3:

$$b = g^2(\gamma 2\delta)^2(\Delta - \delta/6 - \tau/2) \quad (3)$$

Here, g is the strength of the magnetic field gradient, γ is the nucleus gyromagnetic ratio, δ is the duration of an individual magnetic field gradient pulse. Δ is the observation time, and τ is the delay time between pulses.[278] As for now, in situ PFG-NMR has been already reported to determine self-diffusion coefficient of Na^+ in PEDOT:PSS films (no external potential) and is consistent with previous results measured by moving front experiments.[252]

Figure 9 (a) In situ/operando NMR shows the potential for revealing ion/molecule local environment, chemical reactions, and transport dynamics; the chemical structure of a glycolated thiophene-based OMIEC is shown as a representative example with the dashed grey boxes referring to ion coordination, hydration, and transport properties elaborated on in other panels. (b) Operando NMR setup for OMIECs; Adapted from [252] under CC BY 4.0 license. (c) In situ ssNMR determines cation coordinating with glycol chain and its transport rate in Li salt and PEO blends; Reproduced with permission from [268]. Copyright 2020 American Chemical Society. (d) Operando NMR differentiates the free water in electrolyte and the bound water in PEDOT:PSS and tracks the solvent uptake kinetics; Adapted from [252] under CC BY 4.0 license. (e) PFG-

NMR gives diffusion coefficient of ions in graphene. Reproduced with permission from [278].
Copyright 2017 Springer Nature.

To conclude **Section 5**, operando ssNMR demonstrates the potential to distinguish ionic environments and chemically-bound species in OMIECs, as well as to determine ionic dynamics. Despite the widespread coverage of operando ssNMR experiments in recent years, most ssNMR instruments still require anhydrous and low-conductivity powder materials for the measurements that need to be rotated at the magic angle. Also, comparing to the C and H atoms, other elements present hurdles to high quality ssNMR signal with high time resolution, especially for quadrupole atoms (such as Na-23 and K-39). To obtain high quality NMR signals requires bulk polymers, which makes the application of this technique on thin film geometry difficult. The demand for bulk materials also limit operando NMR to materials that have already been commercialized (e.g. PEDOT:PSS), while less accessible to new synthetic exploration.

6. X-ray and Neutron Techniques

X-ray and neutron-based techniques can be divided mainly into absorption and scattering methods. In contrast to the previously discussed optical absorption, which probes molecular vibrations and valence electronic states, X-ray absorption probes the core electronic energy levels of atoms and has a strong elemental specificity, thus allowing for characterization of the chemical composition and atomic/ionic environment of OMIEC materials. X-ray absorption spectroscopy is not currently applied in operando characterization and will be discussed in **6.1** and **6.2** for X-ray absorption and X-ray photoelectron spectroscopy, respectively. Both X-ray scattering and neutron scattering techniques give similar structural information, however they are sensitive to different scattering sources: while X-ray scattering is sensitive to electronic density, neutron scattering probes atomic nuclei. Depending on the collection angle of the X-ray scattering, X-ray scattering techniques are further divided into small-angle X-ray scattering (SAXS) and wide-angle X-ray scattering (WAXS), as described in **6.3**. Small-angle X-ray scattering targets structural information at larger length scales, such as the contrast of different phases in a thin film and the size of domains. WAXS in OMIECs, often carried out in a grazing incidence, gives information about intermolecular packing. Neutron-related techniques will be described in **6.4** and include small angle neutron scattering (SANS), quasi-elastic neutron

1   scattering (QENS) and neutron reflectometry (NR). The information that can be obtained from

2   these techniques is compared in **Table 3**.

3   **Table 3**. Summary of X-ray and neutron techniques employed in operando study of OMIECs.

Method	Description	Electronic carrier Information	Ionic carrier Information	Structural & Morphology Information	Representative operando/ in situ example(s)	Implementation barriers
XRF	Measure elemental specific X-ray florescence	-	Type/ concentration	-	CP/metal composites[280-282]	Background signal from electrolyte
XAFS	Measure the absorption edge of specific elemental electronic transitions	-	Environment, coordination	-	CP/metal composites[280-282]	Low time resolution
XPS	Measure the number and kinetic energy of emitted photoelectrons from X-ray excitation	-	Type/ concentration, vertical distribution	-	PS[283]	Limited to surface, mostly in vacuo
WAXS	Measure the X-ray scattering pattern at wide scattering angles (q between 0.1 Å^{-1} - 3 Å^{-1})	-	-	Crystalline packing, disorder	P3HT[165, 284] PEDOT:PSS[122] Pg2T-TT[33] PB2T-TEG[285]	Electrolyte scattering
SAXS	Measure the X-ray scattering pattern at small scattering angles (q between 0.005 Å^{-1} - 0.2 Å^{-1})	-	-	Meso-scale domain size and purity, phase separation	PBDTTT-C-T[286]	-
XPCS	Measure temporally coherent fluctuations of scattered spots	-	Mobility	Meso-scale domain, phase separation, aggregation/ packing	Li/PEO[287]	Extent of coherence
SANS	Measure the elastic neutron scattering at small scattering angles	-	-	Meso-scale domain, phase separation	P3HT[288]	Long integration time

QENS	Measure quasi-elastic neutron scattering	-	Molecular dynamics	Segmental dynamics	-	Instruments not widely available
NR	Measure neutron reflectivity	-	Chemical composition	Thickness, surface roughness	PEDOT:PSS[2] [89]	Long integration time

6.1 X-ray absorption

X-ray absorption spectroscopy (XAS) techniques have the potential to be performed in operando OMIEC characterization of elemental composition and environment.[290, 291] XAS can be divided into X-ray absorption/fluorescence spectroscopy and X-ray absorption edge techniques. The former monitors selective X-ray absorption through the transition of the inner shell electrons and distinguishes different elements within the sample. The latter scans the energy near the X-ray absorption edge of a particular element to obtain inter-atomic distances and coordination. The region from the pre-edge to tens of eV above the edge is commonly referred to the near-edge X-ray absorption fine structure (NEXAFS) or X-ray absorption near-edge structure (XANES). Experiments that probe wider energy regions up to 1000 eV above edge energy, are named as extended X-ray absorption fine structure (EXAFS).[292] The oscillation of the X-ray absorption above the absorption edge originates from the interference between the wave function of photoelectrons and the backscattering of nearby atoms.[293, 294]

6.1.1 X-ray Fluorescence

The analysis of the elemental composition of soft matter interfaces by X-ray fluorescence (XRF) has been widely reported,[295] and is possible to be applied in operando OMIEC compositional characterization. To avoid the influence of the bulk solution on the analysis, experiments are often performed with a grazing incidence setup. In multilayer polymer films[296] and lipid layers,[297] the absolute ion concentration as well as its vertical distribution has been determined by varying the grazing incidence angle of X-rays. The need to vary the incident angle implies a longer total measurement time such that depth profiling with XRF is not suitable for time-resolved kinetic studies. To fix the incidence angle less than the X-ray critical angle of the substrate (bulk water or solid substrate), total reflection X-ray fluorescence (TRXF) sacrifices

spatial resolution in order to gain a shorter measurement time.[298, 299] The solvent exchange kinetics of chloroform-loaded metal organic framework films in contact with water has been studied by tracking Cl Kα line in TRXF.[300] When compressing the film by applying external pressure, the Cl fluorescence decreases significantly with the increasing surface pressure. The above-mentioned system successfully differentiated the same element (Cl) in solvent background and thin layer materials, which is the key problem to overcome in operando OMIEC compositional characterization. This similarity suggests it may be possible to apply operando TRXF to track the ion composition in OMIEC thin films and allow for non-destructive, real-time readout.

6.1.2 XANES and EXAFS

XANES and EXAFS spectra are obtained by measuring X-ray absorption and fluorescence while the incident X-ray energy is scanned across the absorption edge of peaks of specific elemental electronic transitions. While attractive for operando characterization of OMIEC materials, these techniques have yet to be applied. Instead of time-resolved study, the long single measurement times makes these techniques preferable for steady-state characterization. XANES analysis, which focuses on the near edge features, usually requires the measured energy edge of standard samples and fine control of incident X-ray energy. In the study of CP films, incident angle dependent XANES is generally used to target the C K-edge to distinguish different components and determine the packing direction[301-304] as well as fine grained microstructure in the film.[178, 305, 306] In addition, a high energy resolution XANES library has been established for commonly used conjugated polymers.[307] Recently, in situ XANES on the S K-edge has been employed on the interconversion of lithium-sulfur compounds during the charging and discharging of lithium-sulfur batteries.[308, 309] EXAFS, which measures the interference patterns above the edge is Fourier transformed to give the coordination around the target atom with the average distance to neighboring atoms. The technique has been applied to study the coordination of ions in PEO by measuring the K-edge of metal ions,[310, 311] and provides useful information about the local structure of the amorphous region.[312] For XANES and EXAFS to achieve an in situ ion environment measurement, the influence of background ions in the electrolyte must be overcome. Initial work with metal/CP composite in situ XAS is promising.[280-282] Carried out in transmission, minimizing the thickness of the contacting electrolyte layer may be sufficient, but

1   in the grazing configuration different approaches will need to be developed. It is expected that

2   operando XANES and EXAFS will give ion environment/coordination information in OMIECs

3   if we choose proper doping ions with sensitive X-ray absorption edges. Compared to operando

4   NMR that require thick films or bulk samples, XAS is not limited by the sample geometry and is

5   well suitable for thin film OMIECs.

6   6.2 X-ray Photoelectron Spectroscopy

7   X-ray photoelectron spectroscopy (XPS) is an important elemental analysis tool that can

8   quantitatively differentiate the content of different elements in a sample and distinguish different

9   valence states of the same element. Based on the photoelectric effect, the system detects the

10   number and kinetic energy of emitted photoelectrons arising from X-ray excitation of the atoms

11   on the sample surface. Similar to X-ray fluorescence, XPS is a potential option for revealing the

12   chemical composition of OMIEC materials with voltage applied. In addition, the ability of ion

13   milling/etching allows us to obtain information on the composition of depth profile at the same

14   location of the sample during the measurement. This technique should be applicable to operando

15   experiments of solid-state OMIEC devices that can be operated in high vacuum. However,

16   OMIEC devices that are interfaced with or immersed in electrolyte are likely incompatible with

17   depth profiling XPS.

18
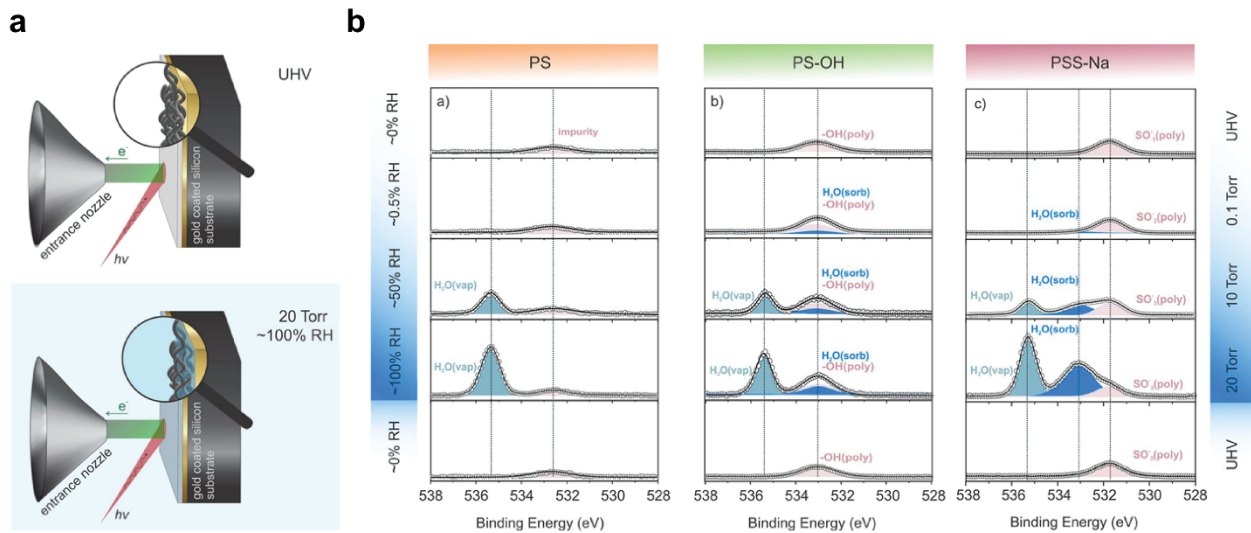
Figure 10 (a) Schematization of the polyelectrolyte hydration probing by in situ APXPS. (b) O 1s spectra of PS, PS-OH and PSS-Na as a function of relative humidity (RH) at room temperature. Intensities are normalized to the O 1s peak from the polymer. The O 1s component from the functional group of the polymer in the surface region is shown in pink, while the absorbed water contribution is shown in blue. Adapted with permission from [283]. Copyright 2020 American Chemical Society.

The biggest obstacle to applying XPS to operando experiments is the vacuum measurement condition due to the small attenuation length of soft X-ray in air. Most in situ experiments with OMIECs have not involved liquid electrolytes, instead monitoring aging in air,[313] or thermal annealing.[314] Recently, in situ XPS studies of water sorption of different chemical modified polystyrene (PS) films has been reported by Gokturk et al.[283] The technique shown in **Figure 10a**, named ambient pressure XPS (APXPS), was performed at pressures below 5 Torr and allowed for the presence of water vapor. To achieve the non-vacuum condition, intense tender X-ray (energy between 1.0 and 5.0 keV) supplied a from synchrotron light source were required. When the sample is cooled below room temperature, 100% relative humidity (RH) can be reached in the chamber. Through the study of three different PS films (PS, PS-OH, and PSSNa), the authors succeeded in distinguishing different oxygens atoms of water and the polymer itself, shown in **Figure 10b**. The water volume adsorbed in the three films as well as stoichiometric ratios of different elements were adequately quantified by fitted peak area and the corresponding photoionization cross sections.

The ability to test from 0% to 100% RH would not only enable XPS studies of vapor swelling in OMIEC materials, but lays the foundation for XPS in the presence of liquid electrolytes. Ideally, operando XPS characterization of OMIECs requires the material being electrochemically biased. Currently, operando APXPS has successfully achieved the characterization of electrochemical oxidation on inorganic electrodes,[315, 316] which implies the feasibility of this technique for application in voltage-dependent CP and OMIEC compositional characterization, especially in cases with solid state and moderately hydrated OMIEC-based devices.

APXPS may be an attractive technical route to operando XPS implementation of OMIEC materials, but there are still some major challenges to overcome. The signal of XPS, although it

can be analyzed quantitatively, is less sensitive compared to the XRF.[317] It is necessary to use a long integration time and integrate multiple times for one element in XPS. In the APXPS experiment mentioned above, the beam was irradiated for 10-15 seconds. Spectra at different positions were summed to improve the signal-to-noise ratio.[283] In addition, condensed matter cannot block the optical path of X-ray beam and emitted photon electrons in XPS, thus requiring the absence of electrolyte above OMIEC film and special design of operando cells. Using ionic liquids (ILs) in replacement of aqueous electrolytes will facilitate XPS measurements due to the low vapor pressure of ILs, and in situ XPS analysis of chemical/electrochemical reactions at IL surface have been reported.[318-320] Lastly, APXPS is not a widespread technology and relies on synchrotron light sources. At present, most benchtop XPS still need to be performed in vacuum. Operando XPS on benchtop is challenging and require a specialized cell with a beam path of few hundred nanometers. Similarly, ultraviolet photoelectron spectroscopy has been employed in ambient to probe the ionization potential of conjugated polymers in situ during electrochemical doping.[321]

6.3 X-ray scattering

X-ray scattering/diffraction techniques are a powerful tool for the characterization of OMIECs. Across the broader fields of organic electronics and polymeric ion conductors, scattering techniques have revealed intermolecular spacings, crystallite size, paracrystallinity, phase separation, domain size/shape/spacing, domain purity, etc[28, 322, 323] at the sub-nm to 100 nm scale. This has facilitated the establishment of structure-property relationships that have driven materials advances. Similarly, X-ray scattering techniques are a straightforward route to improve morphological understanding and establish structure-property design rules in OMIECs.

Undergirding X-ray scattering techniques is a relationship between the scattered X-ray wave vector and characteristic length scales of electron density heterogeneity (intermolecular and/or domain). The instrumental geometry and sample preparation of X-ray scattering techniques show a great diversity. X-ray scattering of OMIEC materials is usually performed in synchrotron with semicrystalline film samples, while X-ray Diffraction (XRD) experiments performed on benchtop require single crystals or powders. X-ray incidence modes tend towards grazing or transmission, and the signal collection ranges from ultra-small to wide angles.

1   Currently, ex situ, in situ, and operando X-ray scattering experiments have been applied to

2   OMIEC materials. Most of the in situ studies have focused on the formation and post-processing

3   of polymeric OMIEC thin films. However, the intermolecular stacking and mesoscale structure

4   of OMIEC material dynamically change during operation and are highly relevant to the electrical

5   properties (ion/hole/electron transport) of the material. Therefore, operando X-ray scattering of

6   OMIECs is primed to provide crucial application related structure-property information and is an

7   indispensable part of the multimodal operando characterization toolbox of OMIEC materials.

8   6.3.1 Wide Angle X-ray Scattering

9   As a widely established technique for molecular packing characterization of conjugated polymer

10   thin films, Wide Angle X-ray Scattering (WAXS) has been performed in operando OMIEC

11   characterization recently. WAXS experiments on OMIEC materials usually apply Grazing

12   Incidence Wide Angle X-ray Scattering (GIWAXS) rather than the transmission mode, because

13   GIWAXS has increased scattering signal (from a larger beam footprint, wave guiding, and

14   scattering events from both the direct and substrate reflected beam) and captures out-of-plane

15   (normal to the sample plane) scattering missing in the transmission mode. The technique focuses

16   on structural information on the periodic repetition within crystalline domains in the range of

17   0.1-5 nm, and the relationship between scattering angle 2θ and interplanar spacing d can be

18   described with Braggs' law (Equation 4): [28]

$$19 \qquad q = \left(\frac{4\pi}{\lambda}\right) sin\theta = \frac{2\pi}{d_{hkl}} \quad (4)$$

20   where q is the scattering vector, λ is the X-ray wavelength and h, k, l are Miller indices for

21   designating planes within a crystal. In the crystalline domain of most OMIECs, polymer chains

22   stack in three dimensions and form lamellar stacks (h00), π stacks (0k0), and backbone repeating

23   structures (00l) that can be identified by their GIWAXS pattern. The coherence length L_c related

24   to the domain size can be calculated from peak width by Scherrer equation (Equation 5):[28]

$$25 \qquad L_c = \frac{2\pi K}{\Delta_q} \quad (5)$$

where K is a shape factor typically from 0.8-1 and Δ_q is the full width at half-maximum (FWHM) of the peak of interest. The pseudo-Voigt mixing parameter η and paracrystallinity g can be extracted from scattering peak shape, and are associated with non-cumulative disorder and cumulative disorder.[324] Since WAXS arises from diffraction in ordered/crystalline domains, it is by definition insensitive to the structure of disordered/amorphous regions. To probe both the crystalline and amorphous domains, WAXS must be combined with complimentary techniques which are sensitive to the amorphous domains (e.g. UV-Vis, Raman, NMR, XPCS, scanning probe, etc).

This structural information as well as the texture information from GIWAXS pattern are often correlated with electronic transport in conjugated polymers. The vast majority of OMIEC studies have been carried out on as cast films or films ex situ processed with electrolyte exposure and/or electrochemical cycling,[82, 186, 285, 325-327] similar to the studies of molecular doping in CPs.[328, 329] While the goal of such ex situ studies is to determine the changes in microstructure and texture following electrolyte exposure and/or electrochemical cycling (doping/dedoping), as discussed previously, such ex situ measurements often fail to mimic application relevant conditions. For example, the structural changes accompanying electrochemical doping/dedoping in OMIEC devices is not guaranteed to persist after the removal from the operating environment due to the absence of continued applied voltages, evaporation of solvent, reactions with ambient, etc. In addition, many parameters, such as diffraction peak intensity and background scattering, complicate quantitative comparisons in diffraction patterns between different exposure sites and samples. Operando GIWAXS enables continuous measurements on the same site in operation relevant conditions with actively applied potentials, thus circumventing the above limitations. Lastly, operando GIWAXS allows direct correlation of structural changes with simultaneously measured electronic properties, and time-resolved scattering patterns can reveal kinetic information on said correlations.

There is a large body of work on the in situ characterization of CP film deposition[38] and post-processing which can be leveraged towards operando GIWAXS studies of OMIECs.[42, 43] In situ studies of vapor annealing of conjugated polymer films present a case that approaches the operating conditions of OMIEC materials.[42, 43] One study traced the lattice swelling in both chloroform (CF) and tetrahydrofuran (THF), demonstrating the applicability of in situ/operando

GIWAXS in different solvent vapors.[42] CP film deposition methods studied by in situ GIWAXS include spin coating,[330, 331] blade coating[332] and slot-die coating.[333] For film deposition, a small amount of solvent remains on the surface of the newly formed film at the initial stage, which is similar to the operando GIWAXS with the presence of liquid electrolyte. These studies capture the changes in coherence lengths as crystallites form and the changes in d-spacing as the film dries, thus identifying different regimes and mechanisms of film formation.[331] With some modifications, these in situ GIWAXS setups can also be used for operando experiments, especially the blade coating setup, creating a rolling drop meniscus cell shown in **Figure 11a,b**.
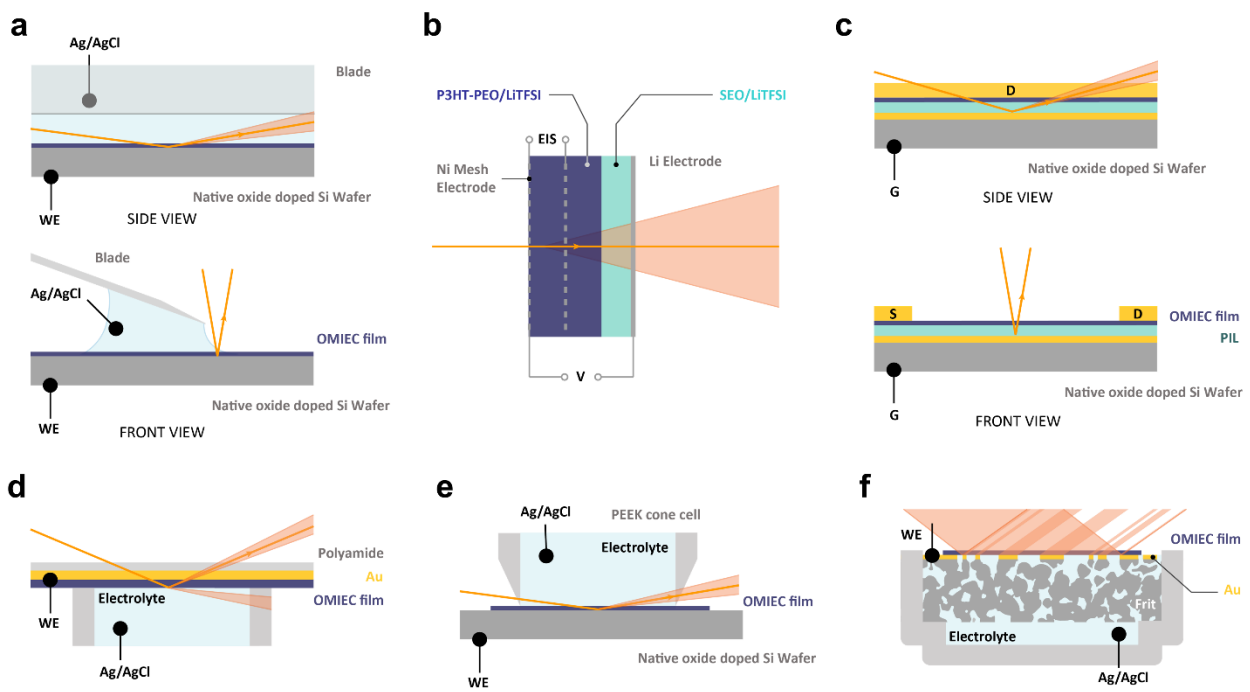
Figure 11 (a) The view perpendicular (top) to and along (bottom) incident X-ray beam of meniscus cell based on blade coating setup. (b) In-situ electrochemical cell for WAXS measurement reported by Thelen et al.. Reproduced with permission from [284]. Copyright 2015 American Chemical Society. (c) The view perpendicular (top) to and along (bottom) incident X-ray beam of operando GIWAXS setup of poly ionic liquid (PIL) device reported by Thomas et al., note that the X-ray beam pass through the thin PIL layer. Reproduced with permission from [165]. Copyright 2018 John Wiley & Sons. (d) The side view of the polyamide cell reported by Bischak et al.. Reproduced with permission from [285]. Copyright 2020 American Chemical

Society. (e) The side view of the cone cell reported by Paulsen et al.; (f) The side view of the frit cell reported by Paulsen et al.;

In recent years, several implementations of operando (GI)WAXS have been reported for solvent-free OMIEC and CP materials. Thelen et al. reported operando transmission WAXS experiments with the Lithium transporting block co-polymer OMIEC material, poly(3-hexylthiophene)-b-poly(ethylene oxide) (P3HT-PEO), in a transmission geometry yielding good resolution of the scattering signal.[284] Expansion of the lamellar spacing and contraction of the π-stacking of P3HT block were observed after electrochemical oxidation, implying the intercalation of anions into the lattice. Ideally, the grazing geometry is preferred for thin film OMIEC materials. An operando GIWAXS analysis of OECT with a P3HT thin film channel cast on polyelectrolyte was carried out to obtain structural information of P3HT under different bias.[165] The incident X-ray beam penetrated the polyelectrolyte layer and was reflected by the gold substrate, as shown in **Figure 11c**. It should be noted that both these experimental setups were solvent free and relevant to solid-state devices of similar arrangement. While relative changes in structure during operation are accessible, solid electrolyte scattering is conflated with OMIEC scattering which could add complication to both data acquisition and analysis of OMIEC-specific information.

Many applications of OMIEC materials are performed in environments with mobile anions, cations, and solvent molecules. In these cases, overcoming scattering from the substrate and/or electrolyte is critical for isolation of OMIEC scattering. One route is to position the X-ray beam on the OMIEC film of interest but well away from the contacting electrolyte, and applying a high voltage to drive the lateral transport of ions into the region of film probed by the X-rays.[334] This approach, however, is limited in the type and quality of data accessible, i.e. lamellar peak changes at large charging voltages (+4V) which may not be relevant in devices. For measurements of thin films immersed in an aqueous environment, Bischak et al. implemented an in situ WAXS experiments (incident angle of 2°) using a cell consisting of PB2T-TEG thin film on a gold-plated polyimide substrate inverted in a well filled with aqueous electrolyte (**Figure 11d**).[285] This revealed a lamellar expansion for ion intercalation in the crystalline region in qualitative agreement with their ex situ results, informing non-Fickian ion transport p-type glycolated thiophenes. During multiple electrochemical cycling, the lamellar peak intensity and position switched between two states, showing that the structure change is reversible. In this

setup, only the incident X-ray beam was isolated from the electrolyte. As the OMIEC of interest was on the underside of the Au coated polyimide window, a grazing incidence was not possible as the beam had to penetrate through the substrate to probe the OMIEC. Thus, the transmitted beam continued through the electrolyte, likely producing electrolyte scattering in the mid to high q scattering vector range (where electrolyte scattering is most problematic); this region of data was not reported. The X-ray beam is not reflected at the interface between the OMIEC material and the electrolyte in this cell, and thus leads to technical difficulties to apply the operando technique for common OMIEC materials. Additionally, the in-plane signal of the scattered pattern was severely diminished, and only the lamellar peak in out-of-plane direction was successfully captured. Thus, while convincingly confirming the particular ion-intercalation phenomena of interest in that work, the cell design employed does not represent a generalizable operando GIWAXS test bed for OMIECs.

Alternatively, Paulsen et al. reported a cone cell (**Figure 11e**) with a knife-edge to seal the liquid electrolyte above the OMIEC material.[122] By reducing the cell material at the cone tip and matching OMIEC films with thickness approaching that of the incident X-ray beam height, the incident and scattered X-rays have a negligible path through the cell wall and a minimal path through the overlaying electrolyte thereby lowering the intensity of background scattering. The authors successfully monitored the real-time lamellar spacing oscillation of acid treated PEDOT:PSS in operating condition and extracted the kinetic time constants of charging/discharging. However, the broad electrolyte scattering peak still persisted to the point that time resolved measurements of π-stack changes were not possible, with π-stack scattering only sufficiently resolved with longer exposures (integration time) at equilibrated potentials. From these scattering patterns at equilibrated potentials, the authors proved the reversibility of both lamellar and π-stack spacing changes. While the operando cone cell is successful for resolving certain features (i.e. lamellar kinetics) and readily allows for typical assembly of electrochemical measurements, it is ultimately only suitable for thick (several microns or more) OMIECs with relatively strong scattering. The low crystalline fraction and the high degree of disorder of most OMIEC materials which make them weakly diffracting,[335] combined with the ubiquity of the thin film geometry (a few 100 nm or less) in OMIEC device applications, may limit the broad applicability of the cone cell for OMIEC operando WAXS.

To enable broadly applicable operando GIWAXS on OMIEC thin films, Paulsen et al. further reported a "frit cell" (**Figure 11f** and **Figure 12a**) for liquid electrolyte-contacting OMIEC charging measurements.[33] The frit cell separates the X-ray path from the electrolyte by using a polished porous X-ray absorbing substrate onto which OMIEC thin films were transferred. Capillary action enabled electrolyte to contact with the OMIEC film from below, leaving the headspace above the film open for the incident and scattered X-rays to pass unencumbered. Thin films of weaker scattering materials shown to be impractical in cone cells were selected for measurement in the frit cell, and high-fidelity time resolved scattering patterns were obtained during electrochemical cycling, as shown in **Figure 12b**. Since the incident beam did not pass through the aqueous electrolyte, both the (010) π-stack scattering and multiple orders of (h00) lamellar scattering of pg2T-TT were well resolved and readily fit, yielding quantitative structural information (d-spacings and coherence lengths, for example). The reversible lamellar and π spacing change during CV cycling was confirmed. Despite the wide applicability and ease of operation for different OMIEC materials, the method still shows room for improvement. While potential control is achieved, the charging current related to the structural changes is overwhelmed by currents arising from electrochemical side reactions due to using a stainless steel frit. In addition, the distribution and homogeneity of pores on the frit surface may affect the uniformity and kinetics of ion migration, which makes the current frit cell only suitable for quasi steady-state measurements, or transient measurements where ion transport in the OMIEC is not the rate limiting step. It is expected that optimized frit materials selection or modification will overcome some of these drawbacks.
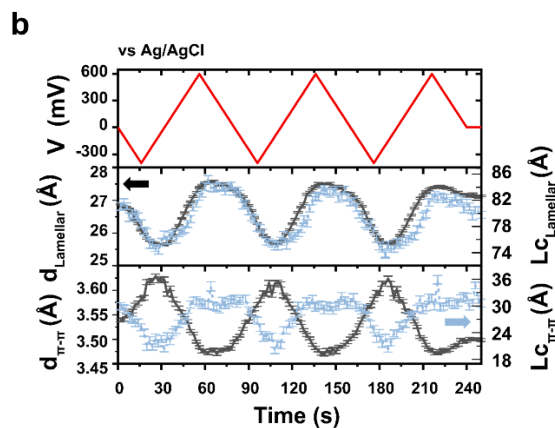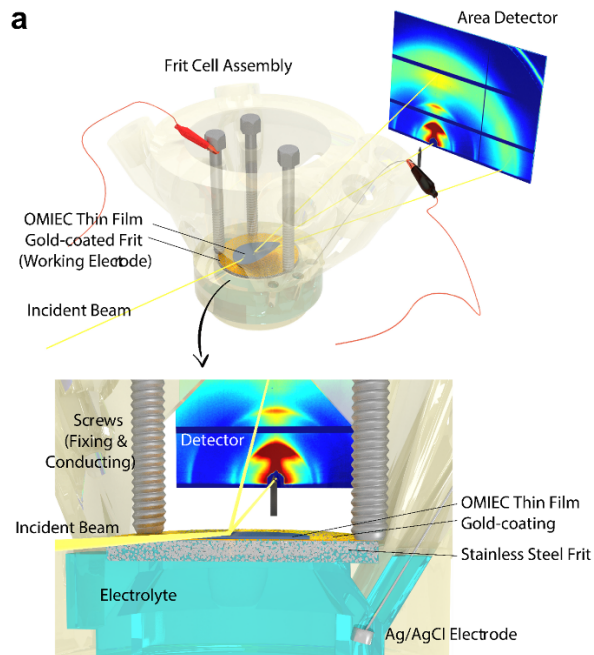
Figure 12 (a) 3D rendering of the printed operando cell with porous frit substrate/working electrode, highlighting the underlying electrolyte reservoir and electrolyte path coupling the film of interest to potentiostatic control; (b) p(g2T-TT) lamellar/π stack peak center over time with swept electrochemical potential.

6.3.2 Small Angle X-ray Scattering

Small Angle X-ray Scattering (SAXS) reveals different domain structures in the range of 1-100 nm (mesoscale). The technique has not been implemented in OMIEC operando characterization, but shows potential for tracking OMIEC domain changes under working conditions. Mesoscale

inhomogeneities of OMIECs are highly probable because OMIECs are often multicomponent systems (CPs combined with polyelectrolyte or polymer electrolyte), with phase inhomogeneity (between crystalline and amorphous domains), along with likely compositional inhomogeneity of ions between components and phases.[1] These complex mesoscale features are sensitive to electrochemical potential, chemical environment, and temperature. With ex situ experiments, the mesoscale structures are significantly altered (due to solvent evaporation, loss of charge state, and ion diffusion), highlighting the importance of operando SAXS characterization. The insensitivity to liquid electrolytes in SAXS is an important prerequisite for operando characterization. While WAXS focuses on molecular packing peaks located in high q range, SAXS concerns the pattern in low q range, corresponding to the size and shape of the aggregates. Due to the small scattering angle change in SAXS, electrolyte background absorption and scattering (in high q range) has little effect on the signal of interest, thus making this technique particularly suitable to study heterogeneous OMIEC morphologies. For example, the use of SAXS in inhomogeneous stirred systems to observe polymer particle aggregation allowed to successfully distinguish between molecularly dissolved copolymer chains and nascent micelle formation in turbid monomer emulsions.[336] The similarity of such systems to OMIECs makes SAXS promising for in situ/operando studies in swollen polymer thin film with and without liquid electrolyte.

In experiments on polymer films, grazing incidence small angle scattering (GISAXS), similar to GIWAXS, is usually employed to increase the effective integration area of the film, to improve the signal-to-noise ratio, and to capture the anisotropic meso-structure often present in thin films. A model with Distorted Wave Born Approximation (DWBA) correction is used to fit the characteristics of the Yoneda peaks (without obvious 2D features) and 2D scattering patterns to correct the multiple reflections due to this geometry.[337] The shape and size information of different domains is extracted from the form factor, and the aggregation distribution is related to the structure factor. If the GISAXS pattern exhibits a distinct peak, its corresponding real space distance responds to the ordered spacing of mesoscale domains and can be calculated from Braggs' law (i.e. in ordered block co-polymer or colloidal crystal systems).

Again, work toward operando SAXS for OMIECs builds on work from across the field of organic electronics and polymer thin films. In situ GISAXS has been reported for block

copolymers [338-342] and BHJ systems during film processing.[42] The studies of block copolymers focused on the thermal and/or vapor annealing. By controlling the flow rate of the solvent-saturated inert gas, the polymer is slowly swollen surrounded by the saturated solvent vapor. During vapor swelling, the distribution of the solvent and the morphology of the individual domains within the polymer can be directly extracted from the 2D diffraction pattern. The characterization of BHJ systems in organic photovoltaics ranges from the crystallization in BHJ film formation[286, 343, 344] to nanoscale phase separation during the annealing of BHJ films.[345, 346] In a three-phase BHJ system with additives, Bokel et al. defined the integrated scattering invariant as $\int_{q_{min}}^{q_{max}} I q^2 dq$, and tracked the relative volume ratio of each phase by this volume-dependent invariant during a blade coating process.[286] By modeling the ternary phase diagram, the function of additive 1,8-diiodoocatane (DIO) was revealed, which brings the BHJ close to the equilibrium liquid-solid phase conditions and allows a steady state phase separation. These successful in situ experiments demonstrate the technical feasibility of operando OMIEC GISAXS characterization.

The successful implementation of operando GISAXS characterization relies on enhancing the domain contrast in OMIEC materials and can be achieved by appropriate selection of both ionic dopant and X-ray energy. The ability of GISAXS to determine the mesoscale inhomogeneity comes from its sensitivity to electron density inhomogeneity, in contrast to the nucleus density in neutron scattering and reflection. From the choice of X-ray wavelength, incident light resonant with elemental absorption edge also increases the phase contrast. Resonant soft X-ray scattering (RSoXS) has been widely employed for polymer studying near the carbon K-edge,[347] and its high chemical sensitivity allows solving morphological and compositional problems in multi-phase, multicomponent systems.[348] Ex situ RSoXS has been reported to determine the absolute PEDOT concentration of the PEDOT:PSS-rich phase and surrounding PSS-rich matrix in PEDOT:PSS.[178] The absence of energetic transitions in the carbon K edge makes dopant ions only contribute to the linear background absorption and can be easily removed. Due to the low penetration depth of soft X-rays, this technique is usually performed in vacuum and is therefore suitable for the characterization of solid-state samples. Sealed microfluidic cells have been reported for in situ studies of the self-assembly kinetics of block polymers, and show the potential for operando characterization of OMIECs requiring additional liquid electrolytes. The

penetration depth can be improved by using hard X-rays especially above 10keV, but the inherent electron density contrast between aggregates might be too low to obtain an analyzable scattering pattern. Choosing tender X-rays for the resonant S K-edge might balance the X-ray penetration depth with a reasonable electron density contrast and is suitable for operando experiments at ambient pressure.

The multimodal use of operando GISAXS with other characterization techniques is another future target. Further confirmation of molecular aggregates can be done using ex situ/in situ probe techniques. In addition, the full-microscale structure of OMIEC films can be fully depicted by incorporating operando GIWAXS described in 6.3.1.

6.3.3 X-ray Photon Correlation Spectroscopy

X-ray photon correlation spectroscopy (XPCS) records temporally coherent fluctuations of scattered spots but has not been applied for OMIEC characterization. The technique shows a µs level time resolution and provides the information of structure relaxation kinetics (mechanical information) and ionic velocity that are especially interesting for operando OMIEC investigations. The spatial inhomogeneity of the material can also be extracted by analyzing the statistics of the diffracted spot distribution and scale. In principle, due to the high coherence of the incident beam, the diffraction pattern obtained by XPCS can directly be used to reconstruct all the structural details inside the material, which is unique among all the operando characterizations. Similar to WAXS and SAXS, choosing low energy coherent X-ray gives higher phase contrast and intense signal but might lead to significant beam damage after long term exposure. Oppositely, high energy X-ray are rarely absorbed by the polymer film and electrolyte but might lose necessary scattering contrast.

1
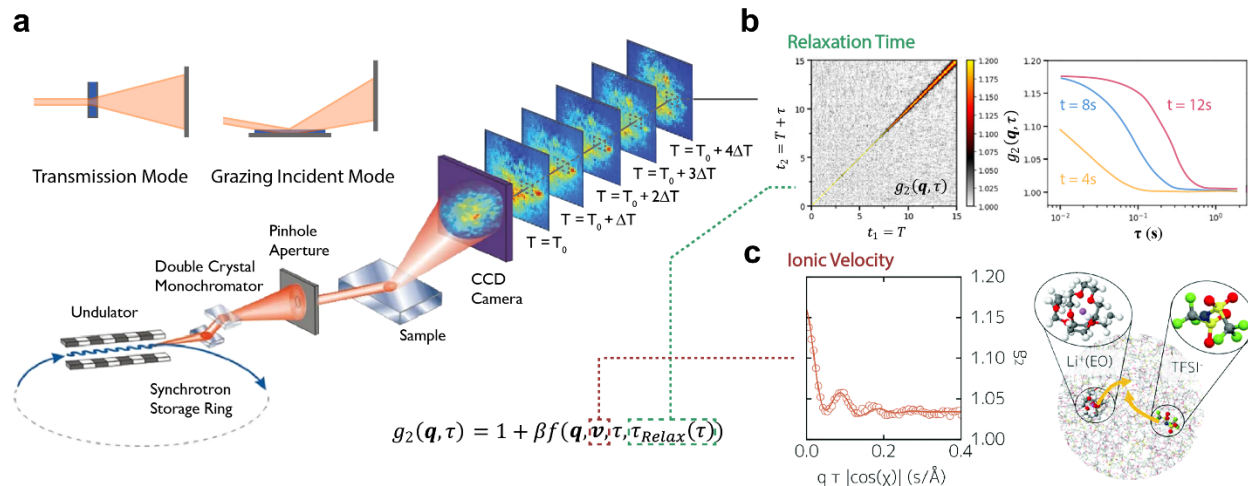
Figure 13 (a) The setup of XPCS. Reproduced with permission from [349]; Copyright 2007 Springer Nature. (b) The structure relaxation curve of epoxy/layered silicate composites after t seconds aging time. The relaxation time τ can be extracted from the curves. Reproduced with permission from [350]. Copyright 2019 American Chemical Society. (c) Local ionic velocity can be extracted from the fitting of time correlation function in Li salt/PEO blends. Adapted with permission from [287]. Copyright 2020 Royal Society of Chemistry.

As shown in **Figure 13a**, XPCS can take both the grazing incidence mode to probe the surface of liquids/thin films,[351, 352] and the transmission mode to acquire bulk information of solid samples or hydrogels.[353, 354] In the transmission mode, the spatial mapping resolution of XPCS is on the order of microns. The thickness of the studied sample in a recent report was only 140μm, which is only a factor of 20x thicker than drop cast OMIEC films.[355] The experimental approach has now been reported for studying soft materials, including the growth and the diffusion of nanoparticles,[356, 357] the cross-linking of polymers[358] under heating[350, 359] and UV curing processes,[360] as well as the stress relaxation of polymer electrolytes.[353, 361]

The statistical interpretation of the XPCS pattern requires the calculation of the time correlation function (Equation 6), and the complex morphology and rheology of material at short time scales can be studied:

$$g_2(\boldsymbol{q}, t, \tau) = \frac{\langle I(\boldsymbol{q}, t) I(\boldsymbol{q}, t+\tau)\rangle_{q, t \to t+\tau}}{\langle I(\boldsymbol{q}, t)\rangle_{q, t \to t+\tau} \langle I(\boldsymbol{q}, t+\tau)\rangle_{q, t \to t+\tau}} \quad (6)$$

Where q is the wave factor of certain points in the scattering pattern and I is the scattered intensity of that point. The average bracket $\langle \cdots \rangle_{q,t\to t+\tau}$ describes an average over correlations within a narrow range of time τ.

The relaxation time constant τ_0 of the system from the correlation function reflects the ability of the polymer to maintain its own microstructure and intermolecular network, as shown in **Figure 13b**. In addition, heterodyne XPCS, which mixes the static reference scattering signal with the dynamic scattering signal of the electrolyte, provides the ionic velocity with voltage applied.[287] The correlation function g is expressed as a function (Equation 7) of the velocity vector v, the scattering vector q, the angle χ between two vectors, and the delay time τ:

$$g_2(q,\tau) = 1 + \beta(1-h)^2 + h^2\beta e^{-2\left(\frac{\tau}{\tau_0(q)}\right)^\gamma} + 2h(1-h)\beta\cos(\omega\tau)e^{-\left(\frac{\tau}{\tau_0(q)}\right)^\gamma} \quad (7)$$

Where h is the heterodyne fraction and ω is derived oscillation frequency (Equation 8):

$$\omega = q \cdot v = qv\cos\chi \quad (8)$$

The local electrolyte velocity can be extracted as the fitting variable by angularly resolved sampling of a series of XPCS frames, as shown in **Figure 13c**. Considering the simultaneous ability to obtain material SAXS or WAXS data in XPCS measurements, it can be expected that XPCS promises to capture mesoscale dynamics by small angle XPCS as well as crystalline chain dynamics by wide angle XPCS during OMIEC operation. The technique has not currently been performed in OMIECs owing to relatively new availability of coherent X-ray sources and in situ/operando cell design to maintain beam coherence. The significant data analysis/modelling requires powerful computing capabilities to handle large data sets and to perform real-time data analysis in experiments. Despite the aforementioned obstacles, XPCS still shows the future for solving the long-standing problem of submicron spatial structure-property relationship of OMIEC during electrochemical doping/dedoping.

6.4 Neutron Scattering and Reflection

6.4.1 Small Angle Neutron Scattering

Small-angle neutron scattering (SANS) is a non-destructive scattering technique to detect the morphology of segregated phases. Neutron beams mainly interact with atomic nuclei to produce isotropic scattering, and the scattering ability is not related to the atomic number but the nuclei density. As a result, SANS is very sensitive to light atoms and has a deeper penetration into the material, making it suitable for OMIECs forming hydrogels or operating in liquid electrolytes. For scattering at small wave vectors, individual atoms are not resolved, and the scattering process is governed by the interference of neutron waves from domain geometry. Therefore, similar to small angle X-ray scattering, SANS provides information on material heterogeneity including domain or particle shape and dimension.

In situ SANS measurements have long been applied to monitor the self-assembly of organic conducting polymers in solution,[362, 363] and are feasible for operando OMIEC characterization. Bastianini et al. used UV-Vis spectroscopy and SANS to trace P3HT in solution and successfully revealed the formation of P3HT nanowires, showing that P3HT molecules first aggregate into one-dimensional rods and then slowly self-assemble into two-dimensional π stacked lamellae.[288] Although there are no relevant reports on the application of SANS for operando measurements of OMIEC materials, SANS has been employed in situ to study the ionic liquid driven formation of PEDOT:PSS microgels[364] and ex situ to study the effects of solvent annealing on PEDOT:PSS thin films.[365] SANS is crucial to probe the internal aggregation shape and distribution for hydrogel OMIEC materials where X-ray diffraction cannot be used. The reasons that hinder the application of SANS include the scarce experimental facilities, the large number of samples required, and the long integration time.

6.4.2 Quasi-elastic Neutron Scattering

Quasi-elastic Neutron Scattering (QENS) reveals picosecond level polymer dynamics and has been performed on polyelectrolytes[366] and conjugated polymers.[367-372] The technique measures the dynamic structure factor $S(\boldsymbol{q}, \omega)$ as a function of the wave factor **q** and the neutron frequency ω around the elastic scattering peak.[373] The incident neutrons exchange their kinetic energy with mobile polymer fragments; the larger the frequency difference $\Delta\omega$, the higher the polymer mobility. The intermediate scattering function $I(\boldsymbol{q}, t)$ is derived from the inverse Fourier transform of the dynamic structure factor.[374] The **q** dependent time constant can be fitted from

the intermediate scattering function and yields polymer dynamics at different length scales.

Classical detectors for QENS are time-of-flight (TOF) and back-scattering (BS) spectrometers

with energy resolution of 10-100 μeV and 1 μeV, respectively.[374]

The Neutron Spin-echo (NSE) method directly measures $I(\boldsymbol{q}, t)$ with incident neutrons of wide

energy distribution.[375] This method does not require a monochromatic incident light, and thus

yields higher signal intensity as well as energy resolution at the neV level.[374] In conjugated

polymers with different side chains, QENS was used to compare temperature dependent polymer

dynamics, including side chain motion and backbone torsion.[368, 369] The technique has also been

applied to molecular doped P3HT for microscale dopant dynamics.[367] In addition, QENS is able

to separate molecular dynamics of different components in P3HT:PCBM blends through

selective deuteration (causing different cross section).[370-372] Due to the time scale matching of

QENS experiments and molecular dynamics simulations (MD), the latter are often combined

with QENS to further characterize the motion of polymers.[368, 371, 376, 377] Probability distribution

functions can be extracted from the QENS fit results[378] and directly compared with simulation

results for different molecular modes. The success of QENS applied to other conjugated

polymers lays the foundation for ultrafast dynamic probing of OMIECs. In association with MD,

this technique can elucidate and distinguish side chain and backbone dynamics, corresponding to

the migration and coupling of ionic and electronic species in operating OMIECs. However, the

application of QNES – particularly for NSE – is still limited by the presence of very few

instruments across the world.

6.4.3 Neutron Reflectometry

Neutron reflectometry (NR), or alternatively neutron reflectivity, shows great opportunity for

operando OMIEC characterization due to its sensitivity to material surface and interfacial

structure, including film thickness, surface roughness, and interfacial roughness. With a known

elemental composition, NR gives the neutron scattering length density of the different layers in a

multilayer film and thus also provides information on the atomic density in the different layers.

Time-resolved neutron reflection experiments have been reported for the study of material

swelling and molecular diffusion in materials, which are core questions in the study of OMIEC

materials that require solvent involvement in operation.[289, 346] Bießmann et al. reported a time-

resolved NR study of the swelling kinetics of PEDOT:PSS by different treatment with the time resolution of 30 seconds.[289] By fitting a multilayer model to the scattering length density in the vertical direction of the film, neutron reflection not only provides information about the vertical layer composition (i.e., dry vs. wet film) and thickness, but also allows accurate calculation of the water content in the film. Another report investigated the phase separation and the distribution of components of P3HT:PCBM during annealing.[346] Combining the data from ex situ experiments, the authors modeled a mixture heterojunction (BHJ) with pre-extracted densities of both materials and successfully obtained the exact thickness and chemical composition of each layer of the whole film at different temperatures. A recent report from Galuska et al. monitored the film thickness and the water content change of polymer floated on the liquid surface,[379] which shows the feasibility of in situ/operando NR on thin film OMIECs. Looking forward, in situ/operando NR has the potential to show the swelling and chemical exchange of OMIEC materials in operation conditions. In addition to conventional thin film state measurements, OMIEC applications with different material geometries, such as hydrogels and thick battery electrodes/polyelectrolytes, can be designed to investigate the device physics of OMIEC materials using the powerful vertical resolution of in situ/operando NR.

7. Quartz Crystal Microbalance

Quartz Crystal Microbalance (QCM) techniques are a powerful gravimetric tool for the operando study of OMIECs, as they provide time resolved information on mass transport of solvent and/or ionic species into or out of a thin film by monitoring nanogram-level mass change, density, and film thickness of OMIEC materials. QCM can be employed to measure the mass change after electrolyte exposure, swelling, or doping/dedoping processes, allowing to accurately characterize the corresponding volume change and contribute to the determination of ion-solvent composition. In addition, the extracted the shear modulus, density, thickness, and viscosity of OMIEC thin films can be used to quantify the film homogeneity. The unique information available through QCM measurements provides data on ion transport dynamics, ionic-electronic interactions and morphology changes in OMIECs during operation.

The QCM mass analysis is based on the piezoelectric effect of quartz crystals. When a sinusoidal voltage is applied to a quartz crystal, the crystal will oscillate mechanically at a precise

vibrational frequency determined by its total mass (with polymer sample loaded) and mechanical properties. In air or near vacuum, the frequency change Δf is proportional to the mass change Δm of a quartz crystal, known as the Sauerbrey equation (Equation 9):

$$\Delta f = -\frac{2{f_0}^2}{A\sqrt{\rho_q \mu_q}}\Delta m \quad (9)$$

Where f_0 is the resonant frequency of the fundamental mode of the chip and A is the piezoelectrically active area, both related to the bare quartz chip. The constants ρ_q and μ_q are the density and shear modulus of quartz, respectively. The experiments require to deposit the OMIEC material on a thin quartz crystal together with connecting electrodes, as shown in **Figure 14a**. The QCM relates changes in the resonant frequency of the crystal to small mass changes occurring in OMIEC thin films upon solvent swelling or ion doping with nanogram-level accuracy. The technique also records the oscillation frequency at multiple overtones of the resonant frequency. The penetration depth decreases as the overtone number increase, thus different orders of overtones reflect the mass change at different vertical regions of the sample.[380] This principle has been applied on ionic liquid[381] and conjugated polymer thin films[379] to qualitatively extract mass change at different vertical depth.

Commonly used QCM sensors also record the dissipation of the vibrational oscillations, known as QCM-D[380] (QCM with dissipation monitoring), which quantifies the oscillation dampening in soft materials (including polymer thin film and electrolytes) due to their viscoelasticity. The dissipation term is proportional to the decay time constant of the oscillation amplitude. Since the frequency domain signal is the Fourier transform of the time domain signal, this term is obtained from the half width at half-maximum of the conductance peak at the resonance frequency.[382] In OMIECs, the dissipation term is not only important to quantify viscoelasticity but is also necessary for quantitative mass analysis. In fact, solvent swelling or changes in the film thickness significantly affect viscoelastic properties of OMIEC films, causing their vibrational oscillation frequency to deviate from the Sauerbrey equation. This phenomenon can be described using the Kelvin-Voigt model (Equation 10), which approximates the dissipation term as the ratio of dissipated energy to stored energy:

$$D \approx \frac{E_{dissipated}}{E_{stored}} \quad (10)$$

Voinova et al. used this model to describe the the QCM-D response in terms of the frequency change Δf (Equation 11) and the dissipation change ΔD (Equation 12) and the viscoelasticity of the adsorbed soft film layer:[383]

$$\Delta f = Im\left(\frac{\beta}{2\pi\rho_q h_q}\right) \quad (11)$$

$$\Delta D = -Re\left(\frac{\beta}{\pi f \rho_q h_q}\right) \quad (12)$$

Where f is the oscillation frequency, h_q and ρ_q are the thickness and density of quartz, respectively; β is a function of the complex shear modulus G*, film thickness h_f and film density ρ_f, is the coefficient of the following wave propagating differential equation (Equation 13):[384]

$$F = -\eta_f \frac{\partial v_x}{\partial z}\bigg|_{z=0} = \beta v_x \quad (13)$$
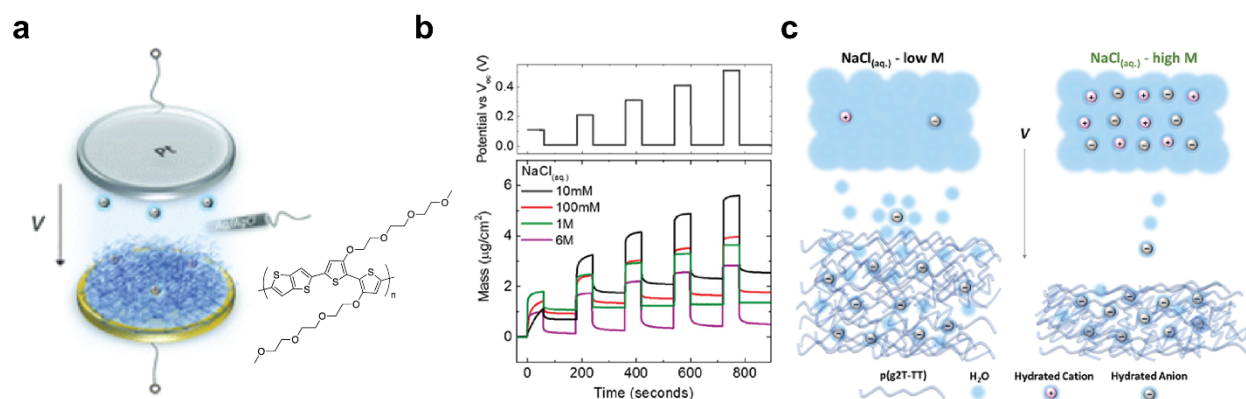
Here, η_f is the film viscosity, x is the quartz oscillation direction, and z is orthogonal to the QCM chip plane. When the film is thinner than the penetration depth of the oscillation wave, the mass change can be calculated from fitted thickness h_f and density ρ_f. This model has been widely used in the quantitative analysis of QCM-D data in liquid-solid interface systems.[385-389] Recently, other QCM-D models have also been proposed to enhance the suitability of the theory for practical applications.[382, 390, 391]

Qualitatively, the dissipation term in QCM-D relates to the viscoelasticity of the film and reflects the change in stiffness of the film, which also serves as an additional check for mass change (e.g. electrochemical doping or biomolecule loading). For example, in the case of an OMIEC-based biosensor, QCM-D was used not only to characterize the mass change of a phospholipid bilayer and protein upon loading, but also to demonstrate the very presence of these molecules by the change of viscoelasticity on the film surface.[392] Cendra et al. corroborated the hydration of the

films in different environments by analyzing the dissipation changes of the solvated OMIEC films. A higher water content in the polymer film led to a decrease in the film stiffness, thus increasing the viscoelastic response.[186] In addition, dissipative QCM studies are an ideal tool to characterize the rheology and mechanical properties of OMIEC materials used in biological environments, notably their stiffness (mis)match to the surrounding tissue.

The electrochemical quartz crystal microbalance with dissipation monitoring (EQCM-D) enables the control of electrochemical potential, thus reproducing the operating conditions of OMIEC devices. In the work of Savva et al., EQCM-D was used to directly monitor voltage-triggered ion uptake and the corresponding current changes in PEDOT:PSS.[44] The reported mass loss in the polymer film upon doping demonstrates that most cations leave the doped OMIEC thin film. Assuming a complete ionic compensation of the holes at the maximum dedoping level and an unchanged cation/water ratio, the authors estimated the dopant concentration at different voltages. The potential dependent doping efficiency, a measure of the ionic-electronic coupling, was defined by the ratio between the dopant concentration and the hole concentration (from CV) of the OMIEC film. In a subsequent study, the authors used EQCM-D on the accumulation mode OMIEC material pg2T-TT by assuming that only anions are involved in electrochemical doping.[45] The EQCM-D analysis showed that the dopant anions entering the pg2T-TT film were hydrated, but the water swelling exceeded the amount needed to solvate the ions. The effect of electrolyte concentration on swelling was also studied: the film swelled more and retained more water at lower electrolyte concentrations, an effect that the authors attributed to osmotic pressure (see **Figure 14b,c**). Similar compositional estimates of swelling OMIECs during electrochemical doping have been reported with different ionic dopants[186] and glycol side chain content.[20, 393] Despite referring to different electrolyte-OMIEC pairs, these studies can still be compared with each other as they are mostly monitoring solvent-induced effects, as opposed to the penetration of bare ions. It is worth noting that the estimation of dopant concentration by EQCM-D relies on assumptions of 100% doping efficiency at the maximum dedoping potential. Given the increasing availability of black box EQCM-D systems, it is important to verify the applicability of common models and assumptions to OMIEC film properties (i.e. thickness, mechanical properties). To further improve data interpretation, EQCM-D could be integrated with other

compositional analysis methods such as XRF and Glow-discharge optical emission spectroscopy (GDOES).[394]

Figure 14 (a) EQCM setup for the study of pg2T-TT, where the OMIEC film is in contact with electrolyte; (b) Changes in the film mass when electrochemical doped in four electrolytes of varying ion concentrations; (c) The polymer–electrolyte interface and the differences in the swelling behavior of the film in low- and high-concentration electrolytes. Adapted with permission from [[45]]. Copyright 2019 American Chemical Society.

8. Scanning Probe Techniques

Operando scanning microprobe techniques have the capability to provide spatially resolved information on the microstructure,[285] charge distribution[86, 395] and chemical composition[396] of OMIEC materials.[396] These include scanning electrochemical microscopy, atomic force microscopy, and its many derivatives. Atomic force microscopy has been applied in the characterization of OMIEC materials due to its adaptability to a wide range of environments as described in **8.1** - **8.5**. Scanning electrochemical microscopy has not yet been directly applied to the real-time operational characterization of OMIEC materials yet. However, imaging of similar systems has been reported in recent years and will be briefly described in **8.6**. Compared to other techniques, probe-based techniques directly image OMIEC materials and spatially resolved morphology, electrical and mechanical properties of the material. A general comparison among these probe techniques is presented in **Table 4**.

Table 4. Summary of probe techniques employed in operando study of OMIECs

| Method	Description	Electronic carrier Information	Ionic carrier Information	Structural & Morphology Information	Representative in situ example	Implementation barriers
KPFM	Map surface potential and morphology	Spatial distribution	-	Domain/phase separation, surface topology	MEH-PPV[86,395]	No electrolyte between probe/sample
cAFM	Map local conductivity and surface morphology	Local conductivity	-		PFBT[397]	Signal screening in electrolyte
IR-AFM	Map high-spatial resolution IR absorption and surface morphology	Spatial distribution/ concentration	Ionic Environment		-	Signal screening in electrolyte
Strain-AFM	Map mechanical properties and surface morphology	-	Ion uptake/ swelling		PEDOT:PSS[396]	-
SECM	Map local electrochemical behavior of solid/liquid interface	-	Redox reaction	-	PEDOT:PSS[398]	Large tip, low spatial resolution

1

8.1 Atomic Force Microscopy

As a well-established technique, atomic force microscopy (AFM) has been widely applied in the morphological characterization of soft materials such as polymers and biological samples,[399-401] especially in the study of phase/domain separation.[401-403] For polymeric samples, AFM acquires three-dimensional topography and phase maps of sample surface, detected by a sharp cantilever probe in tapping (intermittent contact) mode. The height of the AFM probe is usually accurately determined by measuring the deflection of a laser beam, as shown in **Figure 15a**. The phase image, relating to the hardness, elasticity, viscosity and friction of the detected point, is recorded simultaneously with the height map by measuring the fundamental resonant frequency of the probe.[399] The surface morphology of thin films, including phase separation, elastic modulus, roughness, as well as granular size, shape, and distribution can be imaged and quantified in atmospheric and aqueous environments. The material elasticity, viscoelasticity and surface adhesion can be obtained by recording the energy dissipation of probe-sample interaction.[404] Comparing to other microscope techniques such as scanning tunnelling microscopy and

traditional electron microscopy, AFM is suitable for OMIEC materials due to the modest requirements for sample preparation, versatility and widespread commercial availability.[405] In addition, unlike electron microscopy, AFM is a nondestructive technique: surface damage can be avoided simply by using non-contact or tapping modes.

The high spatial resolution and wide environmental adaptability of AFM make this technique highly advantageous for operando characterization of OMIECs. Spatial resolution at the molecular level has been reported for structural characterization at the liquid/solid interface.[406] In situ AFM has also been applied on polyelectrolytes to study the swelling in water vapor[407] and the relaxation process in aqueous solutions.[408] In addition, the interfacial morphology changes during electrochemical polymerization of EDOT has been observed by in situ AFM.[409]

Operando AFM experiments are usually coupled to additional techniques to achieve a two-dimensional image of other physical properties in addition to height and phase profile. These additional techniques include mechanical, optical, and electrical probes. While most of non-scanning probe operando characterization focus on overall changes of OMIEC morphology, operando AFM provides local information on optical,[410] mechanical,[396, 411] electrical,[86, 395, 412] and structural properties,[413-415] as well as their surface distribution. Thanks to the availability of AFM probes made from conductive materials, AFM can be directly used for in situ/operando characterization of OMIECs under applied voltage/current, as shown respectively for Kelvin probe (**Figure 15b**) and conducting probe force microscopy (**Figure 15c**) setups. By scanning the surface of OMIEC materials during electrochemical doping/dedoping, these operando AFM measurements can quantitatively determine the local electrical properties while recording the surface morphology of the material. Meanwhile, infrared photo-atom force microscopy (**Figure 15d**) and strain microscopy (**Figure 15e**) provide spatial optical and mechanical information of the material, respectively. The additional information obtained by these mapping techniques (discussed in the following sections) makes them essential for the study of OMIEC in operation.
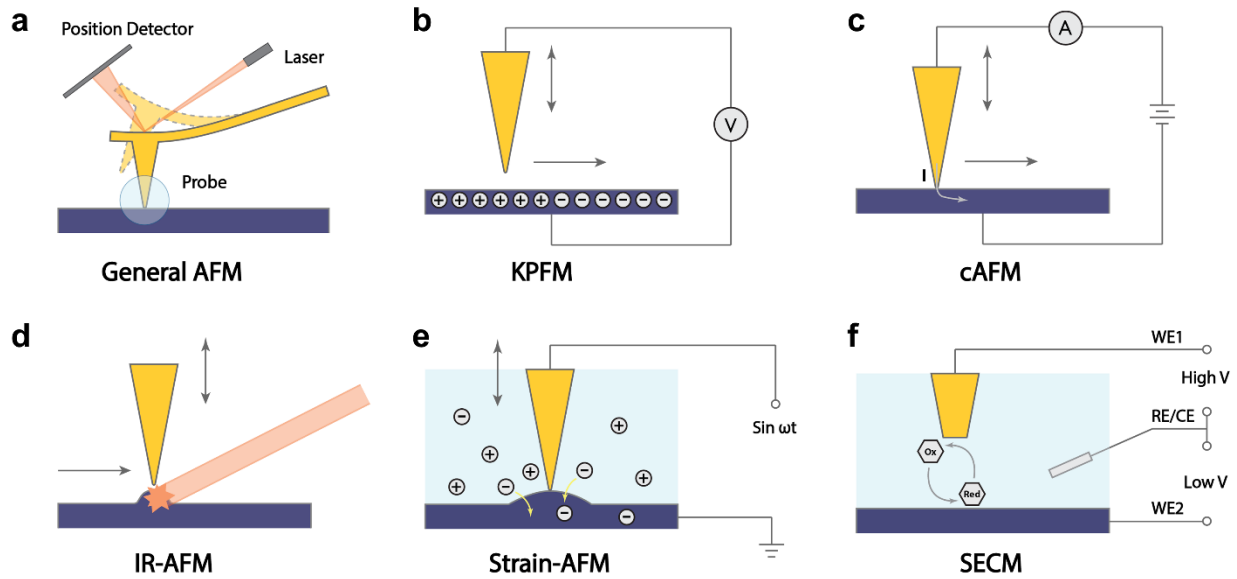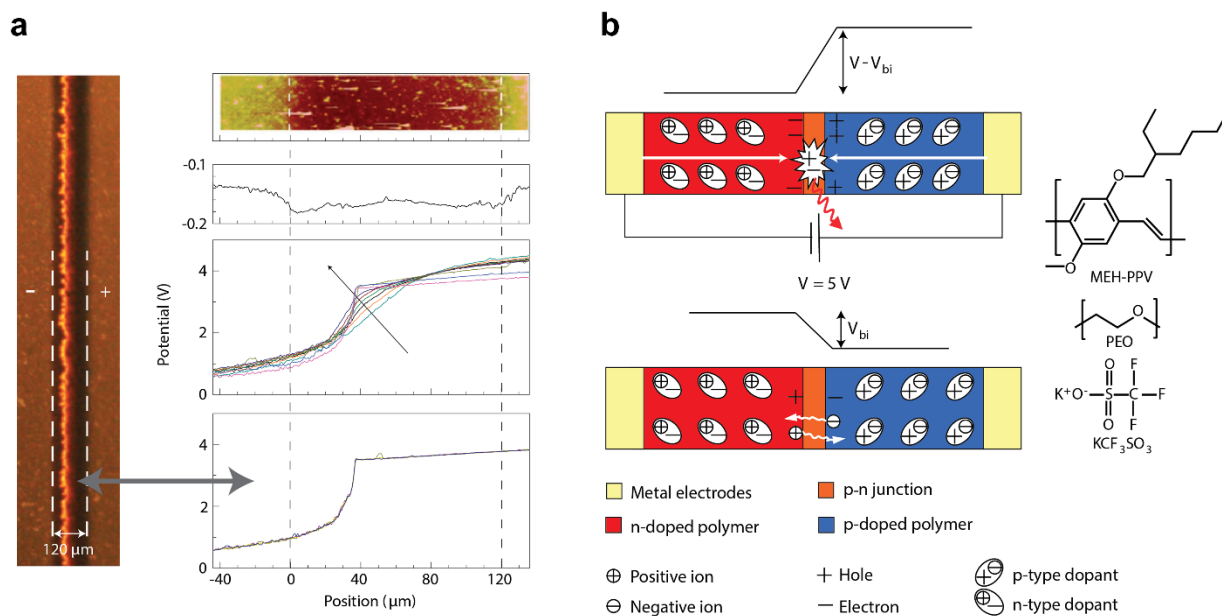
Figure 15 (a) AFM setup in general; The probe tip of (b) Kelvin probe force microscopy (KPFM); (c) conductive AFM; (d) infrared photo-atom force microscopy (IR-AFM); (e) strain AFM; and (f) Scan electrochemistry microscope.

8.2 Kelvin probe force microscopy

Operando Kelvin probe force microscopy (KPFM) has been used for the characterization of OMIEC materials in the absence of an electrolyte. In addition to spatially resolved mechanical properties, this technique enables the mapping of the surface potential of thin films, revealing the spatial distribution of doping[416] and trapped charges.[417] The technique has been applied to the study of phase separation[418, 419] and molecular aggregation by accurately mapping the distribution of HOMO levels in different regions of the film. In KPFM, extra voltage pattern is applied between the tip of a conventional non-contact AFM and the sample. A DC voltage is applied to offset the contact potential difference between the sample surface while a superimposed AC voltage is used to probe the surface potential variations.[420] With a known tip work function (the energy difference between the vacuum and the Fermi level), the work function at single point on the sample surface can be obtained by the compensating DC voltage. The gap between the probe tip and the material surface must be free of contaminants (preferably in vacuum) in order to record a stable signal. Although the technique has achieved a high spatial

resolution under ambient conditions,[421] KPFM remains challenging to carry out in the presence of liquid electrolytes.[422]

KPFM has been applied to the study of solid-state light emitting electrochemical cells (LEECs) in operation. The carrier and electric field distribution in small molecule transition metal complex salts used in LEECs has been studied by KPFM.[423] Similarly, in polymeric OMIEC materials, Matyba et al. measured the spatially resolved potential distribution of ionic doped MEH-PPV under active applied bias, revealing the formation of p-n junctions.[395] A significant potential drop occurs in the center of the material channel, inducing light emission at the boundary between the p- and n-doped regions, shown in **Figure 16a**. With positive bias applied, the anion and the hole on the polymer backbone migrate to opposite electrodes, leading to charge buildup and eventually screening the electric field, as shown in **Figure 16b**. During the relaxation process following the removal of external bias, the change in the potential profile measured by KPFM allowed the estimation of ion mobilities. A similar phenomenon was also revealed in the operando KPFM study of conjugated polyelectrolytes by Collins et al.[86]

Figure 16 (a) Micrograph showing the light emission from a planar LEC device during steady-state operation at V =5 V (left) and the positive and negative electrodes are indicated by the + and − sign, respectively. The right column shows the 2D topographic image, electrostatic

74

potential profile recorded on a pristine device under open-circuit conditions, temporal evolution before balance with V =5 V (the arrow indicates increasing time), and the subsequent steady-state at V =5 V; (b) The transient charge distribution after a shift to the open-circuit condition (top) and the steady-state charge distribution at V =+5 V (bottom), where V_{bi} indicates the built-in potential over the junction. The net charge motion is indicated by the white arrows. Adapted with permission from [395]. Copyright 2009 Springer Nature.

Operando KPFM shows excellent time resolution and has been reported on the characterization of OFETs, in which the charge distribution and trapped charge on the material surface are directly related to the performance of the device. Although OFET devices do not involve ionic conductivity in operation, the following example still demonstrate the insight for electronic charge dynamics. Yamagishi et al. used KPFM to perform millisecond resolution surface potential mapping on OFETs made from DNTT with different gate bias,[424] and successfully revealed the different time scales for the decay of free carriers and trapped carriers inside the film after turning off the device.[417] Additionally, KPFM reveals the spatial inhomogeneity of carrier diffusion rate in operating device channels. Due to the high resistance near the electrode, the carriers accumulated near the electrode edge immediately diffuse to the electrode, while the carriers in the channel center diffuse relatively slowly. This uneven carrier distribution can be confirmed with the results of Raman mapping mentioned in **Section 4.3**.[140] In recent years, KPFM with fast free force reconstruction has been developed using the G-Mode platform. In this technique, the quantitative recovery of the electrostatic force achieves a time resolution of ~10 μs and enables ultrafast surface potential measurements.[425] This breakthrough makes this method suitable for the 2D study of fast carrier kinetics.

8.3 Conducting Probe Microscopy

Conducting Atomic Force Microscopy (cAFM) working in tapping mode already possesses reliable repeatability for soft materials and shows great potential for the operando OMIEC characterization of local conductivity and viscoelastic properties. Unlike KPFM, cAFM works in contact with the sample surface and applies a DC bias voltage between the probe tip and the substrate to measure the I-V response at the desired point. The local conductivity map as well as the surface morphology can be imaged, even on samples that are highly resistive or surrounded

by insulating regions.[426-428] Because the current can be collected from a larger area than the probe tip, the spatial resolution of the conductivity map is lower than the topographic resolution (10-20 nanometers), but still outperforms standard electrical measurement techniques. The technique effectively avoids surface damage caused by the lateral friction of the probe tip and the constant large current densities near the probe tip.[428] For organic conjugated materials, the ability to quantify the local carrier mobility opens up the possibility of identifying the inhomogeneous current paths and quantifying the density of conducting spots in the presence of both crystalline and amorphous domains.[429, 430] cAFM has been used to characterize mechanical properties and charge transport properties of conjugated polymers during thermal annealing[431, 432] and photo induced conductivity.[433, 434] In addition, Yang et al. investigated the local mobility and charge transport process of conjugated polyelectrolytes (PFBT-X, X is the ions) using cAFM by varying the forward and reverse direction of the bias voltage on the substrate (ITO).[397] In samples with small counter anions (PFBT-Br), the tighter interchain contacts with anions cause higher mobility of the material and strongly decrease the charge injection barriers. For OMIEC materials with external electrolyte in operation, the presence of liquid electrolyte and surface contamination can reduce the reproducibility and validity of cAFM experimental results. However, cAFM working in contact mode does not require operation in vacuum, such that hydrated OMIECs (in high RH conditions) can be studied. Ambient operation leaves open the possibility to design in situ/operando electrochemical cells that allow electrolyte contact, similar to the frit cell employed for operando GIWAXS.

8.4 Infrared photo-atom force microscopy (IR-AFM)

Infrared photo-atom force microscopy (IR-AFM) provides high-spatial resolution IR absorption map as well as the surface morphology and is expected to be compatible with operando OMIEC characterization. IR-AFM achieves a tip limited spatial resolution of 10-100 nm, which is unattainable with traditional wavelength limited FTIR technology. After scanning surface height information, the infrared laser is turned on to detect local IR absorption at the sample surface. Based on different method to acquire IR absorption spectra, IR-AFM can be divided into scattering scanning near-field microscopy (s-SNOM), photo-induced force microscopy (PiFM) and photo-thermal induced resonance (PTIR, also known as AFM-IR and photo expansion microscopy).[435] s-SNOM directly measures the scattering IR light and therefore captures a

scatter background. The other two approach variants extract the IR information from the vibration of AFM probe and are more suitable for OMIEC materials than s-SNOM due to their high signal to noise ratio. PiFM measures IR induced dipole-dipole interactions between the AFM probe tip and the sample surface.[436, 437] Due to the ability to distinguish the characteristic absorption of different components in the sample, this technique has now been widely used in the study of phase separation in organic solar cell materials[438] and the distribution of individual components in cast block co-polymer films.[439, 440] In a recent report, PiFM was used to observe the process of ion diffusion relaxation in dry OMIEC films (PB2T-TEG and P3MEEMT) with no potential bias.[285] The sharp ionic moving front between the neutral and oxidized regions of the material were mapped out by following the characteristic IR absorption peaks of the doped anion PF_6^-. Although PiFM shows the highest spatial resolution among all IR-AFM techniques, this technique works in non-contact mode and requires vacuum conditions, thus preventing its application to hydrated OMIEC materials or those requiring aqueous/liquid electrolytes. As an alternative to PiFM, PTIR works in contact or tapping modes,[441] and measures the thermal expansion of the sample correlated to IR absorption.[442] The technique has been applied to characterize the distribution and transport of water molecules in polymer systems,[443, 444] and is promising for in situ spatial resolution of species within OMIEC materials.

8.5 Strain microscopy

Operando electrochemical strain microscopy (ESM) has been applied in OMIEC characterization[396] and works in aqueous electrolytes for potential dependent strain mapping.[445,446] An alternating electric field is applied via a nanoscale conducting probe, inducing an electron transfer between the tip and the material surface. The inhomogeneous electrostatic field redistributes the moving ions in the solid-state material, which triggers a probe vibration caused by local strain on the material surface.[447] In ESM, the conducting probe acts as a counter electrode for the OMIEC material, providing charging voltage to the material to simulate the electrochemical doping/dedoping of the material in the electrolyte, and thus enabling the operando characterization of the OMIEC devices at the nanoscale. ESM is useful for studying ion diffusion and solvent swelling during OMIEC operation: this technique directly reveals the change in viscoelastic properties and volume in different mesoscale domains under doping/dedoping conditions. Together with cAFM, ESM allows to characterize in real time the

electrical and mechanical properties of OMIECs, deduce ion migration mechanisms and

ultimately guide the molecular design and post-processing of materials.[448, 449]
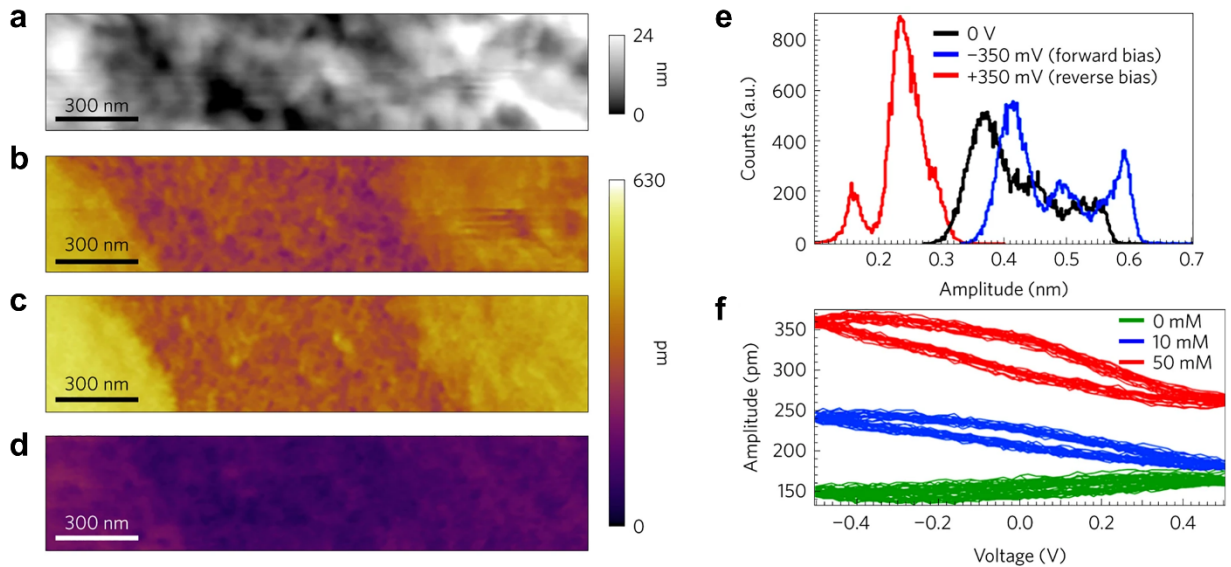
Figure 17 Topography (a) and ESM amplitude images (b–d) of a typical P3HT film in 20 mM KCl. ESM images taken with the tip at 0 V (b), −350 mV (c) and +350 mV (d). (e), Histograms of the ESM amplitude of the same location under different bias conditions, indicating that swelling is primarily observed in forward bias (negative gate voltage) conditions. (f), Switching spectroscopy ESM 'remnant' loops taken at different ionic concentration with the same AFM tip showing enhanced hysteresis at higher concentrations, consistent with a finite ion relaxation time. Adapted with permission from [396]. Copyright 2017 Springer Nature.

The characterization of local variations in ion transport of OMIEC materials by operando ESM was reported by Giridharagopal et al., who measured the sub-nanometer volumetric expansion of a P3HT films due to ion uptake after electrochemical doping.[396] The swelling of P3HT films with different voltage level was explored by applying an additional DC charging voltage to the probe, shown in **Figure 17a-d**. Attributed to counter ion uptake, positive correlation between film swelling and electrochemical doping was observed. In addition to the overall swelling rate, the dispersion (width of distribution, **Figure 17e**), voltage-dependent hysteresis (**Figure 17f**) and local heterogeneity of film swelling were also analyzed. By matching the swelling heterogeneity with the stiffness heterogeneity of the film, the ion uptake was related to the mechanical

1 properties of different domains. This example illustrates how ESM can reveal the strong

2 correlation between morphology, ion concentration, and electrochemical behavior in OMIECs.

3 As this technique is further popularized in the future, the real time monitoring of ion diffusion

4 across different types of OMIEC materials should be within reach.

5 8.6 Scanning electrochemical microscopy

6 Scanning electrochemical microscopy (SECM) employs an electrochemical scanning probe near

7 an electrolyte immersed material to assess its local redox state. This technique can thus be

8 applied to operando OMIEC characterization in the presence of an external electrolyte. SECM

9 quantifies surface fluxes of redox species with high spatial and temporal resolution by recording

10 either the current or potential response.[450] This technique is applicable to various soft matter

11 systems containing liquid electrolytes (such as gels, aqueous electrolytes and ionic liquids) to

12 study ion diffusion,[451] local conductivity[452, 453] and reaction kinetics.[454] Warren et al. reported the

13 use of SECM for imaging modified PEDOT electrodes during biosensing.[398] Regional

14 homogeneity in NADH redox as well as dopant leaking were monitored by SECM and used to

15 optimize the fabrication and post-processing processes of the PEDOT based biosensor. By

16 selecting the appropriate SECM quantification and imaging mode, the redox reactions occurring

17 in both biosensing and small molecule monitoring using OMIEC materials can be monitored in

18 operando conditions. This advantage is particularly relevant for OMIEC devices, as redox active

19 species have been reported to significantly affect the performance, stability and lifetime of

20 OMIEC materials.[185] Mapping these species via SECM is key to better understanding Faradaic

21 reactions in mixed transport devices, and this insight will directly enable the development of

22 improved OMIEC-based devices.

23 The techniques discussed in **Section 8** allow for the direct mapping of physical and chemical

24 processes in OMIECs. Such mapping is amongst the highest resolution that can be achieved for

25 many of these characteristics, however some challenges and drawbacks exist that can limit

26 implementation or applicability. For example, the scanning probe study of charge/potential

27 distributions is limited to devices where charge transport occurs in-plane, which is not

28 necessarily representative of vertically stacked devices; where local microstructural features and

29 transport pathways are likely different in- and out-or-plane. In addition, common to all the

scanning probe approaches is the direct probing of surface properties, which are not necessarily representative of bulk properties. As such, the effect of bulk or out-of-plane morphology is lost and must be assumed or separately investigated.

9. Electron Microscopy

In situ/operando electron microscopy techniques have enabled nanometer-resolution imaging of soft matter samples in ambient and liquid environments,[455] and are thus appealing for applications in OMIEC materials. Conventional scanning transmission electron microscopes (STEM) and transmission electron microscopes (TEM) involve the imaging of solid materials in vacuum, making these techniques suitable only for OMIECs with intrinsic ions working without external electrolytes. In recent years, liquid-phase electron microscopy (LPEM) has enabled the time-resolved characterization of fully solvated soft materials at room temperature.[456] This technique has been widely used for in situ imaging of lithium-ion batteries,[457] biomolecules/cells and molecular dynamic studies of polymerization processes.[458]

Direct imaging of PEDOT clusters formed during electrochemical deposition has been reported by in situ liquid-phase transmission electron microscopy (LPTEM).[459] This technique employs a liquid flow cell (**Figure 18a**) with a channel thickness of 500 nm. Thin (50 nm) electron-transparent silicon nitride films are designed to seal the liquid and enable the cell to withstand the high vacuum of the microscope, as shown in **Figure 18b**. The electrochemical deposition images of PEDOT are shown in **Figure 18c-e**, from which the morphology and coverage ratio of the PEDOT deposited on the glassy electrode can be clearly visualized. This example demonstrates the possibility of in situ/operando imaging of OMIEC materials by LPTEM under different potential, which requires pre-encapsulation of the cast polymer film prior to cell fabrication. In addition to using SiN as the electron window for operando LPEM, graphene has also been chosen in this technique for its excellent mechanical properties, physical impermeability, and chemical stability.[460, 461] Due to the atomic thickness of graphene, the spatial resolution of LPTM can be further increased,[462] from several nanometers to atomic level.[463] Performing operando EM on OMIECs still requires more efforts, including reducing damage of OMIEC materials from the electron beam and solvent perturbation during measurements,[464] as well as controlling decomposition products from radiation exposure of organic materials.[456]
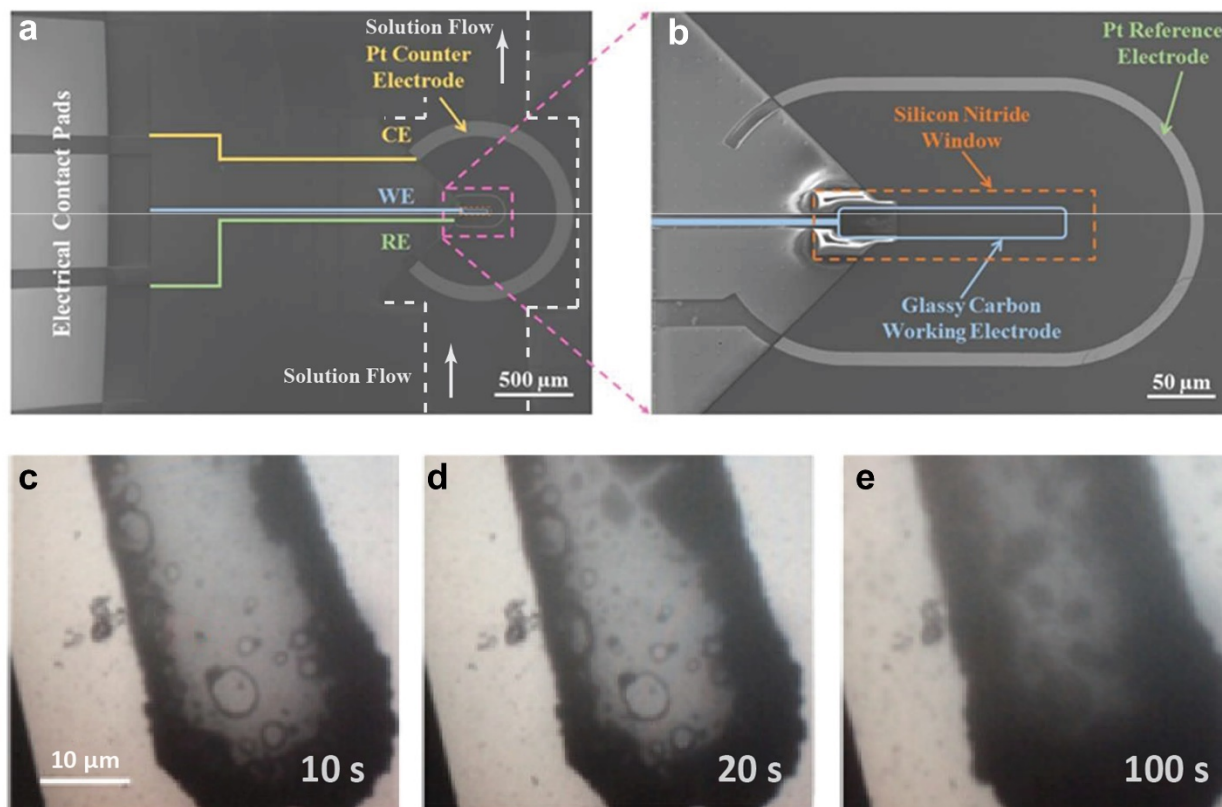
Figure 18 Top view of LPTEM electrochemical chip showing (a) electrical contact pads with the liquid flow cell (white), working (blue), reference (green) and counter electrodes (yellow); b) Higher magnification image for glassy carbon working electrode with thin electron-transparent silicon nitride window. Electrochemical deposition of PEDOT under a constant voltage of +1.2V after (c) 10s, (d) 20s and (e) 100s. Adapted with permission from [459]. Copyright 2015 American Chemical Society.

Apart from the morphology determination, electron microscopy can also combine with X-ray detectors (mostly silicon drift detectors) for elemental analysis, known as energy dispersive X-ray microanalysis (EDS).[465] This technique measures elemental characteristic X-rays produced by outer shell electrons as they fill the inner shell holes created by the incident electron beams.[466] There are two major problems to be solved before EDS can be used for the operando characterization of OMIECs: polymers are notorious for electron beam damages, and the additional EDS measurement would further damage the samples. The outer shell electron transitions of light elements (for example, C, N and O) are known to excite Auger electrons,

causing a decrease in X-rays yield.[467] Consequently, higher incident electron beam doses are required to obtain EDS signals for conjugated polymers. The second problem is the relatively high vacuum requirement for EDS measurements, due to electron beam scattering and X-ray absorption of the atmosphere. There have been reports for environmental EDS at the resin/Al interface with the existence of water vapor and helium (up to 15 torr).[468, 469] However, this is still far away from the operando conditions of most OMIECs, which makes EDS less suitable for mixed conducting applications than other elemental analysis methods such as XRF and APXPS.

10. In Silico Characterization Methods

The advantages of computational approaches when investigating OMIEC materials go beyond simply reproducing experimentally observed trends. On the one hand, the atomistic resolution of the 'computational microscope' offers the possibility to directly observe local events or individual features that most spectroscopic or structural characterization techniques can only capture as the average ensemble of all possible states. Molecular simulations can also have a remarkable predictive power in the rational design of materials. Data-driven approaches that combine inexpensive computational methods with machine learning and high-throughput algorithms have enabled the screening of large libraries of compounds that can be optimized in silico before bench-top testing, thus accelerating innovation.[470-473] Finally, simulations can be used to run 'alchemical' experiments, where the effect of a particular substitution or group on a given material's properties is tested by either removing it, displacing it or chemically altering it; whereas the same wet lab experiment can often be too time consuming or not possible, it can become affordable and sometimes even trivial to run in silico.[474]

In the following subsections, we outline the main advantages and limitations of molecular simulations in complementing operando measurements on OMIECs, focusing mainly on electronic structure calculations and molecular dynamics simulations, and how these two frameworks can be integrated to characterize the structural and transport properties of OMIECs (see **Figure 19**). Among ab initio methods we focus on density functional theory calculations as they are the most widely employed in the computational materials science and organic electronics communities, either as a standalone technique (**Section 10.1.1**) or in combination with classical simulations (**Section 10.1.2-10.1.3**). In **Section 10.2** we discuss classical

molecular dynamics simulations, detailing OMIEC-relevant applications for both atomistic (**Section 10.2.1**) and coarse-grained force fields (**Section 10.2.2**). We leave out of this discussion numerical device models such as Monte Carlo algorithms,[475-478] master equation approaches[479, 480] or drift-diffusion models,[101, 481, 482] as these methods are reliant on parameters derived from ab initio calculations[483] and highly dependent on experimental device setup.[484, 485]
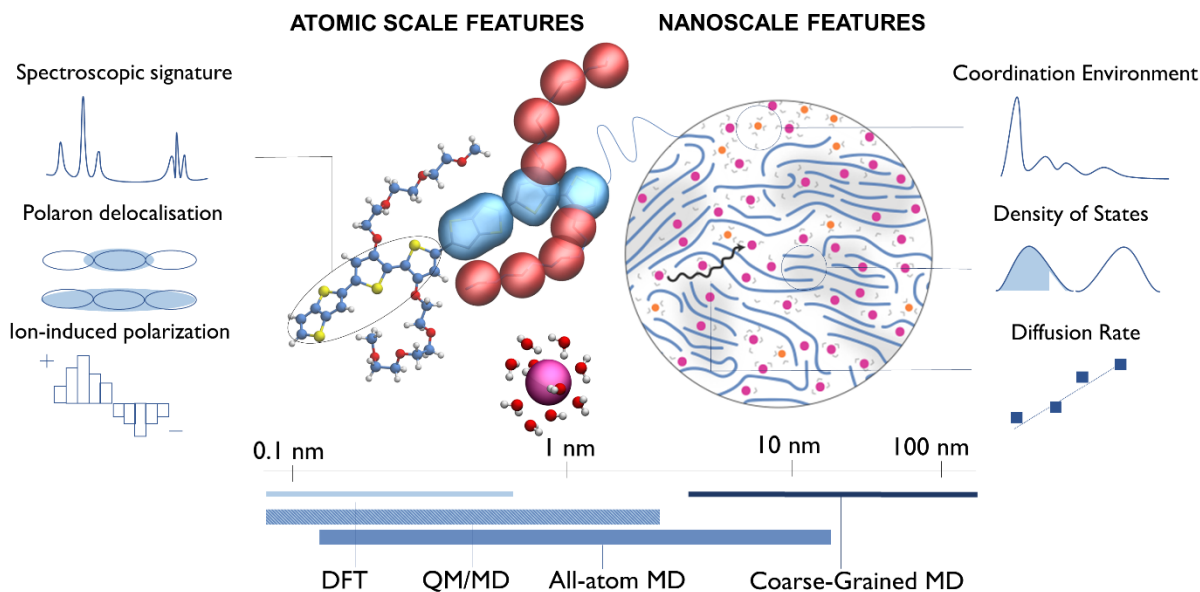
Figure 19: Overview of the computational methods for OMIECs characterization presented in **Section 10**, and representative examples of the information that can be extracted at the atomic scale and nanoscale level.

10.1. Ab initio electronic structure methods

Electronic structure calculations are routinely used in the characterization of OMIECs and the wider class of organic conducting materials. They are essential tools to elucidate the reactivity, spectroscopic signatures (Raman, IR and UV-Vis, see **Section 4**), structural features (conformational energies, steric interactions) as well as electrochemical, electronic and energetic parameters related to electronic mobility (frontier orbital energies, orbital localization, reorganization energies).

Thanks to their optimal balance between accuracy and computational cost,[486, 487] density functional theory (DFT) and its time-dependent formalism (TD-DFT) are the most widely employed electronic structure methods for the study of organic semiconductors and OMIEC materials. For this reason, DFT will be the main focus of the following section. The general principle of DFT states that the electronic properties of a multi-electron system are a functional (function of a function) of its electronic density, however the exact mathematical form describing electron correlation in many body systems is not known.[486, 487] Different approximations have been developed to build functionals of the electronic density, and many density functional approximations (DFAs) are available.[488, 489] While a detailed discussion of DFAs is well beyond the scope of this review, we must mention that many widely used functionals contain empirical parameters, and can therefore fail when applied to different classes of compounds than the data set they were optimized against.

The popularity of DFT and the wide choice of software implementations to perform calculations have essentially turned it into a 'black box' tool;[490, 491] DFT calculations of small OMIEC oligomers are a routinely performed to gain insight on orbital energies, polaron delocalization length or torsional barriers between conjugated units. However, it must be pointed out that many popular DFAs present well known shortcomings[492] that can negatively affect the reliability of the predictions made. For this reason, a range of corrections have been developed to address these issues. For instance, the excessive delocalization of the wavefunction resulting in the underestimation of barrier heights, bandgaps and excited state energies[493] can be prevented by using range-separate functionals.[494] Another important drawback of DFAs is in the incorrect representation of dispersion interactions, that are subtle yet extremely consequential for the stability of organic and biological materials. Dispersion-inclusive functionals are now the standard for the study of non-covalent interactions in systems like molecular crystals or supramolecular complexes.[489, 495]

Semiempirical methods derived from DFT or Hartree-Fock formalisms are commonly used for the calculation of large systems (>100 atoms) or in high-throughput studies, as they afford a computational speed up of three orders of magnitude with respect to DFT.[496] In these methods, interatomic integrals constituting the Hamiltonian are either taken from tabulated, pre-calculated contributions (as in DFTB, where they are calculated from DFT), or partially neglected (as for

HF-based methods). In the latter case, experimental data such as the enthalpy of formation ΔH_f are also used to fit the parameters, therefore these methods can perform poorly for systems falling outside the intended class of materials. Besides, semiempirical methods inherit the shortcomings relative to their parent methods: the lack of electron correlation (particularly for HF)[497, 498] and the poor treatment of dispersion interactions,[499] which is also present in certain DFAs. Just as in the case of DFT, these issues have been addressed by developing dispersion corrections aimed at better reproducing non-bonded interactions such as van der Waals interactions or hydrogen bonds.[496] In the context of OMIECs, semiempirical methods with the appropriate corrections can be a useful, cost effective tool to study charge transport in soft materials.

10.1.1 Standalone DFT methods

In the context of OMIEC and related polymers, DFT calculations have been a key aide in the study of their reactivity,[500-504] conformational[505, 506] and electronic properties,[507, 508] charge transport[509], ion doping[244, 509-513] and thermoelectric properties.[512, 514] Notably, DFT has become the standard computational methodology for the interpretation of spectroscopic features arising from inelastic neutron scattering experiments,[370] UV-Vis,[515, 516] IR and Raman spectroscopy.[146, 245, 517-521] In combination with Raman spectroscopy, insight from DFT calculations can resolve fine polymer stacking features that cannot be fully characterized from X-ray scattering experiments alone.[146, 243, 517] The spectral signatures of organic semiconducting species can be attributed to either internal modes or inter-molecular modes. While internal modes can be studied by performing DFT calculations of single molecules or oligomers in vacuum,[522] those associated with long-range ordering and by intermolecular aggregation can be obtained by performing periodic DFT calculations on crystalline cells.[517, 523] However, the degree of fine tuning and the possibility to apply higher order perturbation corrections (beyond the harmonic approximation)[520, 524, 525] to achieve a correct reproduction of experimental transitions contribute to make theoretical vibrational spectroscopy far from a black-box method.[526, 527] In addition, the $O(N^3)$ scaling of standard DFT methods (where N is the number of atoms) poses a limit in the size of the system as well as the possibility to take into account environmental factors. As an example, the calculation for a single oligomer in DFT is often limited to less than 10 repeat units,

and it is usually necessary to perform calculations for a series of small oligomers in order to verify that Raman spectral features are converged to the polymer limit.[146, 243]

DFT methods have been also used to describe the effect of ion doping on the charge density, charge localization and energy levels of OMIECs and related materials.[509-513, 528] A recent work[529] estimates the capacitive interaction between a p-doped EDOT oligomer and negative ions, arguing that each ion-polaron couple could be considered as an independent capacitor. The calculated capacitance is in qualitative agreement with experiments, despite the lack of polarization and screening effects arising from solvent molecules and electrostatics/dispersion interactions between doped polymer chains. This idealized model is an initial step towards a molecular-scale description of the capacitance of PEDOT and other OMIECs; further work integrating a DFT approach with MD-simulated OMIEC morphologies in the presence of water[530-532] will be key to describe the interactions between OMIECs and electrolytes in operando conditions.

10.1.2 DFT calculations on nanoscale morphologies

Overall, the conformational disorder and heterogeneous morphology that characterize OMIEC materials limit the scope of electronic structure calculations, which on their own can only provide information around a local energy minimum. Conversely, DFT or semiempirical single-point calculations performed on an ensemble of polymer conformations stemming from classical molecular dynamics trajectories can be extremely informative. The data extracted from such a collection allows the calculation of key charge transport parameters such as density of states, localization length, energetic disorder, electronic couplings between chains and percolation pathways for charge carriers, ultimately allowing to estimate the electronic mobility.[533] Rolland and coworkers employ this sequential approach to study amorphous aggregates of PEDOT:Tos at different hydration levels.[534] PEDOT is p-doped by negatively charged Tos molecule in an overall electroneutral simulation box, mimicking operating conditions. The relationship between morphology and mobility is analyzed by calculating percolative networks across the material and evaluating charge mobility through a mean-field approach. For simulations on shorter PEDOT oligomers, as the water content increases, the mobility decreases due to the inter-crystallite links being weakened. In the case of longer chains, however, the mobility plateaus and is not affected

by hydration. These results are in good agreement with experimental reports on conducting polymers,[84] showing how effective π-stacking in small subdomains is more important than long-range order and providing a general framework to describe morphology and mobility trends in PEDOT-based OMIECs.[84]

The mean field approach used by Rolland et al. to calculate charge mobilities is effective to describe general trends, however it should be noted that this approach neglects the interaction between charge carriers at high charge densities,[85] the screening effect of the environment and the electrolyte-polaron interactions that are expected to play a role under device relevant operating conditions. In order to fully elucidate this picture, a new theoretical/computational paradigm able to describe ionic and electronic conduction, and the interaction between ionic and electronic charge carriers, in a high dielectric medium and at high charge density will need to be developed.[79, 535] Structural and spectroscopic information in operando conditions will be critical to achieve a better fundamental understanding of the interplay between electronic processes, ion doping and diffusion across heterogeneous morphologies, thus informing the development of computational and theoretical framework for mixed conduction.

10.1.3 Quantum mechanics/molecular dynamics simulations

Quantum mechanics/molecular mechanics (QM/MM, also known as QM/MD from molecular dynamics) simulations combine the possibility to investigate electronic properties of a system while accounting for dynamic effects with a classical potential.[536, 537] This feature is especially attractive for the study of solvent effects and electrolyte doping in OMIECs. QM/MM algorithms subdivide the system in 2 regions, one treated at QM level and the other with a classical force field. The feedback between the 2 layers can be implemented in different ways,[538-542] but the general feature of these models is that the QM region affects the forces of the MM region while the latter in turn affects the potential energy landscape calculated by the former. The timescale accessible by QM/MM simulations strongly depends on the level of theory and number of atoms in the QM portion of the system. This is because DFT calculations scale with $O(N^3)$ while MD simulations scale with $O(N)$, where N is the number of atoms in the system. QM/MM methods are widely employed in the study of reactivity, solvatochromic effects, photochemical processes and are thus well established in the biomolecular field.[543-546] In the case

of conjugated polymers, polyelectrolytes and OMIECs, these methods have so far been underutilized;[547-549] few examples exist of QM/MM simulation of conjugated polyelectrolytes to investigate solvation effects[550] or study the electronic properties of redox polymers in bulk-like amorphous morphologies.[551] The possibility to describe dynamic polarization effects,[552] charge localization and ion doping at the quantum mechanical level makes QM/MM schemes suitable for the study of mixed ionic/electronic conduction. However, if studying short oligomers at infinite dilution where the QM region is as small and localized is technically possible, this would represent an idealized model. The study of realistic, thin film-like morphologies would create a substantial bottleneck as the entire polymer phase would need to be treated at the QM level. As the computing resources required for large scale, accurate DFT calculations become cheaper, and semiempirical or linear-scaling electronic structure methods reach full maturity, QM/MM schemes could become more widespread in the study of OMIECs and electrolyte interfaces.[553-555]

10.2. Molecular Dynamics Simulations

Molecular dynamics (MD) simulations are a key tool for in silico OMIEC characterization. They can provide valuable insight on both i) dynamical properties such as electrolyte diffusion, segmental chain motion and swelling and ii) equilibrium properties such as aggregation, non-bonding interactions and conformational features (side chain and backbone flexibility, electrolyte coordination). Due to the possibility to apply external forces, MD simulations can also be used to investigate viscoelastic properties[556-559] and thermoelectric behavior.[509, 560-562] In all the instances above, and particularly when studying OMIECs or other polymers, extended sampling of the system is required to capture the full range of thermally accessible states. The structural information obtained from MD simulations includes radial distribution functions, simulated scattering patterns, order parameters, and coordination numbers; making it an ideal complement to X-ray scattering and absorption characterization techniques. Notably, atomistic MD studies have been successfully paired to QENS techniques to investigate the segmental motion of backbone and side chain fragments in polymer melts (see **Section** 6.4.2).

Classical MD simulations describe the time evolution of a system according to Newton's equations of motion, treating atoms as rigid spheres with fixed connectivity and neglecting chemical reactivity and charge polarizability. The system can be defined either at the atomistic

level or at a coarser scale; in order of decreasing resolution and computational cost, they range from all-atom MD simulations, to united-atom models where hydrogens are omitted, to coarse-grained (CG) MD, where each 'bead' can represent multiple atoms or molecules. The collection of parameters describing all bonded and non-bonded interactions in the system is defined as a force field, and is usually parameterized against experimental data and/or quantum chemical calculations for a given class of compounds.[563-565] Simulating a novel system requires a careful selection of the most appropriate force field parameters, and it is common to refine many-body parameters (partial atomic charges and torsional potentials between molecular fragments) using DFT calculations as a reference. This is particularly important in the field of conjugated polymers when dealing with a novel organic fragment or connecting pattern between groups.

10.2.1 Atomistic Molecular Dynamics

Several atomistic MD studies of OMIECs have provided insight on general structure-property relationships that indirectly inform device operation. The prominence of PEDOT and its blends across a wide range of applications has spurred many studies dedicated to understanding its interfacial properties, self-assembly and electronic transport properties.[566-571] Recent studies have focused on understanding electrolyte-polymer interactions[572] and morphological changes[572, 573] in conditions mimicking those of operating devices.[574]

Conjugated polymers bearing glycolated side chains have recently surged as alternatives to PEDOT in mixed conducting devices. Various computational studies on these materials have focused on the interactions between electrolytes and polar side chains in glycolated polythiophenes, highlighting how the choice of anions,[575] as well as the side chain chemistry[21, 576] modulate ion coordination, chelation and conductivity (see also **Figure 20a**).[21, 577] Other studies have leveraged MD simulations jointly with experimental characterization techniques to elucidate morphological trends. Side chain engineering studies[578, 579] have highlighted the key role of the ethylene glycol chain length in determining the balance between ordered and disordered microstructure, where the former is driven by backbone π-stacking and the latter is dominated by increased conformational entropy. The challenge of side chain engineering studies is the simultaneous presence of other concurring variables that cannot be completely decoupled: molecular weight, polydispersity and solubility are just some of them. This results in non-

linearities and hinders a straightforward prediction of mobility trends. In this respect, MD simulations offer an inexpensive way of decoupling these effects by performing computational experiments under controlled conditions.

While most examples reported so far tend to approximate experimental non-operating conditions or do not explicitly account for the doping effect on OMIECs, few studies have attempted the simulation of doped mixed conducting materials to reproduce experimental swelling behavior and electrolyte-polymer interactions. A report by Gladisch et al.[46] uses MD simulations to investigate the reversible swelling and water intake of the glycolated polythiophene p(gT2) in the fully doped state and in the presence of electrolytes. The simulations results show the swelling of the doped polymer aggregate is entirely due to the electrostatic interaction between polymer and electrolyte, which drives the ions with its solvation shell inside the polymer film. This conclusion is corroborated by a counter-experiment in which counterions are already inserted within the polymer aggregate: in this case once the polymer is doped the swelling does not occur. Gosh et al. recently studied another reversible structural change in an OMIEC material (PB2T-TEG) upon oxidation and ion injection.[285, 580] In this case, MD simulations highlight the role of the substrate in promoting a morphology transition during electrochemical oxidation and ion injection; the anisotropy between simulated scattering patterns in-plane and out-of-plane agrees with experimentally reported X-ray diffraction data (see **Figure 20b**).
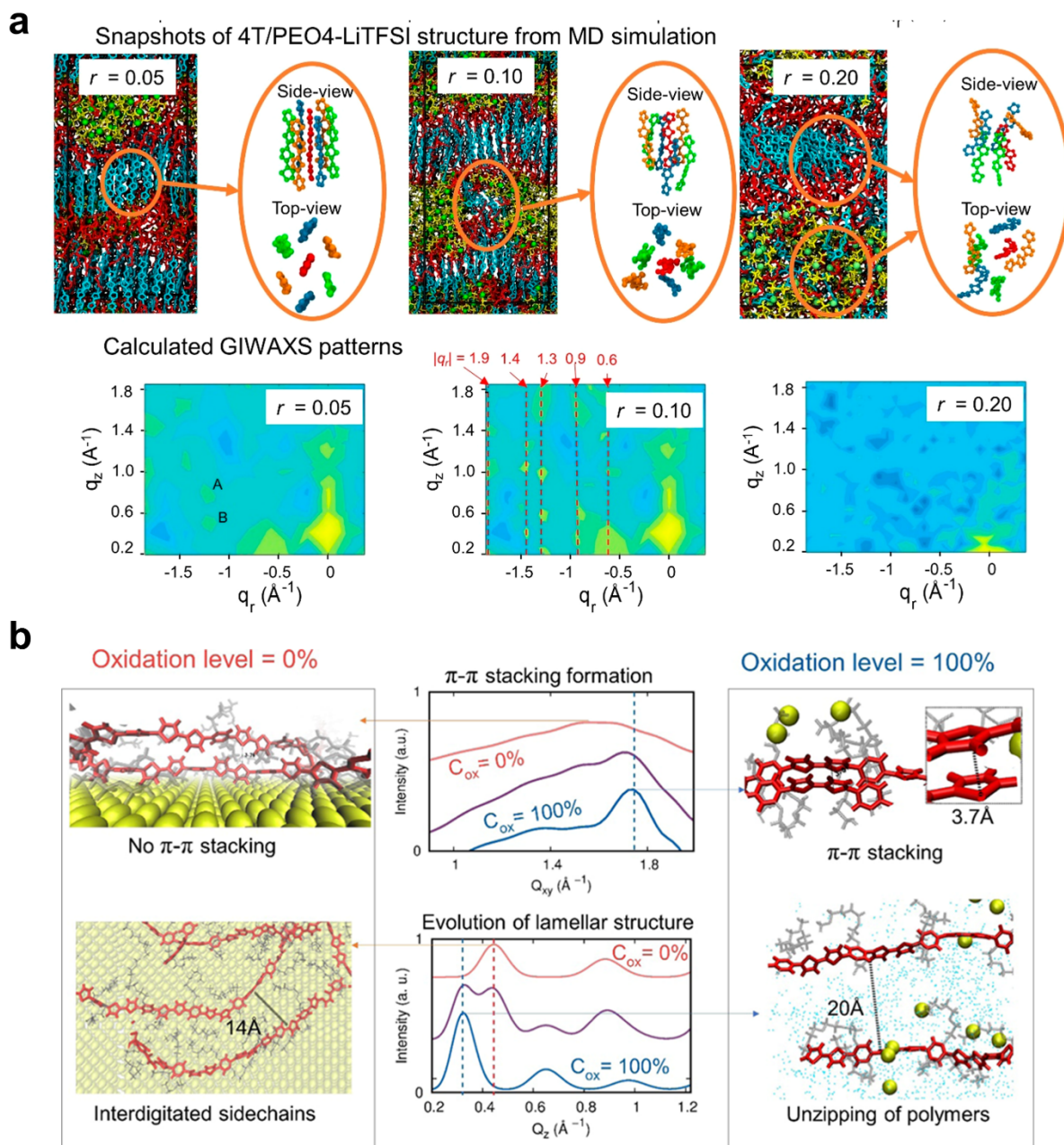
Figure 20. Examples of atomistic MD simulations elucidating structural changes upon ion doping in OMIECs. a) MD simulations of the liquid crystal 4T/PEO4 in the presence of LiTFSI. The morphology and calculated GIWAXS patterns at different values of r = [Li+]/[EO] are shown. Adapted from [577]. Copyright 2019 American Chemical Society. b) MD simulations of a PB2T-TEG hydrated polymer film on a gold substrate at different oxidation degrees. Morphology and X-ray diffraction (XRD) simulated curve plotted along the π-π stacking and lamellar directions. Adapted from [580]. Copyright 2020 American Chemical Society.

It is important to note that the timescales for morphological changes observed in operando experiments transcend those normally achievable with all-atom MD (~1 µs). A study of the structural evolution and swelling behavior of OMIECs with atomistic MD frameworks is possible, albeit only if we limit ourselves to oligomers short enough to escape kinetic traps within this simulation window (see **Section 4.3**). However, it is still possible to gain some insight from the simulation of shorter oligomers. The characteristic polymer length scales observed in scattering experiments are essentially dictated by π-stacking and lamellar spacing, and these features are expected to be found in both short-range and long-range ordered domains, regardless of polymer length. This might explain why computational studies such as the above, despite the smaller system size and shorter timescale, successfully capture the key trends and structural transitions caused by electrolyte insertion and doping.

Nonetheless, atomistic MD simulations present several issues that currently limit their impact on OMIECs studies, particularly for operando conditions. On the one hand, the need to refine and check force field parameters for each new fragment means that a certain degree of manual intervention is always needed, making parameterization and validation rather tedious tasks. In this context, efforts to increase reproducibility by simultaneously standardizing the force field development pipeline and making datasets available on public repositories are underway. Notably, machine learning tools are starting to take off as a way to achieve classic transferable force fields,[581-584] however autonomous learning algorithms present two main issues that currently limit their immediate application to OMIEC materials: the need to gather large training sets, which is challenging given the few available mixed conducting polymers, and the fact that some of these models do not explicitly include long range electrostatic interactions.[585-588]

Indeed, the biggest fundamental obstacle limiting the straightforward application of MD simulations to operando studies of OMIECs is the classical treatment of electrostatic forces. If the structural and morphologic properties of OMIECs cannot be represented successfully with fixed charges, the transport properties associated with operando conditions appear more challenging. The high electrolyte concentrations achieved in mixed conducting devices and the importance of ion-OMIEC electrostatic interactions limit the accuracy of force fields having fixed point charges, which in practice adopt a mean-field approximation. As in the case of ionic liquids, the strong polarization in OMIECs in operating conditions makes this approximation no

longer valid, potentially leading to errors in the estimation of diffusion properties, ion-ion

correlation and screening effects.[589-591] The adoption of fluctuating charge schemes[592] or Drude

oscillator models[593] provide a solution, however at an additional computational cost. The

continuous increase in high-performance computing power has contributed to the

implementation of polarizable models for large-scale simulations.[589, 594-598] The research

community is actively developing models for solid-state polymer electrolytes, given their

relevance for energy storage applications.[599] Overall, this effort will soon make large-scale

accurate atomistic simulations more mainstream, enabling their use for OMIECs.

10.2.2 Coarse-grained models

Classical all-atom MD simulations are not suited for the sampling of rare events or phenomena

having timescales that far exceed those of molecular vibrations, such as those involving

segmental motion and chain relaxation in polymer melts. In relation to OMIECs, polymer

electrolytes and polyelectrolytes, it is well understood that segmental motion is a critical

phenomenon affecting ion transport. Unless simulating short oligomer chains, an 'equilibrated'

morphology cannot be achieved, and the system reaches instead a kinetically trapped state.

Among the solutions to this issue, coarse-grained (CG) models have proven very successful both

to study the general behavior of polymers and to enable the simulation of realistic

morphologies. CG models represent molecules as a collection of beads and springs,[600] each bead

encompassing several atoms. This lower resolution allows to effectively smoothen the potential

energy surface of the system, integrate over the faster degrees of freedom to overcome kinetic

traps and explore materials properties at the mesoscale.

General CG models are 'top down' models, meaning they are not meant to reproduce a specific

molecule but rather apply to a wide class of materials, for which it is possible to extract general

trends and structure-properties rules. They have been applied successfully to investigate the

charge transport in redox-active polymers,[601] the morphology of polymer electrolytes, the ion-

polymer interactions and ion diffusion,[602, 603] A recent work from Khot et al.[604] uses a top-down

approach to model the morphology and ionic/electronic mobility of a generic OMIEC polymer at

different hydration levels and doping levels. The model uses a hybrid coarse grained model that

combines Gay-Berne ellipsoids and spherical MARTINI beads to describe a generic glycolated

conjugated polymer (see **Figure 21a**). The key findings showed that accounting for electrostatic ion-polymer interactions suppressed electronic mobility, however the differences in mobility at different hydration levels cover a relatively small range. On the contrary, ion mobility was found to increase linearly with water content, unlike in other CG simulations of OMIECs.[605]

The opposite, top-down approach in CG simulations is instead to explicitly map a system to a collection of beads, parameterizing the force field to reproduce either the structural,[606, 607] thermodynamic properties,[608] or the forces[609] of the corresponding all-atom system.[610, 611] This method has two main advantages: it is chemistry-specific, and it gives the possibility to 'backmap' to the all-atom model as needed, for instance to perform electronic structure calculations starting from simulation snapshots of the equilibrated system. Although some tools to streamline the mapping and parameterization of CG models are available,[606, 612-615] however there is not a universal guideline or standard as to how to map systems with a low degree of symmetry, such as conjugated fragments or fragments having an uneven number of atoms.

Overall, the longer parameterization procedure is compensated by a substantial speed up of the simulations between 2 and 5 orders of magnitude[616] with respect to all-atom simulations, making CG simulations extremely attractive for the study of experimentally-relevant OMIECs morphologies. Indeed, this approach was used to study the interplay between polymer oxidation, swelling morphology and ion diffusion in PEDOT:Tos[605] (see also **Figure 21b**) and PEDOT:PSS.[617] Modarresi and coworkers simulated the aggregation of PEDOT:PSS in water at different pH (corresponding to different PSS protonation states) starting from either a homogeneous dispersion or a core PEDOT-shell PSS,[618] in the presence of Na^+ and Cl^- ions. For the homogeneous dispersion, the formation of PEDOT crystallites was not observed regardless of the pH level. On the other hand, the core-shell morphology was found to be dependent on the pH. The PEDOT-rich and PSS-rich regions were maintained at pH=0 and pH=5, while at intermediate pH (3.5) the simulations showed a higher degree of dispersion and a more homogeneous phase. Another study from the same group investigated the effect of PEDOT oxidation on swelling.[619] When a net positive charge was added to PEDOT and a corresponding amount of protons were removed from PSS, the PSS-rich phase swelled with water. In the PEDOT-rich phase, swelling was found to be proportional to the oxidation state, with the fully oxidized PEDOT swelling the most.
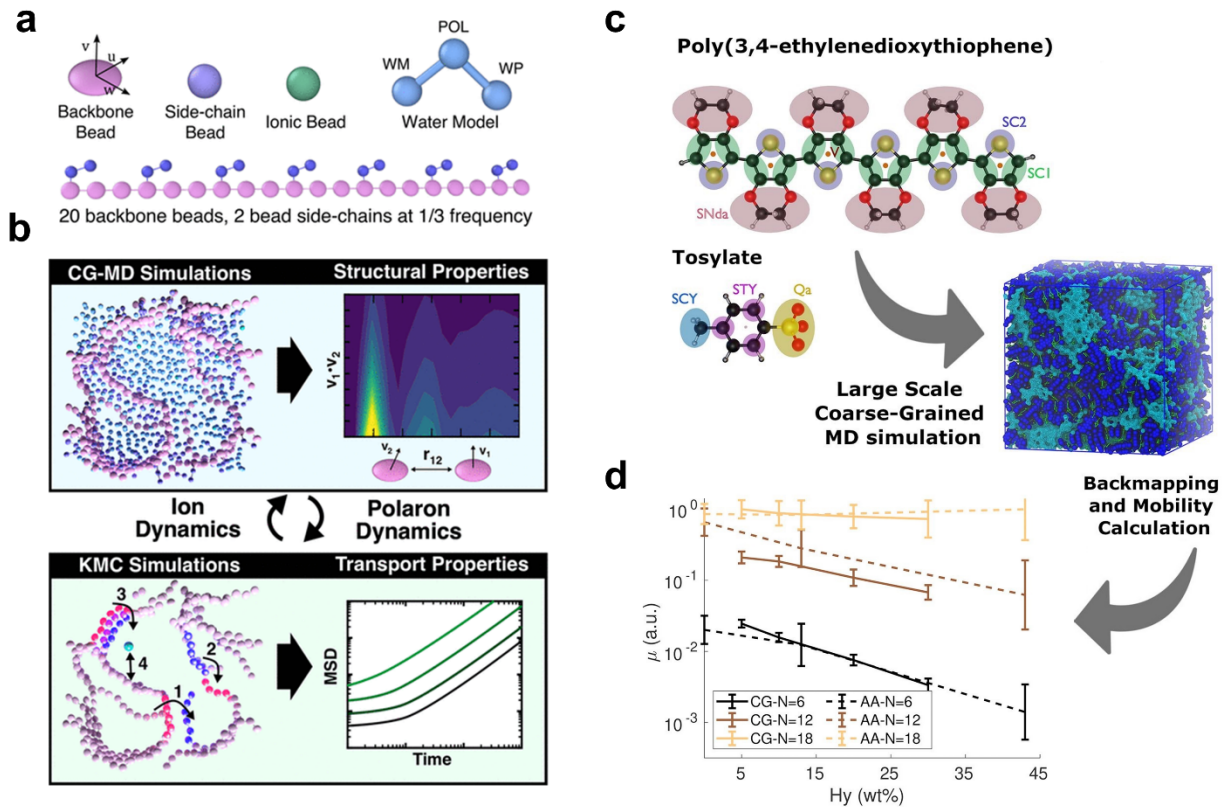
Figure 21. Comparison between top-down (left) and bottom-up (right) coarse grained MD approaches for the study of OMIECs. a) Force field for a generic mixed conducting polymer with polar side chains. b) Overview of the procedure used in ref. [604] to extract information on ion dynamics, electronic transport and mixed conductor morphology. Kinetic Monte Carlo simulations are used to characterize polaron dynamics, in particular (1) interchain charge transfer, (2) intrachain charge transfer, (3) π–π aggregation, and (4) ion–polaron coupling. Adapted with permission from [604]. Copyright 2021 American Chemical Society. c) Coarse-grained force field of PEDOT:Tos used to investigate its aggregation and morphology at different hydration levels. d) Electronic mobility as a function of water content and PEDOT chain length from coarse-grained PEDOT:Tos morphologies backmapped to the atomistic level. Adapted with permission from ref. [618] under CC BY 3.0 license.
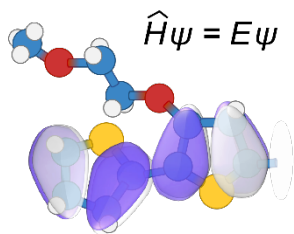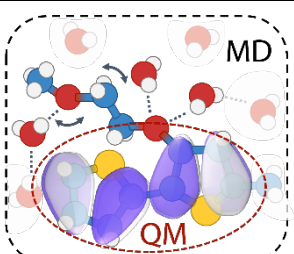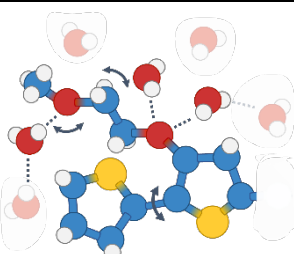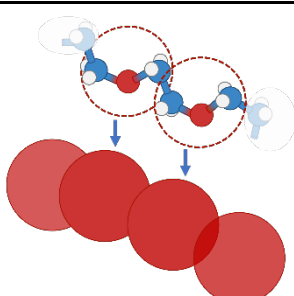
Overall, CG simulations find their ideal application in the study of amphiphilic polymers such as OMIECs and can capture the relevant trends in hydration, electrolyte percolation and polymer aggregation at a device relevant scale. However, these models present the same caveats discussed above regarding the treatment of electrostatic interactions, with some additional issues.

For instance, the loss of directional interactions such as hydrogen bonds means that ad-hoc models that re-insert these features[620] will need to be used for materials where these interactions dictate the nanoscale morphology. In a similar way, losing the atomistic resolution might also preclude the study of systems where confinement effects are important, such as the trapping of solvent or electrolyte inside ordered domains or in gel-like phases.

Moreover, CG trajectories are effectively accelerated with respect to atomistic ones. While in some cases it is possible to apply a 'rescaling factor' to retrieve the corresponding atomistic timescales, in some cases – particularly where multiple CG resolutions are used – the actual scaling factor for dynamical properties will be ambiguous at best.[615, 621] Therefore, when extracting electrolyte diffusion constants from CG dynamics it is best to either report a trend by comparing different ions or simulation conditions or seek a qualitative agreement with experiments. Obtaining accurate estimates of ion/electrolyte diffusion in CG models (as well as in all-atom MD) depends not only on the fine tuning of non-bonded interaction terms of the chosen force field, but also on the presence of friction or dissipative energy terms.[615]

Reverting from the CG system to its all-atom equivalent – an operation known as backmapping – allows to observe atomic-scale interactions at CG-equilibrated morphologies;[617] however this imposes an upper limit on the system size and/or simulation length. If the goal is to perform ab initio calculations on each conjugated fragment to retrieve a distribution of orbital energies or electronic couplings over many trajectory frames, this could mean having to perform hundreds of thousands of calculations - a daunting task even with approximate electronic structure methods. In such a scenario it may seem attractive to bypass the atomistic backmapping altogether, and instead train a machine learning model to reproduce the key electronic properties of a polymer segment directly from the CG trajectory.[622] A fully coarse-grained approach incorporating insight extracted from electronic structure calculations would be an extremely valuable tool to bridge the current divide between device-scale phenomena and simulations in many polymer-based devices, especially those based on OMIECs.

Table 5. Summary of in silico methods employed in the study of OMIECs.

Method	Description	No. of atoms	Timescale	Information extracted	Representative example(s)	Implementation barriers
Electronic structure methods	$\hat{H}\psi = E\psi$ Methods solving the Schrödinger equation at frozen nuclei. DFT is the most widespread.	$10\text{-}10^2$	-	Optimized geometries, conformational energies, electronic energy levels, charge transport parameters	PEDOT[501, 507, 515, 517-519, 528, 529, 623]	Scaling $O(N^3)$; no dynamic or explicit environment effects
QM/MD	MD QM Inner shell treated at QM level; outer shell treated classically (MD)	$10\text{ -}10^2$ (QM shell), $10^3\text{ -}10^8$ (MD shell)	Depends on size and update frequency of QM portion	Adds dynamic and solvation effects to the QM information	Oligothiophenes[549, 550]	Scaling of QM shell; QM/MD boundary can affect results[538, 624, 625]
All-atom MD	Atoms (bonds) treated as rigid spheres (springs) described by classical dynamics	$10^3\text{ -}10^8$	$10^{-6}\text{ -}10^{-4}$ s	Electrolyte diffusion rates, coordination environment, polymer morphology, viscoelastic properties	PEDOT:PSS,[573] PEDOT:Tos,[534] glycolated oligo/polythiophenes,[575, 576, 578, 579] PB2T-TEG[580]	Rare events require enhanced sampling methods[626]
Coarse-Grained MD		-	-	Accelerated dynamics capture self-organization and ion/solvent diffusion in device-scale morphologies	PEDOT:Tos,[605] PEDOT:PSS,[618] generic OMIECs[604]	Cannot correctly describe time-dependent phenomena; requires backmapping to atomistic MD

	Atoms are mapped to beads, reducing the degrees of freedom.					

11. Conclusion and perspectives

Operando characterization aims to perform accurate structural, morphological, mechanical, and compositional analysis of application-relevant OMIECs to reveal their complex structure-property relationships and how they change during device operation. Such insights would guide mechanistic understanding of transport, optoelectronic and mechanical properties, to better understand devices, and to design new high performing materials. This review illustrates recent advances in operando OMIEC characterization, including spectroscopy, scattering, gravimetry, microscope probe techniques and computational simulation. Among these techniques, operando spectroscopies provide valuable insight on electronic transitions, charge populations and molecular packing. Operando scattering techniques focus on structural information at the molecular and domain scale. Scanning probe techniques map spatial resolved morphology, electrical and mechanical properties of OMIEC materials. In silico approaches have provided complementary information to spectroscopic and structural techniques and are being leveraged to unveil electronic and ionic transport at molecular scale. Most of these currently available operando characterizations can be done for OMIECs operating in dry conditions, however many OMIEC based technologies require the presence of residual solvent or an external liquid electrolyte which adds challenges towards experimental implementation. In general, operando characterization for OMIECs requires the enhancement of the effective OMIEC signal as well as the reduction of the background, for example, to separate the electrolyte and the beam path. In addition, operando experiments often demand high temporal resolution, which requires the improvement of the characterization signal-to-noise ratio as well. Operando experiments also seek good spatial resolution, especially for mapping techniques.

On the theoretical side, the framework to describe electronic charge transport in organic semiconductors is well established, but a complete characterization of ion doping, and ionic-electronic coupling is still lacking. If a classic, mean-field picture is perhaps sufficient to describe the behavior of highly doped organic materials,[627] this model may no longer hold for

intermediate or low ionic strengths and charge densities.[79, 535] For these reasons, a comprehensive theory of electronic-ionic transport in OMIECs is a crucial step in the systematic betterment of mixed conducting devices and materials. Conversely, ion diffusion and coordination properties are straightforward observables that naturally emerge from molecular dynamic simulations; although observing these phenomena across device-relevant morphologies is still challenging due to the long simulation times required to study polymer melts.

Existing operando techniques are not yet sufficient to fully elucidate the complex structural and compositional relationships in OMIECs during operation. The introduction of new operando techniques, such as X-ray absorption spectroscopy, X-ray photon correlation spectroscopy, and electron microscopy are promising in future OMIEC characterization. First, these techniques add solid experimental evidence and details to the already existing operando toolbox. For example, electron microscopy directly images the nano scale molecular structure/packing and is a powerful complement to scattering techniques. Second, they provide unique information of OMIECs in working conditions. For example, XAS has the potential to reveal compositional dynamics and molecular coordination, both of which are difficult to elucidate via other techniques. XPCS uniquely tracks the chain dynamics of polymers and opens new perspectives on ion transport.

Finally, we should also look towards the combination of operando techniques to provide comprehensive and accurate description of OMIECs. This has been relatively absent in previous reports. A common approach is to perform separate operando characterizations of the same material and then combine the results. Operando UV-Vis-NIR spectroscopy has been reported to unravel the operational kinetics in combination with operando GIWAXS techniques. This combines the time-revolved charge population and structural information. Joint analysis of multimodal results require caution because different techniques may have different requirements for film geometry. A more challenging yet advantageous approach is to integrate multiple techniques on the same sample for simultaneous multi-modal characterization. The incorporation of mapping means with spectroscopic techniques enables the simultaneous acquisition of spectral information with spatial resolution. The incorporation of an energy detector to an X-ray scattering experiment allows to obtain both structural and compositional changes of the material in single measurement. Some EQCM-D setups have optical transparent windows above the sealed liquid chamber and allow reflective optical measurements. These setups combine

gravimetric and spectroscopic information that is important in OMIECs with external electrolytes.

Lastly, computational characterization has been a key complement for spectroscopic techniques. DFT calculations are routinely compared to UV-Vis-NIR, IR, and Raman spectra. Similarly, MD simulations with scattering experiments have mutually informed each other, advancing the study of OMIECs morphology and structure. The continued integration between experimental and computational work allows the simulation results to inform experiments, while at the same time the experimental input is key to refine in silico predictions.

These developments and efforts for operando characterization will increase the understanding of fundamental process in OMIECs, for instance charge transport, ion-electron coupling, cyclic stability and side reactions/byproducts. This provides better guidance and experimental predictions for application oriented OMIEC molecular design. Operando experiments are also able to direct material processing to achieve desired properties, which is lacking in OMIEC materials processing due to its large parameter space. While operando techniques have no doubt accelerated the study of a wide array of functional, solid-state devices, the incorporation of mixed charged species, mass transport, and often solvent molecules or liquid electrolytes introduces challenges that required added attention and technique development. The targeted material optimization will significantly advance the field of bioelectronics, energy storage, neuromorphic, displays, actuators/soft robotics and drug delivery/ion pumps. The advancement of universal operando characterization tools will also benefit adjacent fields with systems/interfaces similar to OMIECs, such as hybrid organic-inorganics, biopolymers, and hydrogels.

AUTHOR INFORMATION

Corresponding Author

*Email: jrivnay@northwestern.edu

Notes

The authors declare no competing financial interest.

Biographies

Ruiheng Wu got his B.Sc. in Chemistry with a minor in Math from Peking University, China, in 2018. He is a Chemistry PhD candidate in the research group of Prof. Jonathan Rivnay in the Department of Biomedical Engineering at Northwestern University. His research is focused on the in situ/operando characterization of OMIECs to reveal the structure property relationship. The characterization tools he works on include optical and X-ray spectroscopy, X-ray scattering, microbalance, and probe techniques.

[bio of Micaela] Micaela Matta is a Marie Skłodowska-Curie Individual Fellow at the University of Liverpool, hosted in the group of Alessandro Troisi. She is interested in how the macroscopic properties of organic semiconductors are determined at the nanoscale level.

Bryan D. Paulsen S.J. is a postdoctoral researcher in Prof. Jonathan Rivnay's group in the Department of Biomedical Engineering at Northwestern University, where he applies synchrotron scattering to the operando investigations of organic mixed ionic-electronic conductors. He completed his PhD in Materials Science and Engineering studying the electrochemical properties of π-conjugated polymers for transistor and photovoltaic applications under the direction of Prof. C. Daniel Frisbie in the Department of Chemical Engineering and Materials Science at the University of Minnesota, during which he received the EnTISE K-12 STEM outreach fellowship. Prior to this he received a B.S. with Honors in Chemical Engineering at Trine (formerly Tri-State) University. In parallel with his scientific pursuits, he earned a MA in Social Philosophy from Loyola University Chicago and is currently completing a MDiv at the Jesuit School of Theology at Santa Clara University.

REFERENCES

1.   Paulsen, B. D.; Tybrandt, K.; Stavrinidou, E.; Rivnay, J., Organic Mixed Ionic–Electronic Conductors. *Nat. Mater.* **2020,** *19*, 13-26.
2.   Sun, K.; Zhang, S.; Li, P.; Xia, Y.; Zhang, X.; Du, D.; Isikgor, F. H.; Ouyang, J., Review on Application of Pedots and PEDOT:PSS in Energy Conversion and Storage Devices. *J. Mater. Sci.: Mater. Electron.* **2015,** *26*, 4438-4462.

3.   Go, G.-T.; Lee, Y.; Seo, D.-G.; Pei, M.; Lee, W.; Yang, H.; Lee, T.-W., Achieving Microstructure-Controlled Synaptic Plasticity and Long-Term Retention in Ion-Gel-Gated Organic Synaptic Transistors. *Adv. Intell. Syst.* **2020,** *2*, 2000012.

4.   Yamamoto, S.; Malliaras, G. G., Controlling the Neuromorphic Behavior of Organic Electrochemical Transistors by Blending Mixed and Ion Conductors. *ACS Appl. Electron. Mater.* **2020,** *2*, 2224-2228.

5.   Simon, D. T.; Gabrielsson, E. O.; Tybrandt, K.; Berggren, M., Organic Bioelectronics: Bridging the Signaling Gap between Biology and Technology. *Chem. Rev.* **2016,** *116*, 13009-13041.

6.   Van De Burgt, Y.; Melianas, A.; Keene, S. T.; Malliaras, G.; Salleo, A., Organic Electronics for Neuromorphic Computing. *Nat. Electron.* **2018,** *1*, 386-397.

7.   Ji, X.; Paulsen, B. D.; Chik, G. K. K.; Wu, R.; Yin, Y.; Chan, P. K. L.; Rivnay, J., Mimicking Associative Learning Using an Ion-Trapping Non-Volatile Synaptic Organic Electrochemical Transistor. *Nat. Commun.* **2021,** *12*, 2480.

8.   Macchia, E.; Romele, P.; Manoli, K.; Ghittorelli, M.; Magliulo, M.; Kovaacs-Vajna, Z. M.; Torricelli, F.; Torsi, L., Ultra-Sensitive Protein Detection with Organic Electrochemical Transistors Printed on Plastic Substrates. *Flex Print Electron* **2018,** *3*, 034002.

9.   Khodagholy, D.; Gelinas, J. N.; Thesen, T.; Doyle, W.; Devinsky, O.; Malliaras, G. G.; Buzsaki, G., Neurogrid: Recording Action Potentials from the Surface of the Brain. *Nat. Neurosci.* **2015,** *18*, 310-315.

10.   Keene, S. T.; Lubrano, C.; Kazemzadeh, S.; Melianas, A.; Tuchman, Y.; Polino, G.; Scognamiglio, P.; Cinà, L.; Salleo, A.; Van De Burgt, Y., et al., A Biohybrid Synapse with Neurotransmitter-Mediated Plasticity. *Nat. Mater.* **2020,** *19*, 969-973.

11.   Yang, A. N.; Li, Y. Z.; Yang, C. X.; Fu, Y.; Wang, N. X.; Li, L.; Yan, F., Fabric Organic Electrochemical Transistors for Biosensors. *Adv. Mater.* **2018,** *30*, 1800051.

12.   Chen, D.; Pei, Q., Electronic Muscles and Skins: A Review of Soft Sensors and Actuators. *Chem. Rev.* **2017,** *117*, 11239-11268.

13.   Hu, F.; Xue, Y.; Xu, J.; Lu, B., PEDOT-Based Conducting Polymer Actuators. *Front. Robot. AI* **2019,** *6*, 114.

14.   Jonsson, A.; Song, Z.; Nilsson, D.; Meyerson, B. A.; Simon, D. T.; Linderoth, B.; Berggren, M., Therapy Using Implanted Organic Bioelectronics. *Sci. Adv.* **2015,** *1*, e1500039.

15.   Jonsson, A.; Sjöström, T. A.; Tybrandt, K.; Berggren, M.; Simon, D. T., Chemical Delivery Array with Millisecond Neurotransmitter Release. *Sci. Adv.* **2016,** *2*, e1601340.

16.   Nevers, D. R.; Brushett, F. R.; Wheeler, D. R., Engineering Radical Polymer Electrodes for Electrochemical Energy Storage. *J. Power Sources* **2017,** *352*, 226-244.

17.   Costa, R. D.; Ortí, E.; Bolink, H. J.; Monti, F.; Accorsi, G.; Armaroli, N., Luminescent Ionic Transition-Metal Complexes for Light-Emitting Electrochemical Cells. *Angew. Chem. Int. Ed.* **2012,** *51*, 8178-8211.

18.   Liu, Z.; Dong, B. X.; Misra, M.; Sun, Y.; Strzalka, J.; Patel, S. N.; Escobedo, F. A.; Nealey, P. F.; Ober, C. K., Self-Assembly Behavior of an Oligothiophene-Based Conjugated

Liquid Crystal and Its Implication for Ionic Conductivity Characteristics. *Adv. Funct. Mater.* **2019,** *29*, 1805220.

19. Moser, M.; Hidalgo, T. C.; Surgailis, J.; Gladisch, J.; Ghosh, S.; Sheelamanthula, R.; Thiburce, Q.; Giovannitti, A.; Salleo, A.; Gasparini, N., et al., Side Chain Redistribution as a Strategy to Boost Organic Electrochemical Transistor Performance and Stability. *Adv. Mater.* **2020,** *32*, 2002748.

20. Savva, A.; Hallani, R.; Cendra, C.; Surgailis, J.; Hidalgo, T. C.; Wustoni, S.; Sheelamanthula, R.; Chen, X.; Kirkus, M.; Giovannitti, A., et al., Balancing Ionic and Electronic Conduction for High-Performance Organic Electrochemical Transistors. *Adv. Funct. Mater.* **2020,** *30*, 1907657.

21. Dong, B. X.; Nowak, C.; Onorato, J. W.; Strzalka, J.; Escobedo, F. A.; Luscombe, C. K.; Nealey, P. F.; Patel, S. N., Influence of Side-Chain Chemistry on Structure and Ionic Conduction Characteristics of Polythiophene Derivatives: A Computational and Experimental Study. *Chem. Mater.* **2019,** *31*, 1418-1429.

22. Liang, Z.; Zou, Q.; Wang, Y.; Lu, Y.-C., Recent Progress in Applying in Situ/Operando Characterization Techniques to Probe the Solid/Liquid/Gas Interfaces of Li-O2batteries. *Small Methods* **2017,** *1*, 1700150.

23. Peterson, V. K.; Papadakis, C. M., Functional Materials Analysis Usingin Situandin Operandox-Ray and Neutron Scattering. *IUCrJ* **2015,** *2*, 292-304.

24. Yang, Y.; Xiong, Y.; Zeng, R.; Lu, X.; Krumov, M.; Huang, X.; Xu, W.; Wang, H.; Disalvo, F. J.; Brock, J. D., et al., Operando Methods in Electrocatalysis. *ACS Catal.* **2021,** *11*, 1136-1178.

25. Souza, J. C. P.; Macedo, L. J. A.; Hassan, A.; Sedenho, G. C.; Modenez, I. A.; Crespilho, F. N., In Situ and Operando Techniques for Investigating Electron Transfer in Biological Systems. *ChemElectroChem* **2021,** *8*, 431-446.

26. Liu, D.; Shadike, Z.; Lin, R.; Qian, K.; Li, H.; Li, K.; Wang, S.; Yu, Q.; Liu, M.; Ganapathy, S., et al., Review of Recent Development of in Situ/Operando Characterization Techniques for Lithium Battery Research. *Adv. Mater.* **2019,** *31*, 1806620.

27. Choi, J. I. J.; Kim, T.-S.; Kim, D.; Lee, S. W.; Park, J. Y., Operando Surface Characterization on Catalytic and Energy Materials from Single Crystals to Nanoparticles. *ACS Nano* **2020,** *14*, 16392-16413.

28. Rivnay, J.; Mannsfeld, S. C. B.; Miller, C. E.; Salleo, A.; Toney, M. F., Quantitative Determination of Organic Semiconductor Microstructure from the Molecular to Device Scale. *Chem. Rev.* **2012,** *112*, 5488-5519.

29. Skompska, M.; Szkurlat, A.; Kowal, A.; Szklarczyk, M., Spectroelectrochemical and AFM Studies of Doping-Undoping of Poly(3-Hexylthiophene) Films in Propylene Carbonate and Aqueous Solutions of Liclo4. *Langmuir* **2003,** *19*, 2318-2324.

30. Chua, L.-L.; Dipankar, M.; Sivaramakrishnan, S.; Gao, X.; Qi, D.; Wee, A. T. S.; Ho, P. K. H., Large Damage Threshold and Small Electron Escape Depth in X-Ray Absorption Spectroscopy of a Conjugated Polymer Thin Film. *Langmuir* **2006,** *22*, 8587-8594.

31. Salmeron, M.; Schlögl, R., Ambient Pressure Photoelectron Spectroscopy: A New Tool for Surface Science and Nanotechnology. *Surf. Sci. Rep.* **2008,** *63*, 169-199.

32. Ando, T., High-Speed Atomic Force Microscopy Coming of Age. *Nanotechnology* **2012,** *23*, 062001.

33. Paulsen, B. D.; Giovannitti, A.; Wu, R. H.; Strzalka, J.; Zhang, Q. T.; Rivnay, J.; Takacs, C. J., Electrochemistry of Thin Films with in Situ/Operando Grazing Incidence X-Ray Scattering: Bypassing Electrolyte Scattering for High Fidelity Time Resolved Studies. *Small* **2021,** *17*, 2103213.

34. Boroudjerdi, H.; Kim, Y. W.; Naji, A.; Netz, R. R.; Schlagberger, X.; Serr, A., Statics and Dynamics of Strongly Charged Soft Matter. *Physics Reports-Review Section of Physics Letters* **2005,** *416*, 129-199.

35. Camurlu, P.; Toppare, L., Dual Type Complementary Colored Polymer Electrochromic Devices Based on Conducting Polymers of Poly(Hexanedioic Acid Bis-(2-Thiophen-3-Yl-Ethyl Ester). *J. Macromol. Sci., Part A* **2006,** *43*, 449-458.

36. Yue, H.; Guo, X.; Du, Y.; Zhang, Y.; Du, H.; Zhao, J.; Zhang, J., Synthesis and Characterization of Donor–Acceptor Type Quinoxaline-Based Polymers and the Corresponding Electrochromic Devices with Satisfactory Open Circuit Memory. *Synth. Met.* **2021,** *271*, 116619.

37. Buchhorn, M.; Wedler, S.; Panzer, F., Setup to Study the in Situ Evolution of Both Photoluminescence and Absorption During the Processing of Organic or Hybrid Semiconductors. *J. Phys. Chem. A* **2018,** *122*, 9115-9122.

38. Richter, L. J.; Delongchamp, D. M.; Amassian, A., Morphology Development in Solution-Processed Functional Organic Blend Films: An in Situ Viewpoint. *Chem. Rev.* **2017,** *117*, 6332-6366.

39. Koch, F. P. V.; Heeney, M.; Smith, P., Thermal and Structural Characteristics of Oligo(3-Hexylthiophene)S (3HT)N, N = 4–36. *J. Am. Chem. Soc.* **2013,** *135*, 13699-13709.

40. Arnold, S. P.; Harris, J. K.; Neelamraju, B.; Rudolph, M.; Ratcliff, E. L., Microstructure-Dependent Electrochemical Properties of Chemical-Vapor Deposited Poly(3,4-Ethylenedioxythiophene) (PEDOT) Films. *Synth. Met.* **2019,** *253*, 26-33.

41. Lilliu, S.; Agostinelli, T.; Pires, E.; Hampton, M.; Nelson, J.; Macdonald, J. E., Dynamics of Crystallization and Disorder During Annealing of P3HT/PCBM Bulk Heterojunctions. *Macromolecules* **2011,** *44*, 2725-2734.

42. Engmann, S.; Ro, H. W.; Herzing, A.; Snyder, C. R.; Richter, L. J.; Geraghty, P. B.; Jones, D. J., Film Morphology Evolution During Solvent Vapor Annealing of Highly Efficient Small Molecule Donor/Acceptor Blends. *J. Mater. Chem. A* **2016,** *4*, 15511-15521.

43. Huq, A. F.; Karim, A., Comparative Solvent Quality Dependent Crystallization in Solvent Vapor Annealing of P3HT:PCBM Thin Films by in-Situ GIWAXS. *Polymer* **2019,** *165*, 101-111.

44. Savva, A.; Wustoni, S.; Inal, S., Ionic-to-Electronic Coupling Efficiency in PEDOT:PSS Films Operated in Aqueous Electrolytes. *J. Mater. Chem. C* **2018,** *6*, 12023-12030.

45.   Savva, A.; Cendra, C.; Giugni, A.; Torre, B.; Surgailis, J.; Ohayon, D.; Giovannitti, A.; McCulloch, I.; Di Fabrizio, E.; Salleo, A., et al., Influence of Water on the Performance of Organic Electrochemical Transistors. *Chem. Mater.* **2019,** *31*, 927-937.

46.   Gladisch, J.; Stavrinidou, E.; Ghosh, S.; Giovannitti, A.; Moser, M.; Zozoulenko, I.; McCulloch, I.; Berggren, M., Reversible Electronic Solid–Gel Switching of a Conjugated Polymer. *Adv. Sci.* **2020,** *7*, 1901144.

47.   Jimison, L. H.; Toney, M. F.; McCulloch, I.; Heeney, M.; Salleo, A., Charge-Transport Anisotropy Due to Grain Boundaries in Directionally Crystallized Thin Films of Regioregular Poly(3-Hexylthiophene). *Adv. Mater.* **2009,** *21*, 1568-1572.

48.   Lee, M. J.; Gupta, D.; Zhao, N.; Heeney, M.; McCulloch, I.; Sirringhaus, H., Anisotropy of Charge Transport in a Uniaxially Aligned and Chain-Extended, High-Mobility, Conjugated Polymer Semiconductor. *Adv. Funct. Mater.* **2011,** *21*, 932-940.

49.   Sumboja, A.; Tefashe, U. M.; Wittstock, G.; Lee, P. S., Investigation of Charge Transfer Kinetics of Polyaniline Supercapacitor Electrodes by Scanning Electrochemical Microscopy. *Adv. Mater. Interfaces* **2015,** *2*, 1400154.

50.   Monge-Romero, I. C.; Suarez-Herrera, M. F., Electrocatalysis of the Hydroquinone/Benzoquinone Redox Couple at Platinum Electrodes Covered by a Thin Film of Poly(3,4-Ethylenedioxythiophene). *Synth. Met.* **2013,** *175*, 36-41.

51.   Pei, Q. B.; Yu, G.; Zhang, C.; Yang, Y.; Heeger, A. J., Polymer Light-Emitting Electrochemical-Cells. *Science* **1995,** *269*, 1086-1088.

52.   Creager, S., Solvents and Supporting Electrolytes. In *Handbook of Electrochemistry*, Elsevier: 2007; pp 57-72.

53.   Maitra, A.; Heuer, A., Cation Transport in Polymer Electrolytes: A Microscopic Approach. *Phys. Rev. Lett.* **2007,** *98*, 227802.

54.   Kuwabata, S.; Tsuda, T.; Torimoto, T., Room-Temperature Ionic Liquid. A New Medium for Material Production and Analyses under Vacuum Conditions. *J. Phys. Chem. Lett.* **2010,** *1*, 3177-3188.

55.   Wu, K.-Y.; Yu, S.-Y.; Tao, Y.-T., Continuous Modulation of Electrode Work Function with Mixed Self-Assembled Monolayers and Its Effect in Charge Injection. *Langmuir* **2009,** *25*, 6232-6238.

56.   Coropceanu, V.; Li, H.; Winget, P.; Zhu, L.; Brédas, J.-L., Electronic-Structure Theory of Organic Semiconductors: Charge-Transport Parameters and Metal/Organic Interfaces. *Annu. Rev. Mater. Res.* **2013,** *43*, 63-87.

57.   Paterson, A. F.; Faber, H.; Savva, A.; Nikiforidis, G.; Gedda, M.; Hidalgo, T. C.; Chen, X.; McCulloch, I.; Anthopoulos, T. D.; Inal, S., On the Role of Contact Resistance and Electrode Modification in Organic Electrochemical Transistors. *Adv. Mater.* **2019,** *31*, 1902291.

58.   Braga, D.; Ha, M.; Xie, W.; Frisbie, C. D., Ultralow Contact Resistance in Electrolyte-Gated Organic Thin Film Transistors. *Appl. Phys. Lett.* **2010,** *97*, 193311.

59.   Friedlein, J. T.; Rivnay, J.; Dunlap, D. H.; McCulloch, I.; Shaheen, S. E.; McLeod, R. R.; Malliaras, G. G., Influence of Disorder on Transfer Characteristics of Organic Electrochemical Transistors. *Appl. Phys. Lett.* **2017,** *111*, 023301.

60.   Kim, S.-M.; Kim, C.-H.; Kim, Y.; Kim, N.; Lee, W.-J.; Lee, E.-H.; Kim, D.; Park, S.; Lee, K.; Rivnay, J., et al., Influence of PEDOT:PSS Crystallinity and Composition on Electrochemical Transistor Performance and Long-Term Stability. *Nat. Commun.* **2018,** *9*, 3858.

61.   Kaphle, V.; Liu, S.; Al-Shadeedi, A.; Keum, C.-M.; Lüssem, B., Contact Resistance Effects in Highly Doped Organic Electrochemical Transistors. *Adv. Mater.* **2016,** *28*, 8766-8770.

62.   Thomas, E. M.; Peterson, K. A.; Balzer, A. H.; Rawlings, D.; Stingelin, N.; Segalman, R. A.; Chabinyc, M. L., Effects of Counter-Ion Size on Delocalization of Carriers and Stability of Doped Semiconducting Polymers. *Adv. Electron. Mater.* **2020,** *6*, 2000595.

63.   Burke, J. H.; Bird, M. J., Energetics and Escape of Interchain-Delocalized Ion Pairs in Nonpolar Media. *Adv. Mater.* **2019,** *31*, 1806863.

64.   Takeda, N.; Miller, J. R., Poly(3-Decylthiophene) Radical Anions and Cations in Solution: Single and Multiple Polarons and Their Delocalization Lengths in Conjugated Polymers. *J. Phys. Chem. B* **2012,** *116*, 14715-14723.

65.   Djellab, H.; Armand, M.; Delabouglise, D., Stabilization of the Conductivity of Poly(3-Methylthiophene) by Triflimide Anions. *Synth. Met.* **1995,** *74*, 223-226.

66.   Paulsen, B. D.; Fabiano, S.; Rivnay, J., Mixed Ionic-Electronic Transport in Polymers. *Annu. Rev. Mater. Res.* **2021,** *51*, 73-99.

67.   Xue, Z.; He, D.; Xie, X., Poly(Ethylene Oxide)-Based Electrolytes for Lithium-Ion Batteries. *J. Mater. Chem. A* **2015,** *3*, 19218-19253.

68.   Shah, D. B.; Olson, K. R.; Karny, A.; Mecham, S. J.; Desimone, J. M.; Balsara, N. P., Effect of Anion Size on Conductivity and Transference Number of Perfluoroether Electrolytes with Lithium Salts. *J. Electrochem. Soc.* **2017,** *164*, A3511-A3517.

69.   Stavrinidou, E.; Leleux, P.; Rajaona, H.; Khodagholy, D.; Rivnay, J.; Lindau, M.; Sanaur, S.; Malliaras, G. G., Direct Measurement of Ion Mobility in a Conducting Polymer. *Adv. Mater.* **2013,** *25*, 4488-4493.

70.   Toss, H.; Suspène, C.; Piro, B.; Yassar, A.; Crispin, X.; Kergoat, L.; Pham, M.-C.; Berggren, M., On the Mode of Operation in Electrolyte-Gated Thin Film Transistors Based on Different Substituted Polythiophenes. *Org. Electron.* **2014,** *15*, 2420-2427.

71.   Pacheco-Moreno, C. M.; Schreck, M.; Scaccabarozzi, A. D.; Bourgun, P.; Wantz, G.; Stevens, M. M.; Dautel, O. J.; Stingelin, N., The Importance of Materials Design to Make Ions Flow: Toward Novel Materials Platforms for Bioelectronics Applications. *Adv. Mater.* **2017,** *29*, 1604446.

72.   Giovannitti, A.; Sbircea, D.-T.; Inal, S.; Nielsen, C. B.; Bandiello, E.; Hanifi, D. A.; Sessolo, M.; Malliaras, G. G.; McCulloch, I.; Rivnay, J., Controlling the Mode of Operation of Organic Transistors through Side-Chain Engineering. *Proc. Natl. Acad. Sci.* **2016,** *113*, 12017-12022.

73.   Liu, J.; Davis, N. R.; Liu, D. S.; Hammond, P. T., Highly Transparent Mixed Electron and Proton Conducting Polymer Membranes. *J. Mater. Chem.* **2012,** *22*, 15534.

74.   Melianas, A.; Quill, T. J.; Lecroy, G.; Tuchman, Y.; Loo, H. V.; Keene, S. T.; Giovannitti, A.; Lee, H. R.; Maria, I. P.; McCulloch, I., et al., Temperature-Resilient Solid-State Organic Artificial Synapses for Neuromorphic Computing. *Sci. Adv.* **2020,** *6*, eabb2958.

75.   Mazzini, V.; Craig, V. S. J., What Is the Fundamental Ion-Specific Series for Anions and Cations? Ion Specificity in Standard Partial Molar Volumes of Electrolytes and Electrostriction in Water and Non-Aqueous Solvents. *Chem. Sci.* **2017,** *8*, 7052-7065.

76.   Schauser, N. S.; Seshadri, R.; Segalman, R. A., Multivalent Ion Conduction in Solid Polymer Systems. *Mol. Syst. Des. Eng.* **2019,** *4*, 263-279.

77.   Choo, Y.; Halat, D. M.; Villaluenga, I.; Timachova, K.; Balsara, N. P., Diffusion and Migration in Polymer Electrolytes. *Prog. Polym. Sci.* **2020,** *103*, 101220.

78.   Hallinan, D. T.; Balsara, N. P., Polymer Electrolytes. *Annu. Rev. Mater. Res.* **2013,** *43*, 503-525.

79.   Fratini, S.; Nikolka, M.; Salleo, A.; Schweicher, G.; Sirringhaus, H., Charge Transport in High-Mobility Conjugated Polymers and Molecular Semiconductors. *Nat. Mater.* **2020,** *19*, 491-502.

80.   Craciun, N. I.; Wildeman, J.; Blom, P. W. M., Universal Arrhenius Temperature Activated Charge Transport in Diodes from Disordered Organic Semiconductors. *Phys. Rev. Lett.* **2008,** *100*, 056601.

81.   Coropceanu, V.; Cornil, J.; Da Silva Filho, D. A.; Olivier, Y.; Silbey, R.; Brédas, J.-L., Charge Transport in Organic Semiconductors. *Chem. Rev.* **2007,** *107*, 926-952.

82.   Surgailis, J.; Savva, A.; Druet, V.; Paulsen, B. D.; Wu, R.; Hamidi-Sakr, A.; Ohayon, D.; Nikiforidis, G.; Chen, X.; McCulloch, I., et al., Mixed Conduction in an N-Type Organic Semiconductor in the Absence of Hydrophilic Side-Chains. *Adv. Funct. Mater.* **2021,** 2010165.

83.   Flagg, L. Q.; Bischak, C. G.; Onorato, J. W.; Rashid, R. B.; Luscombe, C. K.; Ginger, D. S., Polymer Crystallinity Controls Water Uptake in Glycol Side-Chain Polymer Organic Electrochemical Transistors. *J. Am. Chem. Soc.* **2019,** *141*, 4345-4354.

84.   Noriega, R.; Rivnay, J.; Vandewal, K.; Koch, F. P. V.; Stingelin, N.; Smith, P.; Toney, M. F.; Salleo, A., A General Relationship between Disorder, Aggregation and Charge Transport in Conjugated Polymers. *Nat. Mater.* **2013,** *12*, 1038-1044.

85.   Paulsen, B. D.; Frisbie, C. D., Dependence of Conductivity on Charge Density and Electrochemical Potential in Polymer Semiconductors Gated with Ionic Liquids. *J. Phys. Chem. C* **2012,** *116*, 3132-3141.

86.   Collins, S. D.; Mikhnenko, O. V.; Nguyen, T. L.; Rengert, Z. D.; Bazan, G. C.; Woo, H. Y.; Nguyen, T.-Q., Observing Ion Motion in Conjugated Polyelectrolytes with Kelvin Probe Force Microscopy. *Adv. Electron. Mater.* **2017,** *3*, 1700005.

87.   Wang, S.; Ha, M.; Manno, M.; Daniel Frisbie, C.; Leighton, C., Hopping Transport and the Hall Effect near the Insulator–Metal Transition in Electrochemically Gated Poly(3-Hexylthiophene) Transistors. *Nat. Commun.* **2012,** *3*, 1210.

88.   Giannini, S.; Carof, A.; Blumberger, J., Crossover from Hopping to Band-Like Charge Transport in an Organic Semiconductor Model: Atomistic Nonadiabatic Molecular Dynamics Simulation. *J. Phys. Chem. Lett.* **2018,** *9*, 3116-3123.

89.   Xie, Q. J.; Kuwabata, S.; Yoneyama, H., Eqcm Studies on Polypyrrole in Aqueous Solutions. *J. Electroanal. Chem.* **1997,** *420*, 219-225.

90.   Prokes, J.; Varga, M.; Vrnata, M.; Valtera, S.; Stejskal, J.; Kopecky, D., Nanotubular Polypyrrole: Reversibility of Protonation/Deprotonation Cycles and Long-Term Stability. *Eur. Polym. J.* **2019,** *115*, 290-297.

91.   Kang, S. D.; Snyder, G. J., Charge-Transport Model for Conducting Polymers. *Nat. Mater.* **2017,** *16*, 252-257.

92.   Gregory, S. A.; Hanus, R.; Atassi, A.; Rinehart, J. M.; Wooding, J. P.; Menon, A. K.; Losego, M. D.; Snyder, G. J.; Yee, S. K., Quantifying Charge Carrier Localization in Chemically Doped Semiconducting Polymers. *Nat. Mater.* **2021,** *20*, 1414–1421.

93.   Riess, I., Polymeric Mixed Ionic Electronic Conductors. *Solid State Ion.* **2000,** *136-137*, 1119-1130.

94.   Riess, I., I-V Relations in Semiconductors with Ionic Motion. *J Electroceram* **2006,** *17*, 247-253.

95.   Riess, I., Current-Voltage Relation and Charge Distribution in Mixed Ionic Electronic Solid Conductors. *J. Phys. Chem. Solids* **1986,** *47*, 129-138.

96.   Bernards, D. A.; Flores-Torres, S.; Abruna, H. D.; Malliaras, G. G., Observation of Electroluminescence and Photovoltaic Response in Ionic Junctions. *Science* **2006,** *313*, 1416-1419.

97.   Merkle, R.; Gutbrod, P.; Reinold, P.; Katzmaier, M.; Tkachov, R.; Maier, J.; Ludwigs, S., Mixed Conductivity of Polythiophene-Based Ionic Polymers under Controlled Conditions. *Polymer* **2017,** *132*, 216-226.

98.   Zayat, B.; Das, P.; Thompson, B. C.; Narayan, S. R., In Situ Measurement of Ionic and Electronic Conductivities of Conductive Polymers as a Function of Electrochemical Doping in Battery Electrolytes. *J. Phys. Chem. C* **2021,** *125*, 7533-7541.

99.   Feldberg, S. W., Reinterpretation of Polypyrrole Electrochemistry. Consideration of Capacitive Currents in Redox Switching of Conducting Polymers. *J. Am. Chem. Soc.* **1984,** *106*, 4671-4674.

100.   Volkov, A. V.; Wijeratne, K.; Mitraka, E.; Ail, U.; Zhao, D.; Tybrandt, K.; Andreasen, J. W.; Berggren, M.; Crispin, X.; Zozoulenko, I. V., Understanding the Capacitance of PEDOT:PSS. *Adv. Funct. Mater.* **2017,** *27*, 1700329.

101.   Tybrandt, K.; Zozoulenko, I. V.; Berggren, M., Chemical Potential–Electric Double Layer Coupling in Conjugated Polymer–Polyelectrolyte Blends. *Sci. Adv.* **2017,** *3*, eaao3659.

102.   Österholm, A. M.; Ponder, J. F.; De Keersmaecker, M.; Shen, D. E.; Reynolds, J. R., Disentangling Redox Properties and Capacitance in Solution-Processed Conjugated Polymers. *Chem. Mater.* **2019,** *31*, 2971-2982.

103.   Inal, S.; Malliaras, G. G.; Rivnay, J., Benchmarking Organic Mixed Conductors for Transistors. *Nat. Commun.* **2017,** *8*, 1767.

104.   Jamnik, J.; Maier, J., Treatment of the Impedance of Mixed Conductors Equivalent Circuit Model and Explicit Approximate Solutions. *J. Electrochem. Soc.* **1999,** *146*, 4183-4188.

105.   Lai, W.; Haile, S. M., Impedance Spectroscopy as a Tool for Chemical and Electrochemical Analysis of Mixed Conductors: A Case Study of Ceria. *J. Am. Ceram. Soc.* **2005,** *88*, 2979-2997.

106.   Garcia-Belmonte, G.; Pomerantz, Z.; Bisquert, J.; Lellouche, J.-P.; Zaban, A., Analysis of Ion Diffusion and Charging in Electronically Conducting Polydicarbazole Films by Impedance Methods. *Electrochim. Acta* **2004,** *49*, 3413-3417.

107.   Li, G.; Pickup, P. G., Ion Transport in Poly(3,4-Ethylenedioxythiophene)–Poly(Styrene-4-Sulfonate) Composites. *Phys. Chem. Chem. Phys.* **2000,** *2*, 1255-1260.

108.   Sheliakina, M.; Mostert, A. B.; Meredith, P., Decoupling Ionic and Electronic Currents in Melanin. *Adv. Funct. Mater.* **2018,** *28*, 1805514.

109.   Harris, J. K.; Ratcliff, E. L., Ion Diffusion Coefficients in Poly(3-Alkylthiophenes) for Energy Conversion and Biosensing: Role of Side-Chain Length and Microstructure. *J. Mater. Chem. C* **2020,** *8*, 13319-13327.

110.   Garcia-Belmonte, G.; Bisquert, J.; Popkirov, G. S., Determination of the Electronic Conductivity of Polybithiophene Films at Different Doping Levels Using in Situ Electrochemical Impedance Measurements. *Appl. Phys. Lett.* **2003,** *83*, 2178-2180.

111.   Bisquert, J.; Fabregat-Santiago, F.; Mora-Seró, I.; Garcia-Belmonte, G.; Barea, E. M.; Palomares, E., A Review of Recent Results on Electrochemical Determination of the Density of Electronic States of Nanostructured Metal-Oxide Semiconductors and Organic Hole Conductors. *Inorg. Chim. Acta* **2008,** *361*, 684-698.

112.   Thackeray, J. W.; White, H. S.; Wrighton, M. S., Poly (3-Methylthiophene)-Coated Electrodes: Optical and Electrical Properties as a Function of Redox Potential and Amplification of Electrical and Chemical Signals Using Poly (3-Methylthiophene)-Based Microelectrochemical Transistors. *J. Phys. Chem.* **1985,** *89*, 5133-5140.

113.   Rivnay, J.; Inal, S.; Salleo, A.; Owens, R. M.; Berggren, M.; Malliaras, G. G., Organic Electrochemical Transistors. *Nat. Rev. Mater.* **2018,** *3*, 17086.

114.   Bernards, D. A.; Malliaras, G. G., Steady-State and Transient Behavior of Organic Electrochemical Transistors. *Adv. Funct. Mater.* **2007,** *17*, 3538-3544.

115.   Chun, H.; Chung, T. D., Iontronics. *Annual Review of Analytical Chemistry* **2015,** *8*, 441-462.

116.   Yang, C.; Suo, Z., Hydrogel Ionotronics. *Nat. Rev. Mater.* **2018,** *3*, 125-142.

117.   Arbring Sjöström, T.; Berggren, M.; Gabrielsson, E. O.; Janson, P.; Poxson, D. J.; Seitanidou, M.; Simon, D. T., A Decade of Iontronic Delivery Devices. *Adv. Mater. Technol.* **2018,** *3*, 1700360.

118.   Lim, S.-M.; Yoo, H.; Oh, M.-A.; Han, S. H.; Lee, H.-R.; Chung, T. D.; Joo, Y.-C.; Sun, J.-Y., Ion-to-Ion Amplification through an Open-Junction Ionic Diode. *Proc. Natl. Acad. Sci.* **2019,** *116*, 13807-13815.

119.   Sun, G.; Senapati, S.; Chang, H.-C., High-Flux Ionic Diodes, Ionic Transistors and Ionic Amplifiers Based on External Ion Concentration Polarization by an Ion Exchange Membrane: A New Scalable Ionic Circuit Platform. *Lab Chip* **2016,** *16*, 1171-1177.

120.   Zhao, Y.; Dai, S.; Chu, Y.; Wu, X.; Huang, J., A Flexible Ionic Synaptic Device and Diode-Based Aqueous Ion Sensor Utilizing Asymmetric Polyelectrolyte Distribution. *Chem. Commun. (Cambridge, U. K.)* **2018,** *54*, 8186-8189.

121.   Savagian, L. R.; Österholm, A. M.; Ponder, J. F.; Barth, K. J.; Rivnay, J.; Reynolds, J. R., Balancing Charge Storage and Mobility in an Oligo(Ether) Functionalized Dioxythiophene Copolymer for Organic- and Aqueous- Based Electrochemical Devices and Transistors. *Adv. Mater.* **2018,** *30*, 1804647.

122.   Paulsen, B. D.; Wu, R.; Takacs, C. J.; Steinrück, H. G.; Strzalka, J.; Zhang, Q.; Toney, M. F.; Rivnay, J., Time-Resolved Structural Kinetics of an Organic Mixed Ionic–Electronic Conductor. *Adv. Mater.* **2020,** *32*, 2003404.

123.   Bargigia, I.; Savagian, L. R.; Österholm, A. M.; Reynolds, J. R.; Silva, C., Charge-Transfer Intermediates in the Electrochemical Doping Mechanism of Conjugated Polymers. *J. Am. Chem. Soc.* **2021,** *143*, 294-308.

124.   Bischak, C. G.; Flagg, L. Q.; Yan, K.; Li, C.-Z.; Ginger, D. S., Fullerene Active Layers for N-Type Organic Electrochemical Transistors. *ACS Appl. Mater. Interfaces* **2019,** *11*, 28138-28144.

125.   Chen, X.; Marks, A.; Paulsen, B. D.; Wu, R.; Rashid, R. B.; Chen, H.; Alsufyani, M.; Rivnay, J.; McCulloch, I., N -Type Rigid Semiconducting Polymers Bearing Oligo(Ethylene Glycol) Side Chains for High-Performance Organic Electrochemical Transistors. *Angew. Chem. Int. Ed.* **2021,** *60*, 9368–9373.

126.   Sun, H.; Vagin, M.; Wang, S.; Crispin, X.; Forchheimer, R.; Berggren, M.; Fabiano, S., Complementary Logic Circuits Based on High-Performance N-Type Organic Electrochemical Transistors. *Adv. Mater.* **2018,** *30*, 1704916.

127.   Moia, D.; Giovannitti, A.; Szumska, A. A.; Maria, I. P.; Rezasoltani, E.; Sachs, M.; Schnurr, M.; Barnes, P. R. F.; McCulloch, I.; Nelson, J., Design and Evaluation of Conjugated Polymers with Polar Side Chains as Electrode Materials for Electrochemical Energy Storage in Aqueous Electrolytes. *Energy Environ. Sci.* **2019,** *12*, 1349-1357.

128.   Meier, S. B.; Hartmann, D.; Tordera, D.; Bolink, H. J.; Winnacker, A.; Sarfert, W., Dynamic Doping and Degradation in Sandwich-Type Light-Emitting Electrochemical Cells. *Phys. Chem. Chem. Phys.* **2012,** *14*, 10886.

129.   Edman, L.; Summers, M. A.; Buratto, S. K.; Heeger, A. J., Polymer Light-Emitting Electrochemical Cells: Doping, Luminescence, and Mobility. *Phys. Rev. B* **2004,** *70*, 115212.

130.   Hu, Y.; Gao, J., Direct Imaging and Probing of the P−N Junction in a Planar Polymer Light-Emitting Electrochemical Cell. *J. Am. Chem. Soc.* **2011,** *133*, 2227-2231.

131. Van Dijken, A.; Perro, A.; Meulenkamp, E. A.; Brunner, K., The Influence of a PEDOT:PSS Layer on the Efficiency of a Polymer Light-Emitting Diode. *Org. Electron.* **2003,** *4*, 131-141.

132. Pathak, G.; Krasińska-Krawet, Z.; Szyk-Warszyńska, L.; Čakara, D., Doping of Poly(3,4-Ethylenedioxythiophene):Poly(Styrenesulfonate) Films Studied by Means of Electrochemical Variable Angle Spectroscopic Ellipsometry. *Thin Solid Films* **2018,** *651*, 31-38.

133. Enengl, C.; Enengl, S.; Pluczyk, S.; Havlicek, M.; Lapkowski, M.; Neugebauer, H.; Ehrenfreund, E., Doping-Induced Absorption Bands in P3HT: Polarons and Bipolarons. *ChemPhysChem* **2016,** *17*, 3836-3844.

134. Shiri, P.; Dacanay, E. J. S.; Hagen, B.; Kaake, L. G., Vogel-Tammann-Fulcher Model for Charging Dynamics in an Organic Electrochemical Transistor. *J. Mater. Chem. C* **2019,** *7*, 12935-12941.

135. Shiri, P.; Neusser, D.; Malacrida, C.; Ludwigs, S.; Kaake, L. G., Mixed Ion-Carrier Diffusion in Poly(3-Hexyl Thiophene)/Perchlorate Electrochemical Systems. *J. Phys. Chem. C* **2021,** *125*, 536-545.

136. Yohannes, T.; Neugebauer, H.; Jenekhe, S. A.; Sariciftci, N. S., Multiple Reduction States with Different Conductivities of Polybenzimidazobenzophenanthroline (BBL) Studied with Infrared Spectroelectrochemistry. *Synth. Met.* **2001,** *116*, 241-245.

137. Cooke, D. G.; Krebs, F. C.; Jepsen, P. U. In *Multi-THz Spectroscopy of Mobile Charge Carriers in P3HT: PCBM on a Sub-100 fs Time Scale*, Physical Chemistry of Interfaces and Nanomaterials XII, International Society for Optics and Photonics: 2013; p 88111H.

138. Garreau, S.; Louarn, G.; Buisson, J. P.; Froyer, G.; Lefrant, S., In Situ Spectroelectrochemical Raman Studies of Poly(3,4-Ethylenedioxythiophene) (PEDT). *Macromolecules* **1999,** *32*, 6807-6812.

139. Enokida, I.; Furukawa, Y., Doping-Level Dependent Mobilities of Positive Polarons and Bipolarons in Poly(2,5-Bis(3-Hexadecylthiophen-2-Yl)Thieno[3,2-B]Thiophene) (PBTTT-C16) Based on an Ionic-Liquid-Gated Transistor Configuration. *Org. Electron.* **2019,** *68*, 28-34.

140. Wada, Y.; Enokida, I.; Yamamoto, J.; Furukawa, Y., Raman Imaging of Carrier Distribution in the Channel of an Ionic Liquid-Gated Transistor Fabricated with Regioregular Poly(3-Hexylthiophene). *Spectrochim. Acta Part A Mol. Biomol. Spectrosc.* **2018,** *197*, 166-169.

141. Furukawa, Y.; Akiyama, K.; Enokida, I.; Yamamoto, J., Raman Spectra of Carriers in Ionic-Liquid-Gated Transistors Fabricated with Poly(2,5-Bis(3-Tetradecylthiophen-2-Yl)Thieno[3,2-B]Thiophene). *Vib. Spectrosc.* **2016,** *85*, 29-34.

142. Yamamoto, J.; Furukawa, Y., Raman Characterization and Electrical Properties Of poly(3-Hexylthiophene) Doped Electrochemically in an Ionic Liquid-Gated Transistor Geometry. *Org. Electron.* **2016,** *28*, 82-87.

143. Nightingale, J.; Wade, J.; Moia, D.; Nelson, J.; Kim, J.-S., Impact of Molecular Order on Polaron Formation in Conjugated Polymers. *J. Phys. Chem. C* **2018,** *122*, 29129-29140.

144. Stewart, K.; Limbu, S.; Nightingale, J.; Pagano, K.; Park, B.; Hong, S.; Lee, K.; Kwon, S.; Kim, J.-S., Molecular Understanding of a π-Conjugated Polymer/Solid-State Ionic

Liquid Complex as a Highly Sensitive and Selective Gas Sensor. *J. Mater. Chem. C* **2020,** *8*, 15268-15276.

145.   Tan, E.; Pappa, A. M.; Pitsalidis, C.; Nightingale, J.; Wood, S.; Castro, F. A.; Owens, R. M.; Kim, J. S., A Highly Sensitive Molecular Structural Probe Applied to in Situ Biosensing of Metabolites Using PEDOT:PSS. *Biotechnol. Bioeng.* **2020,** *117*, 291-299.

146.   Francis, C.; Fazzi, D.; Grimm, S. B.; Paulus, F.; Beck, S.; Hillebrandt, S.; Pucci, A.; Zaumseil, J., Raman Spectroscopy and Microscopy of Electrochemically and Chemically Doped High-Mobility Semiconducting Polymers. *J. Mater. Chem. C* **2017,** *5*, 6176-6184.

147.   Ohayon, D.; Nikiforidis, G.; Savva, A.; Giugni, A.; Wustoni, S.; Palanisamy, T.; Chen, X.; Maria, I. P.; Di Fabrizio, E.; Costa, P. M. F. J., et al., Biofuel Powered Glucose Detection in Bodily Fluids with an N-Type Conjugated Polymer. *Nat. Mater.* **2020,** *19*, 456-463.

148.   Spano, F. C., The Spectral Signatures of Frenkel Polarons in H- and J-Aggregates. *Acc. Chem. Res.* **2010,** *43*, 429-439.

149.   Yamagata, H.; Spano, F. C., Interplay between Intrachain and Interchain Interactions in Semiconducting Polymer Assemblies: The Hj-Aggregate Model. *J. Chem. Phys.* **2012,** *136*, 184901.

150.   Spano, F. C.; Silva, C., H- and J-Aggregate Behavior in Polymeric Semiconductors. *Annu. Rev. Phys. Chem.* **2014,** *65*, 477-500.

151.   Bredas, J. L.; Street, G. B., Polarons, Bipolarons, and Solitons in Conducting Polymers. *Acc. Chem. Res.* **1985,** *18*, 309-315.

152.   Colaneri, N.; Nowak, M.; Spiegel, D.; Hotta, S.; Heeger, A. J., Bipolarons in Poly(3-Methylthiophene): Spectroscopic, Magnetic, and Electrochemical Measurements. *Phys. Rev. B* **1987,** *36*, 7964-7968.

153.   Patil, A. O.; Heeger, A. J.; Wudl, F., Optical-Properties of Conducting Polymers. *Chem. Rev.* **1988,** *88*, 183-200.

154.   Vernitskaya, T. V.; Efimov, O. N., Polypyrrole: A Conducting Polymer (Synthesis, Properties, and Applications). *Usp. Khim.* **1997,** *66*, 489-505.

155.   Alkan, F.; Salzner, U., Theoretical Investigation of Excited States of Oligothiophene Anions. *J. Phys. Chem. A* **2008,** *112*, 6053-6058.

156.   Massonnet, N.; Carella, A.; Jaudouin, O.; Rannou, P.; Laval, G.; Celle, C.; Simonato, J. P., Improvement of the Seebeck Coefficient of PEDOT:PSS by Chemical Reduction Combined with a Novel Method for its Transfer Using Free-Standing Thin Films. *J. Mater. Chem. C* **2014,** *2*, 1278-1283.

157.   Kendrick, W. J.; Jirasek, M.; Peeks, M. D.; Greetham, G. M.; Sazanovich, I. V.; Donaldson, P. M.; Towrie, M.; Parker, A. W.; Anderson, H. L., Mechanisms of IR Amplification in Radical Cation Polarons. *Chem. Sci.* **2020,** *11*, 2112-2120.

158.   Zuppiroli, L.; Bieber, A.; Michoud, D.; Galli, G.; Gygi, F.; Bussac, M. N.; Andre, J. J., Polaron Formation and Symmetry Breaking. *Chem. Phys. Lett.* **2003,** *374*, 7-12.

159. Hwang, J.; Tanner, D. B.; Schwendeman, I.; Reynolds, J. R., Optical Properties of Nondegenerate Ground-State Polymers: Three Dioxythiophene-Based Conjugated Polymers. *Phys. Rev. B* **2003,** *67*, 115205.

160. Zozoulenko, I.; Singh, A.; Singh, S. K.; Gueskine, V.; Crispin, X.; Berggren, M., Polarons, Bipolarons, and Absorption Spectroscopy of PEDOT. *ACS Appl. Polym. Mater.* **2019,** *1*, 83-94.

161. Inal, S.; Malliaras, G. G.; Rivnay, J., Optical Study of Electrochromic Moving Fronts for the Investigation of Ion Transport in Conducting Polymers. *J. Mater. Chem. C* **2016,** *4*, 3942-3947.

162. Clark, J.; Silva, C.; Friend, R. H.; Spano, F. C., Role of Intermolecular Coupling in the Photophysics of Disordered Organic Semiconductors: Aggregate Emission in Regioregular Polythiophene. *Phys. Rev. Lett.* **2007,** *98*, 206406.

163. Ghosh, R.; Spano, F. C., Excitons and Polarons in Organic Materials. *Acc. Chem. Res.* **2020,** *53*, 2201-2211.

164. Martin, T. P.; Wise, A. J.; Busby, E.; Gao, J.; Roehling, J. D.; Ford, M. J.; Larsen, D. S.; Moulé, A. J.; Grey, J. K., Packing Dependent Electronic Coupling in Single Poly(3-Hexylthiophene) H- and J-Aggregate Nanofibers. *J. Phys. Chem. B* **2013,** *117*, 4478-4487.

165. Thomas, E. M.; Brady, M. A.; Nakayama, H.; Popere, B. C.; Segalman, R. A.; Chabinyc, M. L., X-Ray Scattering Reveals Ion-Induced Microstructural Changes During Electrochemical Gating of Poly(3-Hexylthiophene). *Adv. Funct. Mater.* **2018,** *28*, 1803687.

166. Rawlings, D.; Thomas, E. M.; Segalman, R. A.; Chabinyc, M. L., Controlling the Doping Mechanism in Poly(3-Hexylthiophene) Thin-Film Transistors with Polymeric Ionic Liquid Dielectrics. *Chem. Mater.* **2019,** *31*, 8820-8829.

167. Spano, F. C., Modeling Disorder in Polymer Aggregates: The Optical Spectroscopy of Regioregular Poly(3-Hexylthiophene) Thin Films. *J. Chem. Phys.* **2005,** *122*, 234701.

168. Brown, P. J.; Thomas, D. S.; Köhler, A.; Wilson, J. S.; Kim, J.-S.; Ramsdale, C. M.; Sirringhaus, H.; Friend, R. H., Effect of Interchain Interactions on the Absorption and Emission of Poly(3-Hexylthiophene). *Phys. Rev. B* **2003,** *67*, 064203.

169. Scharsich, C.; Lohwasser, R. H.; Sommer, M.; Asawapirom, U.; Scherf, U.; Thelakkat, M.; Neher, D.; Köhler, A., Control of Aggregate Formation in Poly(3-Hexylthiophene) by Solvent, Molecular Weight, and Synthetic Method. *J. Polym. Sci., Part B: Polym. Phys.* **2012,** *50*, 442-453.

170. Schrader, B.; Hoffmann, A.; Keller, S., Near-Infrared Fourier Transform Raman Spectroscopy: Facing Absorption and Background. *Spectrochim. Acta Part A Mol. Spectrosc.* **1991,** *47*, 1135-1148.

171. Yang, L.; Yu, Y.; Zhang, J.; Chen, F.; Meng, X.; Qiu, Y.; Dan, Y.; Jiang, L., In-Situ Fabrication of Diketopyrrolopyrrole-Carbazole-Based Conjugated Polymer/Tio2 Heterojunction for Enhanced Visible Light Photocatalysis. *Appl. Surf. Sci.* **2018,** *434*, 796-805.

172. Yu, F.; Wang, Z.; Zhang, S.; Ye, H.; Kong, K.; Gong, X.; Hua, J.; Tian, H., Molecular Engineering of Donor-Acceptor Conjugated Polymer/G-C3 N4 Heterostructures for

Significantly Enhanced Hydrogen Evolution under Visible-Light Irradiation. *Adv. Funct. Mater.* **2018,** *28*, 1804512.

173.   Lan, Z.-A.; Ren, W.; Chen, X.; Zhang, Y.; Wang, X., Conjugated Donor-Acceptor Polymer Photocatalysts with Electron-Output "Tentacles" for Efficient Hydrogen Evolution. *Applied Catalysis B: Environmental* **2019,** *245*, 596-603.

174.   Gao, X.; Jehng, J.-M.; Wachs, I. E., In Situ UV–Vis–NIR Diffuse Reflectance and Raman Spectroscopic Studies of Propane Oxidation over ZrO2-Supported Vanadium Oxide Catalysts. *J. Catal.* **2002,** *209*, 43-50.

175.   Gao, X.; Bañares, M. A.; Wachs, I. E., Ethane and N-Butane Oxidation over Supported Vanadium Oxide Catalysts: An in Situ UV–Visible Diffuse Reflectance Spectroscopic Investigation. *J. Catal.* **1999,** *188*, 325-331.

176.   Negri, C.; Signorile, M.; Porcaro, N. G.; Borfecchia, E.; Berlier, G.; Janssens, T. V. W.; Bordiga, S., Dynamic CuII/CuI Speciation in Cu-CHA Catalysts by in Situ Diffuse Reflectance UV–Vis-NIR Spectroscopy. *Applied Catalysis A: General* **2019,** *578*, 1-9.

177.   Mirabella, F. M., Strength of Interaction and Penetration of Infrared Radiation for Polymer Films in Internal Reflection Spectroscopy. *J. Polym. Sci.: Polym. Phys. Ed.* **1983,** *21*, 2403-2417.

178.   Rivnay, J.; Inal, S.; Collins, B. A.; Sessolo, M.; Stavrinidou, E.; Strakosas, X.; Tassone, C.; Delongchamp, D. M.; Malliaras, G. G., Structural Control of Mixed Ionic and Electronic Transport in Conducting Polymers. *Nat. Commun.* **2016,** *7*, 11287.

179.   Lapkowski, M.; Pron, A., Electrochemical Oxidation of Poly(3,4-Ethylenedioxythiophene) - "in Situ" Conductivity and Spectroscopic Investigations. *Synth. Met.* **2000,** *110*, 79-83.

180.   Chen, X. W.; Inganas, O., Three-Step Redox in Polythiophenes: Evidence from Electrochemistry at an Ultramicroelectrode. *J. Phys. Chem.* **1996,** *100*, 15202-15206.

181.   Parr, Z. S.; Rashid, R. B.; Paulsen, B. D.; Poggi, B.; Tan, E.; Freeley, M.; Palma, M.; Abrahams, I.; Rivnay, J.; Nielsen, C. B., Semiconducting Small Molecules as Active Materials for P-Type Accumulation Mode Organic Electrochemical Transistors. *Adv. Electron. Mater.* **2020,** *6*, 2000215.

182.   Moser, M.; Savva, A.; Thorley, K.; Paulsen, B. D.; Hidalgo, T. C.; Ohayon, D.; Chen, H.; Giovannitti, A.; Marks, A.; Gasparini, N., et al., Polaron Delocalization in Donor–Acceptor Polymers and its Impact on Organic Electrochemical Transistor Performance. *Angew. Chem. Int. Ed.* **2021,** *60*, 7777-7785.

183.   Döbbelin, M.; Pozo-Gonzalo, C.; Marcilla, R.; Blanco, R.; Segura, J. L.; Pomposo, J. A.; Mecerreyes, D., Electrochemical Synthesis of PEDOT Derivatives Bearing Imidazolium-Ionic Liquid Moieties. *J. Polym. Sci., Part A: Polym. Chem.* **2009,** *47*, 3010-3021.

184.   Cutler, C. A.; Bouguettaya, M.; Kang, T.-S.; Reynolds, J. R., Alkoxysulfonate-Functionalized PEDOT Polyelectrolyte Multilayer Films: Electrochromic and Hole Transport Materials. *Macromolecules* **2005,** *38*, 3068-3074.

185.   Giovannitti, A.; Rashid, R. B.; Thiburce, Q.; Paulsen, B. D.; Cendra, C.; Thorley, K.; Moia, D.; Mefford, J. T.; Hanifi, D.; Weiyuan, D., et al., Energetic Control of Redox-Active Polymers toward Safe Organic Bioelectronic Materials. *Adv. Mater.* **2020,** *32*, 1908047.

186.   Cendra, C.; Giovannitti, A.; Savva, A.; Venkatraman, V.; McCulloch, I.; Salleo, A.; Inal, S.; Rivnay, J., Role of the Anion on the Transport and Structure of Organic Mixed Conductors. *Adv. Funct. Mater.* **2019,** *29*, 1807034.

187.   Rebetez, G.; Bardagot, O.; Affolter, J.; Réhault, J.; Banerji, N., What Drives the Kinetics and Doping Level in the Electrochemical Reactions of PEDOT:PSS? *Adv. Funct. Mater.* **2021,** 2105821.

188.   Knowles, K. E.; Koch, M. D.; Shelton, J. L., Three Applications of Ultrafast Transient Absorption Spectroscopy of Semiconductor Thin Films: Spectroelectrochemistry, Microscopy, and Identification of Thermal Contributions. *J. Mater. Chem. C* **2018,** *6*, 11853-11867.

189.   Zhu, T.; Snaider, J. M.; Yuan, L.; Huang, L., Ultrafast Dynamic Microscopy of Carrier and Exciton Transport. *Annu. Rev. Phys. Chem.* **2019,** *70*, 219-244.

190.   Park, J.; Reid, O. G.; Rumbles, G., Photoinduced Carrier Generation and Recombination Dynamics of a Trilayer Cascade Heterojunction Composed of Poly(3-Hexylthiophene), Titanyl Phthalocyanine, and C60. *J. Phys. Chem. B* **2015,** *119*, 7729-7739.

191.   Virgili, T.; Grancini, G.; Molotokaite, E.; Suarez-Lopez, I.; Rajendran, S. K.; Liscio, A.; Palermo, V.; Lanzani, G.; Polli, D.; Cerullo, G., Confocal Ultrafast Pump–Probe Spectroscopy: A New Technique to Explore Nanoscale Composites. *Nanoscale* **2012,** *4*, 2219.

192.   Itskos, G.; Othonos, A.; Rauch, T.; Tedde, S. F.; Hayden, O.; Kovalenko, M. V.; Heiss, W.; Choulis, S. A., Optical Properties of Organic Semiconductor Blends with near-Infrared Quantum-Dot Sensitizers for Light Harvesting Applications. *Adv. Energy Mater.* **2011,** *1*, 802-812.

193.   Singh, S.; Pandit, B.; Basel, T. P.; Li, S.; Laird, D.; Vardeny, Z. V., Two-Step Charge Photogeneration Dynamics in Polymer/Fullerene Blends for Photovoltaic Applications. *Phys. Rev. B* **2012,** *85*, 205206.

194.   Eng, M. P.; Barnes, P. R. F.; Durrant, J. R., Concentration-Dependent Hole Mobility and Recombination Coefficient in Bulk Heterojunctions Determined from Transient Absorption Spectroscopy. *J. Phys. Chem. Lett.* **2010,** *1*, 3096-3100.

195.   Tsokkou, D.; Peterhans, L.; Cao, D. X.; Mai, C. K.; Bazan, G. C.; Nguyen, T. Q.; Banerji, N., Excited State Dynamics of a Self-Doped Conjugated Polyelectrolyte. *Adv. Funct. Mater.* **2020,** *30*, 1906148.

196.   Ruhe, J.; Colaneri, N. F.; Bradley, D. D. C.; Friend, R. H.; Wegner, G., Photoexcited States in Poly(3-Alkyl Thienylenes). *J Phys-Condens Mat* **1990,** *2*, 5465-5477.

197.   Xu, B.; Holdcroft, S., Molecular Control of Luminescence from Poly(3-Hexylthiophenes). *Macromolecules* **1993,** *26*, 4457-4460.

198.   Zhou, Q.; Swager, T. M., Fluorescent Chemosensors Based on Energy Migration in Conjugated Polymers: The Molecular Wire Approach to Increased Sensitivity. *J. Am. Chem. Soc.* **1995,** *117*, 12593-12602.

199.   Sim, M.; Shin, J.; Shim, C.; Kim, M.; Jo, S. B.; Kim, J.-H.; Cho, K., Dependence of Exciton Diffusion Length on Crystalline Order in Conjugated Polymers. *J. Phys. Chem. C* **2014,** *118*, 760-766.

200.   Martinez, L.; Higuchi, S.; Maclachlan, A. J.; Stavrinadis, A.; Miller, N. C.; Diedenhofen, S. L.; Bernechea, M.; Sweetnam, S.; Nelson, J.; Haque, S. A., et al., Improved Electronic Coupling in Hybrid Organic–Inorganic Nanocomposites Employing Thiol-Functionalized P3HT and Bismuth Sulfide Nanocrystals. *Nanoscale* **2014,** *6*, 10018-10026.

201.   Benatto, L.; Moraes, C. A. M.; De Jesus Bassi, M.; Wouk, L.; Roman, L. S.; Koehler, M., Kinetic Modeling of the Electric Field Dependent Exciton Quenching at the Donor–Acceptor Interface. *J. Phys. Chem. C* **2021,** *125*, 4436-4448.

202.   Song, P.; Li, Y.; Ma, F.; Pullerits, T.; Sun, M., External Electric Field-Dependent Photoinduced Charge Transfer in a Donor–Acceptor System for an Organic Solar Cell. *J. Phys. Chem. C* **2013,** *117*, 15879-15889.

203.   Zhang, K.-N.; Jiang, Z.-N.; Wang, T.; Qiao, J.-W.; Feng, L.; Qin, C.-C.; Yin, H.; So, S.-K.; Hao, X.-T., Exploring the Mechanisms of Exciton Diffusion Improvement in Ternary Polymer Solar Cells: From Ultrafast to Ultraslow Temporal Scale. *Nano Energy* **2021,** *79*, 105513.

204.   Ward, A. J.; Ruseckas, A.; Samuel, I. D. W., A Shift from Diffusion Assisted to Energy Transfer Controlled Fluorescence Quenching in Polymer–Fullerene Photovoltaic Blends. *J. Phys. Chem. C* **2012,** *116*, 23931-23937.

205.   Jiang, H.; Zhao, X.; Schanze, K. S., Amplified Fluorescence Quenching of a Conjugated Polyelectrolyte Mediated by Ca^{2+}. *Langmuir* **2006,** *22*, 5541-5543.

206.   Wang, Y.; Zhang, Y.; Liu, B., Conjugated Polyelectrolyte Based Fluorescence Turn-on Assay for Real-Time Monitoring of Protease Activity. *Anal. Chem.* **2010,** *82*, 8604-8610.

207.   Gaylord, B. S.; Heeger, A. J.; Bazan, G. C., DNA Detection Using Water-Soluble Conjugated Polymers and Peptide Nucleic Acid Probes. *Proc. Natl. Acad. Sci.* **2002,** *99*, 10954-10957.

208.   Bolinger, J. C.; Traub, M. C.; Adachi, T.; Barbara, P. F., Ultralong-Range Polaron-Induced Quenching of Excitons in Isolated Conjugated Polymers. *Science* **2011,** *331*, 565-567.

209.   Held, M.; Zakharko, Y.; Wang, M.; Jakubka, F.; Gannott, F.; Rumer, J. W.; Ashraf, R. S.; McCulloch, I.; Zaumseil, J., Photo- and Electroluminescence of Ambipolar, High-Mobility, Donor-Acceptor Polymers. *Org. Electron.* **2016,** *32*, 220-227.

210.   Al-Ibrahim, M.; Roth, H. K.; Schroedner, M.; Konkin, A.; Zhokhavets, U.; Gobsch, G.; Scharff, P.; Sensfuss, S., The Influence of the Optoelectronic Properties of Poly(3-Alkylthiophenes) on the Device Parameters in Flexible Polymer Solar Cells. *Org. Electron.* **2005,** *6*, 65-77.

211.   Kadashchuk, A.; Arkhipov, V. I.; Kim, C.-H.; Shinar, J.; Lee, D. W.; Hong, Y. R.; Jin, J.-I.; Heremans, P.; Bässler, H., Localized Trions in Conjugated Polymers. *Phys. Rev. B* **2007,** *76*, 235205.

212.   Drori, T.; Gershman, E.; Sheng, C. X.; Eichen, Y.; Vardeny, Z. V.; Ehrenfreund, E., Illumination-Induced Metastable Polaron-Supporting State in Poly(P-Phenylene Vinylene) Films. *Phys. Rev. B* **2007,** *76*, 033203.

213.   Wedler, S.; Zhou, C.; Bazan, G. C.; Panzer, F.; Köhler, A., Role of Torsional Flexibility in the Film Formation Process in Two π-Conjugated Model Oligomers. *J. Phys. Chem. Lett.* **2020,** *11*, 9379-9386.

214.   Ionov, L.; Sidorenko, A.; Eichhorn, K. J.; Stamm, M.; Minko, S.; Hinrichs, K., Stimuli-Responsive Mixed Grafted Polymer Films with Gradually Changing Properties: Direct Determination of Chemical Composition. *Langmuir* **2005,** *21*, 8711-8716.

215.   Jellison, G. E., Ellipsometry. In *Encyclopedia of Spectroscopy and Spectrometry*, Lindon, J. C., Ed. Elsevier: 1999; pp 402-411.

216.   Ogieglo, W.; Stenbock-Fermor, A.; Juraschek, T. M.; Bogdanova, Y.; Benes, N.; Tsarkova, L. A., Synergic Swelling of Interactive Network Support and Block Copolymer Films During Solvent Vapor Annealing. *Langmuir* **2018,** *34*, 9950-9960.

217.   Campoy-Quiles, M.; Alonso, M. I.; Bradley, D. D. C.; Richter, L. J., Advanced Ellipsometric Characterization of Conjugated Polymer Films. *Adv. Funct. Mater.* **2014,** *24*, 2116-2134.

218.   Jellison, G. E.; Modine, F. A., Parameterization of the Optical Functions of Amorphous Materials in the Interband Region (Vol 69, Pg 371, 1996). *Appl. Phys. Lett.* **1996,** *69*, 2137-2137.

219.   Chen, S.; Kühne, P.; Stanishev, V.; Knight, S.; Brooke, R.; Petsagkourakis, I.; Crispin, X.; Schubert, M.; Darakchieva, V.; Jonsson, M. P., On the Anomalous Optical Conductivity Dispersion of Electrically Conducting Polymers: Ultra-Wide Spectral Range Ellipsometry Combined with a Drude–Lorentz Model. *J. Mater. Chem. C* **2019,** *7*, 4350-4362.

220.   Merryweather, A. J.; Schnedermann, C.; Jacquet, Q.; Grey, C. P.; Rao, A., Operando Optical Tracking of Single-Particle Ion Dynamics in Batteries. *Nature* **2021,** *594*, 522-528.

221.   Neelamraju, B.; Watts, K. E.; Pemberton, J. E.; Ratcliff, E. L., Correlation of Coexistent Charge Transfer States in F4TCNQ-Doped P3HT with Microstructure. *J. Phys. Chem. Lett.* **2018,** *9*, 6871-6877.

222.   Enengl, S.; Enengl, C.; Pluczyk, S.; Glowacki, E. D.; Lapkowski, M.; Ehrenfreund, E.; Neugebauer, H.; Sariciftci, N. S., Spectroscopic Characterization of Charge Carriers of the Organic Semiconductor Quinacridone Compared with Pentacene During Redox Reactions. *J. Mater. Chem. C* **2016,** *4*, 10265-10278.

223.   Kvarnström, C.; Neugebauer, H.; Blomquist, S.; Ahonen, H. J.; Kankare, J.; Ivaska, A., In Situ Spectroelectrochemical Characterization of Poly(3,4-Ethylenedioxythiophene). *Electrochim. Acta* **1999,** *44*, 2739-2750.

224.   Grieco, C.; Kohl, F. R.; Hanes, A. T.; Kohler, B., Probing the Heterogeneous Structure of Eumelanin Using Ultrafast Vibrational Fingerprinting. *Nat. Commun.* **2020,** *11*, 4569.

225.   Grabow, K.; Bentrup, U., Homogeneous Catalytic Processes Monitored by Combined in Situ ATR-IR, UV–Vis, and Raman Spectroscopy. *ACS Catal.* **2014,** *4*, 2153-2164.

226.   Ulbricht, R.; Hendry, E.; Shan, J.; Heinz, T. F.; Bonn, M., Carrier Dynamics in Semiconductors Studied with Time-Resolved Terahertz Spectroscopy. *Rev. Mod. Phys.* **2011,** *83*, 543-586.

227.   Tan, P.; Huang, J.; Liu, K. F.; Xiong, Y. Q.; Fan, M. W., Terahertz Radiation Sources Based on Free Electron Lasers and Their Applications. *Sci. China. Inform. Sci.* **2012,** *55*, 1-15.

228.   Zhang, B.; He, T.; Shen, J. L.; Hou, Y. B.; Hu, Y. F.; Zang, M. D.; Chen, T. J.; Feng, S. F.; Teng, F.; Qin, L., Conjugated Polymer-Based Broadband Terahertz Wave Modulator. *Opt. Lett.* **2014,** *39*, 6110-6113.

229.   Zhong, L.; Zhang, B.; He, T.; Lv, L. F.; Hou, Y. B.; Shen, J. L., Conjugated Polymer Based Active Electric-Controlled Terahertz Device. *Appl. Phys. Lett.* **2016,** *108*, 103301.

230.   He, T.; Zhang, B.; Wang, G. C.; Zang, M. D.; Hou, Y. B.; Shen, J. L., High Efficiency THz-Wave Modulators Based on Conjugated Polymer-Based Organic Films. *J. Phys. D Appl. Phys.* **2016,** *49*, 075111.

231.   Smith, N., Classical Generalization of the Drude Formula for the Optical Conductivity. *Phys. Rev. B* **2001,** *64*, 155106.

232.   Drori, T.; Sheng, C. X.; Ndobe, A.; Singh, S.; Holt, J.; Vardeny, Z. V., Below-Gap Excitation of π-Conjugated Polymer-Fullerene Blends: Implications for Bulk Organic Heterojunction Solar Cells. *Phys. Rev. Lett.* **2008,** *101*, 037401.

233.   Krauspe, P.; Tsokkou, D.; Causa, M.; Buchaca-Domingo, E.; Fei, Z. P.; Heeney, M.; Stingelin, N.; Banerji, N., Terahertz Short-Range Mobilities in Neat and Intermixed Regions of Polymer: Fullerene Blends with Controlled Phase Morphology. *J. Mater. Chem. A* **2018,** *6*, 22301-22309.

234.   Wang, Z. Y.; Di Virgilio, L.; Yao, Z. F.; Yu, Z. D.; Wang, X. Y.; Zhou, Y. Y.; Li, Q. Y.; Lu, Y.; Zou, L.; Wang, H. I., et al., Correlating Charge Transport Properties of Conjugated Polymers in Solution Aggregates and Thin-Film Aggregates. *Angew. Chem. Int. Ed.* **2021,** *60*, 20483-20488.

235.   Němec, H.; Kužel, P.; Sundström, V., Charge Transport in Nanostructured Materials for Solar Energy Conversion Studied by Time-Resolved Terahertz Spectroscopy. *J. Photochem. Photobiol. A Chem.* **2010,** *215*, 123-139.

236.   Zhuldybina, M.; Ropagnol, X.; Trudeau, C.; Bolduc, M.; Zednik, R.; Blanchard, F., Contactless in Situ Electrical Characterization Method of Printed Electronic Devices with Terahertz Spectroscopy. *Sensors* **2019,** *19*, 444.

237.   Nemes, C. T.; Swierk, J. R.; Schmuttenmaer, C. A., A Terahertz-Transparent Electrochemical Cell for in Situ Terahertz Spectroelectrochemistry. *Anal. Chem.* **2018,** *90*, 4389-4396.

238.   Shi, H.; Lercher, J. A.; Yu, X.-Y., Sailing into Uncharted Waters: Recent Advances in the in Situ Monitoring of Catalytic Processes in Aqueous Environments. *Catal. Sci. Technol.* **2015,** *5*, 3035-3060.

239.   Kitano, H., Characterization of Polymer Materials Based on Structure Analyses of Vicinal Water. *Polym. J. (Tokyo, Jpn.)* **2016,** *48*, 15-24.

240. Bukowska, J.; Jackowska, K., In Situ Raman Studies of Polypyrrole and Polythiophene Films on Pt Electrodes. *Synth. Met.* **1990,** *35*, 143-150.

241. Bazzaoui, E. A.; Levi, G.; Aeiyach, S.; Aubard, J.; Marsault, J. P.; Lacaze, P. C., Sers Spectra of Polythiophene in Doped and Undoped States. *J. Phys. Chem.* **1995,** *99*, 6628-6634.

242. Yokonuma, N.; Furukawa, Y.; Tasumi, M.; Kuroda, M.; Nakayama, J., Electronic Absorption and Raman Studies of Bf4−-Doped Polythiophene Based on the Spectra of the Radical Cation and Dication of A-Sexithiophene. *Chem. Phys. Lett.* **1996,** *255*, 431-436.

243. Khlaifia, D.; Ewels, C. P.; Massuyeau, F.; Chemek, M.; Faulques, E.; Duvail, J. L.; Alimi, K., Unraveling the Real Structures of Solution-Based and Surface-Bound Poly(3-Hexylthiophene) (P3HT) Oligomers: A Combined Theoretical and Experimental Study. *Rsc Advances* **2016,** *6*, 56174-56182.

244. Anderson, M.; Ramanan, C.; Fontanesi, C.; Frick, A.; Surana, S.; Cheyns, D.; Furno, M.; Keller, T.; Allard, S.; Scherf, U., et al., Displacement of Polarons by Vibrational Modes in Doped Conjugated Polymers. *Phys. Rev. Mater.* **2017,** *1*, 055604.

245. Wood, S.; Hollis, J. R.; Kim, J. S., Raman Spectroscopy as an Advanced Structural Nanoprobe for Conjugated Molecular Semiconductors. *J. Phys. D Appl. Phys.* **2017,** *50*, 073001.

246. Tsoi, W. C.; James, D. T.; Kim, J. S.; Nicholson, P. G.; Murphy, C. E.; Bradley, D. D. C.; Nelson, J.; Kim, J.-S., The Nature of in-Plane Skeleton Raman Modes of P3HT and Their Correlation to the Degree of Molecular Order in P3HT:PCBM Blend Thin Films. *J. Am. Chem. Soc.* **2011,** *133*, 9834-9843.

247. Razzell-Hollis, J.; Limbu, S.; Kim, J.-S., Spectroscopic Investigations of Three-Phase Morphology Evolution in Polymer: Fullerene Solar Cell Blends. *J. Phys. Chem. C* **2016,** *120*, 10806-10814.

248. Razzell-Hollis, J.; Fleischli, F.; Jahnke, A. A.; Stingelin, N.; Seferos, D. S.; Kim, J.-S., Effects of Side-Chain Length and Shape on Polytellurophene Molecular Order and Blend Morphology. *J. Phys. Chem. C* **2017,** *121*, 2088-2098.

249. Yamamoto, J.; Furukawa, Y., Electronic and Vibrational Spectra of Positive Polarons and Bipolarons in Regioregular Poly(3-Hexylthiophene) Doped with Ferric Chloride. *J. Phys. Chem. B* **2015,** *119*, 4788-4794.

250. Cadusch, P. J.; Hlaing, M. M.; Wade, S. A.; McArthur, S. L.; Stoddart, P. R., Improved Methods for Fluorescence Background Subtraction from Raman Spectra. *J. Raman Spectrosc.* **2013,** *44*, 1587-1595.

251. Magnitskii, S. A.; Malachova, V. I.; Tarasevich, A. P.; Tunkin, V. G.; Yakubovich, S. D., Generation of Bandwidth-Limited Tunable Picosecond Pulses by Injection-Locked Optical Parametric Oscillators. *Opt. Lett.* **1986,** *11*, 18-20.

252. Jin, Y.; Magusin, P.; Sturniolo, S.; Zhao, E. W.; Lyu, D.; Yamamoto, S.; Malliaras, G.; Grey, C., Operando NMR Visualization of Ion Dynamics in PEDOT:PSS. Research Square Platform LLC: 2021.

253. Zykwinska, A.; Domagala, W.; Czardybon, A.; Pilawa, B.; Lapkowski, M., In Situ EPR Spectroelectrochemical Studies of Paramagnetic Centres in Poly(3,4-Ethylenedioxythiophene)

(PEDOT) and Poly(3,4-Butylenedioxythiophene) (PBuDOT) Films. *Chem. Phys.* **2003,** *292*, 31-45.

254.   Zykwinska, A.; Domagala, W.; Pilawa, B.; Lapkowski, M., Electrochemical Overoxidation of Poly(3,4-Ethylenedioxythiophene)—PEDOT Studied by Means of in Situ ESR Spectroelectrochemistry. *Electrochim. Acta* **2005,** *50*, 1625-1633.

255.   Domagala, W.; Pilawa, B.; Lapkowski, M., Quantitative in-Situ EPR Spectroelectrochemical Studies of Doping Processes in Poly(3,4-Alkylenedioxythiophene)S. *Electrochim. Acta* **2008,** *53*, 4580-4590.

256.   Wang, P.-C.; Yu, J.-Y., Dopant-Dependent Variation in the Distribution of Polarons and Bipolarons as Charge-Carriers in Polypyrrole Thin Films Synthesized by Oxidative Chemical Polymerization. *React. Funct. Polym.* **2012,** *72*, 311-316.

257.   Tanaka, H.; Kanahashi, K.; Takekoshi, N.; Mada, H.; Ito, H.; Shimoi, Y.; Ohta, H.; Takenobu, T., Thermoelectric Properties of a Semicrystalline Polymer Doped Beyond the Insulator-to-Metal Transition by Electrolyte Gating. *Sci. Adv.* **2020,** *6*, eaay8065.

258.   Jiang, X.; Patil, R.; Harima, Y.; Ohshita, J.; Kunai, A., Influences of Self-Assembled Structure on Mobilities of Charge Carriers in π-Conjugated Polymers. *J. Phys. Chem. B* **2005,** *109*, 221-229.

259.   Schott, S.; Chopra, U.; Lemaur, V.; Melnyk, A.; Olivier, Y.; Di Pietro, R.; Romanov, I.; Carey, R. L.; Jiao, X.; Jellett, C., et al., Polaron Spin Dynamics in High-Mobility Polymeric Semiconductors. *Nat. Phys.* **2019,** *15*, 814-822.

260.   Sterby, M.; Emanuelsson, R.; Mamedov, F.; Strømme, M.; Sjödin, M., Investigating Electron Transport in a PEDOT/Quinone Conducting Redox Polymer with in Situ Methods. *Electrochim. Acta* **2019,** *308*, 277-284.

261.   Seifrid, M.; Reddy, G. N. M.; Chmelka, B. F.; Bazan, G. C., Insight into the Structures and Dynamics of Organic Semiconductors through Solid-State NMR Spectroscopy. *Nat. Rev. Mater.* **2020,** *5*, 910-930.

262.   Hope, M. A.; Rinkel, B. L. D.; Gunnarsdóttir, A. B.; Märker, K.; Menkin, S.; Paul, S.; Sergeyev, I. V.; Grey, C. P., Selective NMR Observation of the Sei–Metal Interface by Dynamic Nuclear Polarisation from Lithium Metal. *Nat. Commun.* **2020,** *11*, 2224.

263.   Wang, L.; Menakath, A.; Han, F.; Wang, Y.; Zavalij, P. Y.; Gaskell, K. J.; Borodin, O.; Iuga, D.; Brown, S. P.; Wang, C., et al., Identifying the Components of the Solid–Electrolyte Interphase in Li-Ion Batteries. *Nat. Chem.* **2019,** *11*, 789-796.

264.   Jin, Y.; Kneusels, N.-J. H.; Grey, C. P., NMR Study of the Degradation Products of Ethylene Carbonate in Silicon–Lithium Ion Batteries. *J. Phys. Chem. Lett.* **2019,** *10*, 6345-6350.

265.   Pirnat, K.; Bitenc, J.; Vizintin, A.; Krajnc, A.; Tchernychova, E., Indirect Synthesis Route toward Cross-Coupled Polymers for High Voltage Organic Positive Electrodes. *Chem. Mater.* **2018,** *30*, 5726-5732.

266.   Miroshnikov, M.; Wang, H.; Thangavel, N. K.; Mahankali, K.; Satapathy, S.; Kato, K.; Babu, G.; Divya, K. P.; Arava, L. M. R.; Ajayan, P. M., et al., Nature-Inspired Purpurin

Polymer for Li-Ion Batteries: Mechanistic Insights into Energy Storage via Solid-State NMR and Computational Studies. *J. Phys. Chem. C* **2020,** *124*, 17939-17948.

267.	Yurash, B.; Cao, D. X.; Brus, V. V.; Leifert, D.; Wang, M.; Dixon, A.; Seifrid, M.; Mansour, A. E.; Lungwitz, D.; Liu, T., et al., Towards Understanding the Doping Mechanism of Organic Semiconductors by Lewis Acids. *Nat. Mater.* **2019,** *18*, 1327-1334.

268.	Fu, X.; Liu, Y.; Wang, W.; Han, L.; Yang, J.; Ge, M.; Yao, Y.; Liu, H., Probing the Fast Lithium-Ion Transport in Small-Molecule Solid Polymer Electrolytes by Solid-State NMR. *Macromolecules* **2020,** *53*, 10078-10085.

269.	Cheung, I. W.; Chin, K. B.; Greene, E. R.; Smart, M. C.; Abbrent, S.; Greenbaum, S. G.; Prakash, G. K. S.; Surampudi, S., Electrochemical and Solid State NMR Characterization of Composite PEO-Based Polymer Electrolytes. *Electrochim. Acta* **2003,** *48*, 2149-2156.

270.	Voigt, N.; Van Wüllen, L., The Effect of Plastic-Crystalline Succinonitrile on the Electrolyte System PEO:LiBF4: Insights from Solid State NMR. *Solid State Ion.* **2014,** *260*, 65-75.

271.	Gotoh, K.; Yamakami, T.; Nishimura, I.; Kometani, H.; Ando, H.; Hashi, K.; Shimizu, T.; Ishida, H., Mechanisms for Overcharging of Carbon Electrodes in Lithium-Ion/Sodium-Ion Batteries Analysed by Operando Solid-State NMR. *J. Mater. Chem. A* **2020,** *8*, 14472-14481.

272.	Freitag, K. M.; Walke, P.; Nilges, T.; Kirchhain, H.; Spranger, R. J.; van Wullen, L., Electrospun-Sodiumtetrafluoroborate-Polyethylene Oxide Membranes for Solvent-Free Sodium Ion Transport in Solid State Sodium Ion Batteries. *J. Power Sources* **2018,** *378*, 610-617.

273.	Forse, A. C.; Merlet, C.; Grey, C. P.; Griffin, J. M., NMR Studies of Adsorption and Diffusion in Porous Carbonaceous Materials. *Prog. Nucl. Magn. Reson. Spectrosc.* **2021,** *124*, 57-84.

274.	Kataoka, H.; Saito, Y.; Tabuchi, M.; Wada, Y.; Sakai, T., Ionic Conduction Mechanism of PEO-Type Polymer Electrolytes Investigated by the Carrier Diffusion Phenomenon Using PGSE-NMR. *Macromolecules* **2002,** *35*, 6239-6244.

275.	Gouverneur, M.; Kopp, J.; van Wullen, L.; Schonhoff, M., Direct Determination of Ionic Transference Numbers in Ionic Liquids by Electrophoretic NMR. *Phys. Chem. Chem. Phys.* **2015,** *17*, 30680-30686.

276.	Zhao, J.; Wang, L.; He, X.; Wan, C.; Jiang, C., Determination of Lithium-Ion Transference Numbers in LiPF6–PC Solutions Based on Electrochemical Polarization and NMR Measurements. *J. Electrochem. Soc.* **2008,** *155*, A292.

277.	Halat, D. M.; Snyder, R. L.; Sundararaman, S.; Choo, Y.; Gao, K. W.; Hoffman, Z. J.; Abel, B. A.; Grundy, L. S.; Galluzzo, M. D.; Gordon, M. P., et al., Modifying Li+ and Anion Diffusivities in Polyacetal Electrolytes: A Pulsed-Field-Gradient NMR Study of Ion Self-Diffusion. *Chem. Mater.* **2021,** *33*, 4915–4926.

278.	Forse, A.; Griffin, J.; Merlet, C.; Carretero-Gonzalez, J.; Abdul, R.; Nicole; Grey, C., Direct Observation of Ion Dynamics in Supercapacitor Electrodes Using In situ Diffusion NMR Spectroscopy. *Nature Energy* **2017,** *2*, 16216.

279. Hostnik, G.; Bončina, M.; Dolce, C.; Mériguet, G.; Rollet, A.-L.; Cerar, J., Influence of Counterions on the Conformation of Conjugated Polyelectrolytes: The Case of Poly(Thiophen-3-Ylacetic Acid). *Phys. Chem. Chem. Phys.* **2016,** *18*, 25036-25047.

280. Bocchetta, P.; Gianoncelli, A.; Abyaneh, M. K.; Kiskinova, M.; Amati, M.; Gregoratti, L.; Jezeršek, D.; Mele, C.; Bozzini, B., Electrosynthesis of Co/Ppy Nanocomposites for Orr Electrocatalysis: A Study Based on Quasi-in Situ X-Ray Absorption, Fluorescence and in Situ Raman Spectroscopy. *Electrochim. Acta* **2014,** *137*, 535-545.

281. Bozzini, B.; Gianoncelli, A.; Bocchetta, P.; Dal Zilio, S.; Kourousias, G., Fabrication of a Sealed Electrochemical Microcell for in Situ Soft X-Ray Microspectroscopy and Testing with in Situ Co-Polypyrrole Composite Electrodeposition for Pt-Free Oxygen Electrocatalysis. *Anal. Chem.* **2014,** *86*, 664-670.

282. Bozzini, B.; Bocchetta, P.; Gianoncelli, A.; Kourousias, G.; Kiskinova, M.; Zilio, S. D., In Situ Soft X-Ray Fluorescence and Absorption Microspectroscopy: A Study of Mn-Co/Polypyrrole Electrodeposition. *Journal of Vacuum Science & Technology A: Vacuum, Surfaces, and Films* **2015,** *33*, 031102.

283. Gokturk, P. A.; Barry, M.; Segalman, R.; Crumlin, E. J., Directly Probing Polymer Thin Film Chemistry and Counterion Influence on Water Sorption. *ACS Appl. Polym. Mater.* **2020,** *2*, 4752-4761.

284. Thelen, J. L.; Wu, S. L.; Jayier, A. E.; Srinivasan, V.; Balsara, N. P.; Patel, S. N., Relationship between Mobility and Lattice Strain in Electrochemically Doped Poly(3-Hexylthiophene). *ACS Macro Lett.* **2015,** *4*, 1386-1391.

285. Bischak, C. G.; Flagg, L. Q.; Yan, K.; Rehman, T.; Davies, D. W.; Quezada, R. J.; Onorato, J. W.; Luscombe, C. K.; Diao, Y.; Li, C.-Z., et al., A Reversible Structural Phase Transition by Electrochemically-Driven Ion Injection into a Conjugated Polymer. *J. Am. Chem. Soc.* **2020,** *142*, 7434-7442.

286. Bokel, F. A.; Engmann, S.; Herzing, A. A.; Collins, B. A.; Ro, H. W.; Delongchamp, D. M.; Richter, L. J.; Schaible, E.; Hexemer, A., In Situ X-Ray Scattering Studies of the Influence of an Additive on the Formation of a Low-Bandgap Bulk Heterojunction. *Chem. Mater.* **2017,** *29*, 2283-2293.

287. Steinruck, H. G.; Takacs, C. J.; Kim, H. K.; Mackanic, D. G.; Holladay, B.; Cao, C. T.; Narayanan, S.; Dufresne, E. M.; Chushkin, Y.; Ruta, B., et al., Concentration and Velocity Profiles in a Polymeric Lithium-Ion Battery Electrolyte. *Energy Environ. Sci.* **2020,** *13*, 4312-4321.

288. Bastianini, F.; Pérez, G. E.; Hobson, A. R.; Rogers, S. E.; Parnell, A. J.; Grell, M.; Gutiérrez, A. F.; Dunbar, A. D. F., In−Situ Monitoring Poly(3-Hexylthiophene) Nanowire Formation and Shape Evolution in Solution via Small Angle Neutron Scattering. *Sol. Energy Mater. Sol. Cells* **2019,** *202*, 110128.

289. Bießmann, L.; Kreuzer, L. P.; Widmann, T.; Hohn, N.; Moulin, J.-F.; Müller-Buschbaum, P., Monitoring the Swelling Behavior of PEDOT:PSS Electrodes under High Humidity Conditions. *ACS Appl. Mater. Interfaces* **2018,** *10*, 9865-9872.

290. Van Bokhoven, J. A.; Lamberti, C., X-Ray Absorption and X-Ray Emission Spectroscopy: Theory and Applications. John Wiley & Sons: 2016; Vol. 1, pp 99-124.

291. Evans, J., X-Ray Absorption Spectroscopy for the Chemical and Materials Sciences. John Wiley & Sons: 2018; pp 117-161.

292. Smith, J. W.; Saykally, R. J., Soft X-Ray Absorption Spectroscopy of Liquids and Solutions. *Chem. Rev.* **2017,** *117*, 13909-13934.

293. Yano, J.; Yachandra, V. K., X-Ray Absorption Spectroscopy. *Photosynth. Res.* **2009,** *102*, 241-254.

294. Rehr, J. J.; Albers, R. C., Theoretical Approaches to X-Ray Absorption Fine Structure. *Rev. Mod. Phys.* **2000,** *72*, 621-654.

295. Schneck, E.; Demé, B., Structural Characterization of Soft Interfaces by Standing-Wave Fluorescence with X-Rays and Neutrons. *Curr. Opin. Colloid Interface Sci.* **2015,** *20*, 244-252.

296. Schollmeyer, H.; Guenoun, P.; Daillant, J.; Novikov, D. V., Ion Distribution in Polyelectrolyte Multilayers with Standing-Wave X-Ray Fluorescence. *J. Phys. Chem. B* **2007,** *111*, 4036-4042.

297. Schneck, E.; Schubert, T.; Konovalov, O. V.; Quinn, B. E.; Gutsmann, T.; Brandenburg, K.; Oliveira, R. G.; Pink, D. A.; Tanaka, M., Quantitative Determination of Ion Distributions in Bacterial Lipopolysaccharide Membranes by Grazing-Incidence X-Ray Fluorescence. *Proc. Natl. Acad. Sci.* **2010,** *107*, 9147-9151.

298. Shapovalov, V. L.; Ryskin, M. E.; Konovalov, O. V.; Hermelink, A.; Brezesinski, G., Elemental Analysis within the Electrical Double Layer Using Total Reflection X-Ray Fluorescence Technique. *J. Phys. Chem. B* **2007,** *111*, 3927-3934.

299. Brezesinski, G.; Schneck, E., Investigating Ions at Amphiphilic Monolayers with X-Ray Fluorescence. *Langmuir* **2019,** *35*, 8531-8542.

300. Andrés, M. A.; Fontaine, P.; Goldmann, M.; Serre, C.; Roubeau, O.; Gascón, I., Solvent-Exchange Process in Mof Ultrathin Films and its Effect on CO2 and Methanol Adsorption. *J. Colloid Interface Sci.* **2021,** *590*, 72-81.

301. Park, J.; Yang, R.; Hoven, C. V.; Garcia, A.; Fischer, D. A.; Nguyen, T. Q.; Bazan, G. C.; Delongchamp, D. M., Structural Characterization of Conjugated Polyelectrolyte Electron Transport Layers by NEXAFS Spectroscopy. *Adv. Mater.* **2008,** *20*, 2491-2496.

302. Germack, D. S.; Chan, C. K.; Hamadani, B. H.; Richter, L. J.; Fischer, D. A.; Gundlach, D. J.; Delongchamp, D. M., Substrate-Dependent Interface Composition and Charge Transport in Films for Organic Photovoltaics. *Appl. Phys. Lett.* **2009,** *94*, 233303.

303. Chan, C. K.; Richter, L. J.; Dinardo, B.; Jaye, C.; Conrad, B. R.; Ro, H. W.; Germack, D. S.; Fischer, D. A.; Delongchamp, D. M.; Gundlach, D. J., High Performance Airbrushed Organic Thin Film Transistors. *Appl. Phys. Lett.* **2010,** *96*, 133304.

304. Wu, D.; Kaplan, M.; Ro, H. W.; Engmann, S.; Fischer, D. A.; Delongchamp, D. M.; Richter, L. J.; Gann, E.; Thomsen, L.; McNeill, C. R., et al., Blade Coating Aligned, High-Performance, Semiconducting-Polymer Transistors. *Chem. Mater.* **2018,** *30*, 1924-1936.

305. Schuettfort, T.; Huettner, S.; Lilliu, S.; Macdonald, J. E.; Thomsen, L.; McNeill, C. R., Surface and Bulk Structural Characterization of a High-Mobility Electron-Transporting Polymer. *Macromolecules* **2011,** *44*, 1530-1539.

306. Carpenter, J. H.; Ghasemi, M.; Gann, E.; Angunawela, I.; Stuard, S. J.; Rech, J. J.; Ritchie, E.; O'Connor, B. T.; Atkin, J.; You, W., et al., Competition between Exceptionally Long-Range Alkyl Sidechain Ordering and Backbone Ordering in Semiconducting Polymers and Its Impact on Electronic and Optoelectronic Properties. *Adv. Funct. Mater.* **2019,** *29*, 1806977.

307. Watts, B.; Swaraj, S.; Nordlund, D.; Lüning, J.; Ade, H., Calibrated NEXAFS Spectra of Common Conjugated Polymers. *J. Chem. Phys.* **2011,** *134*, 024702.

308. Yan, Y.; Cheng, C.; Zhang, L.; Li, Y.; Lu, J., Deciphering the Reaction Mechanism of Lithium–Sulfur Batteries by in Situ/Operando Synchrotron-Based Characterization Techniques. *Adv. Energy Mater.* **2019,** *9*, 1900148.

309. Bak, S.-M.; Shadike, Z.; Lin, R.; Yu, X.; Yang, X.-Q., In Situ/Operando Synchrotron-Based X-Ray Techniques for Lithium-Ion Battery Research. *NPG Asia Mater.* **2018,** *10*, 563-580.

310. Catlow, C. R. A.; Chadwick, A. V.; Greaves, G. N.; Moroney, L. M.; Worboys, M. R., An EXAFS Study of the Structure of Rubidium Polyethyleneoxide Salt Complexes. *Solid State Ion.* **1983,** *9-10*, 1107-1113.

311. Latham, R. J.; Linford, R. G.; Pynenburg, R.; Schlindwein, W. S., EXAFS and Related Studies of Mixed Ion Polymer Electrolytes. *Electrochim. Acta* **1992,** *37*, 1529-1531.

312. Linford, R. G., Exafs Studies of Polymer Electrolytes. *Chem. Soc. Rev.* **1995,** *24*, 267-&.

313. Yun, D. J.; Jung, J.; Sung, Y. M.; Ra, H.; Kim, J. M.; Chung, J.; Kim, S. Y.; Kim, Y. S.; Heo, S.; Kim, K. H., et al., In-Situ Photoelectron Spectroscopy Study on the Air Degradation of PEDOT:PSS in Terms of Electrical and Thermoelectric Properties. *Adv. Electron. Mater.* **2020,** *6*, 2000620.

314. Yun, D.-J.; Park, S.-H.; Hwang, J.; Ra, H.; Kim, J.-M.; Chung, J.; Kim, S. H.; Kim, Y.-S.; Heo, S.; Kim, K.-H., In Situ Photoelectron Spectroscopy Study on the Buffer Role of Multiwalled Carbon Nanotubes against Thermal Degradation in Organic Conducting Composite Films with PEDOT:PSS. *J. Phys. Chem. C* **2019,** *123*, 2238-2247.

315. Saveleva, V. A.; Papaefthimiou, V.; Daletou, M. K.; Doh, W. H.; Ulhaq-Bouillet, C.; Diebold, M.; Zafeiratos, S.; Savinova, E. R., Operando near Ambient Pressure XPS (NAP-XPS) Study of the Pt Electrochemical Oxidation in H2O and H2O/O2 Ambients. *J. Phys. Chem. C* **2016,** *120*, 15930-15940.

316. Zhang, C.; Grass, M. E.; Yu, Y.; Gaskell, K. J.; Decaluwe, S. C.; Chang, R.; Jackson, G. S.; Hussain, Z.; Bluhm, H.; Eichhorn, B. W., et al., Multielement Activity Mapping and Potential Mapping in Solid Oxide Electrochemical Cells through the Use of Operando XPS. *ACS Catal.* **2012,** *2*, 2297-2304.

317. Walton, J.; Fairley, N., Noise Reduction in X-Ray Photoelectron Spectromicroscopy by a Singular Value Decomposition Sorting Procedure. *J. Electron Spectrosc. Relat. Phenom.* **2005,** *148*, 29-40.

318.   Song, Y.; Huo, F.; Jiang, Y.; Zhang, S.; Chen, S., In Situ Tracking of Organic Reactions at the Vapor/Liquid Interfaces of Ionic Liquids. *ChemPhysChem* **2018,** *19*, 2741-2750.

319.   Wibowo, R.; Aldous, L.; Jacobs, R. M. J.; Manan, N. S. A.; Compton, R. G., Monitoring Potassium Metal Electrodeposition from an Ionic Liquid Using in Situ Electrochemical-X-Ray Photoelectron Spectroscopy. *Chem. Phys. Lett.* **2011,** *509*, 72-76.

320.   Weingarth, D.; Foelske-Schmitz, A.; Wokaun, A.; Kotz, R., In Situ Electrochemical XPS Study of the Pt/[Emim][Bf4] System. *Electrochem. Commun.* **2011,** *13*, 619-622.

321.   Tada, K.; Takaishi, S.; Onoda, M., In-Situmeasurement of Ionization Potential of Conjugated Polymer During Electrochemical Doping Using Photoelectron Spectroscopy in Air. *Appl. Phys. Express* **2008,** *1*, 071801.

322.   Takahara, A.; Higaki, Y.; Hirai, T.; Ishige, R., Application of Synchrotron Radiation X-Ray Scattering and Spectroscopy to Soft Matter. *Polymers* **2020,** *12*, 1624.

323.   Kusoglu, A.; Weber, A. Z., New Insights into Perfluorinated Sulfonic-Acid Ionomers. *Chem. Rev.* **2017,** *117*, 987-1104.

324.   Rivnay, J.; Noriega, R.; Northrup, J. E.; Kline, R. J.; Toney, M. F.; Salleo, A., Structural Origin of Gap States in Semicrystalline Polymers and the Implications for Charge Transport. *Phys. Rev. B* **2011,** *83*, 121306(R).

325.   Guardado, J. O.; Salleo, A., Structural Effects of Gating Poly(3-Hexylthiophene) through an Ionic Liquid. *Adv. Funct. Mater.* **2017,** *27*, 1701791.

326.   Ohayon, D.; Savva, A.; Du, W.; Paulsen, B. D.; Uguz, I.; Ashraf, R. S.; Rivnay, J.; McCulloch, I.; Inal, S., Influence of Side Chains on the N-Type Organic Electrochemical Transistor Performance. *ACS Appl. Mater. Interfaces* **2021,** *13*, 4253-4266.

327.   Maria, I. P.; Paulsen, B. D.; Savva, A.; Ohayon, D.; Wu, R.; Hallani, R.; Basu, A.; Du, W.; Anthopoulos, T. D.; Inal, S., et al., The Effect of Alkyl Spacers on the Mixed Ionic-Electronic Conduction Properties of N-Type Polymers. *Adv. Funct. Mater.* **2021,** 2008718.

328.   Mahmood, A.; Wang, J. L., A Review of Grazing Incidence Small- and Wide-Angle X-Ray Scattering Techniques for Exploring the Film Morphology of Organic Solar Cells. *Solar RRL* **2020,** *4*, 2000337.

329.   Hildner, R.; Köhler, A.; Müller-Buschbaum, P.; Panzer, F.; Thelakkat, M., π-Conjugated Donor Polymers: Structure Formation and Morphology in Solution, Bulk and Photovoltaic Blends. *Adv. Energy Mater.* **2017,** *7*, 1700314.

330.   Manley, E. F.; Strzalka, J.; Fauvell, T. J.; Jackson, N. E.; Leonardi, M. J.; Eastham, N. D.; Marks, T. J.; Chen, L. X., In Situ GIWAXS Analysis of Solvent and Additive Effects on PTB7 Thin Film Microstructure Evolution During Spin Coating. *Adv. Mater.* **2017,** *29*, 1703933.

331.   Palumbiny, C. M.; Liu, F.; Russell, T. P.; Hexemer, A.; Wang, C.; Müller-Buschbaum, P., The Crystallization of PEDOT:PSS Polymeric Electrodes Probed in Situ During Printing. *Adv. Mater.* **2015,** *27*, 3391-3397.

332.   Kim, Y.-J.; Lee, S.; Niazi, M. R.; Hwang, K.; Tang, M.-C.; Lim, D.-H.; Kang, J.-S.; Smilgies, D.-M.; Amassian, A.; Kim, D.-Y., Systematic Study on the Morphological

Development of Blade-Coated Conjugated Polymer Thin Films via in Situ Measurements. *ACS Appl. Mater. Interfaces* **2020,** *12*, 36417-36427.

333.   Dauzon, E.; Mansour, A. E.; Niazi, M. R.; Munir, R.; Smilgies, D.-M.; Sallenave, X.; Plesse, C.; Goubard, F.; Amassian, A., Conducting and Stretchable PEDOT:PSS Electrodes: Role of Additives on Self-Assembly, Morphology, and Transport. *ACS Appl. Mater. Interfaces* **2019,** *11*, 17570-17582.

334.   Troughton, J. G.; Marchiori, B.; Delattre, R.; Escoubas, S.; Aliouat, M. Y.; Grigorian, S.; Ramuz, M., Simultaneous Measurement of Electrical Characteristics and Microstructure of Crystallised PEDOT:PSS Based Oects under Strain. *Org. Electron.* **2021,** *92*, 106108.

335.   Rivnay, J.; Noriega, R.; Kline, R. J.; Salleo, A.; Toney, M. F., Quantitative Analysis of Lattice Disorder and Crystallite Size in Organic Semiconductor Thin Films. *Phys. Rev. B* **2011,** *84*, 045203.

336.   Brotherton, E. E.; Hatton, F. L.; Cockram, A. A.; Derry, M. J.; Czajka, A.; Cornel, E. J.; Topham, P. D.; Mykhaylyk, O. O.; Armes, S. P., In Situ Small-Angle X-Ray Scattering Studies During Reversible Addition–Fragmentation Chain Transfer Aqueous Emulsion Polymerization. *J. Am. Chem. Soc.* **2019,** *141*, 13664-13675.

337.   Renaud, G.; Lazzari, R.; Leroy, F., Probing Surface and Interface Morphology with Grazing Incidence Small Angle X-Ray Scattering. *Surf. Sci. Rep.* **2009,** *64*, 255-380.

338.   Gu, X.; Gunkel, I.; Hexemer, A.; Gu, W.; Russell, T. P., An in Situ Grazing Incidence X-Ray Scattering Study of Block Copolymer Thin Films During Solvent Vapor Annealing. *Adv. Mater.* **2014,** *26*, 273-281.

339.   Gu, X.; Gunkel, I.; Hexemer, A.; Russell, T. P., Controlling Domain Spacing and Grain Size in Cylindrical Block Copolymer Thin Films by Means of Thermal and Solvent Vapor Annealing. *Macromolecules* **2016,** *49*, 3373-3381.

340.   Posselt, D.; Zhang, J.; Smilgies, D.-M.; Berezkin, A. V.; Potemkin, I. I.; Papadakis, C. M., Restructuring in Block Copolymer Thin Films: In Situ GISAXS Investigations During Solvent Vapor Annealing. *Prog. Polym. Sci.* **2017,** *66*, 80-115.

341.   Berezkin, A. V.; Jung, F.; Posselt, D.; Smilgies, D. M.; Papadakis, C. M., In Situ Tracking of Composition and Morphology of a Diblock Copolymer Film with GISAXS During Exchange of Solvent Vapors at Elevated Temperatures. *Adv. Funct. Mater.* **2018,** *28*, 1706226.

342.   Tian, T.; Yin, S.; Tu, S.; Weindl, C. L.; Wienhold, K. S.; Liang, S.; Schwartzkopf, M.; Roth, S. V.; Müller-Buschbaum, P., Morphology Transformation Pathway of Block Copolymer-Directed Cooperative Self-Assembly of ZnO Hybrid Films Monitored in Situ During Slot-Die Coating. *Adv. Funct. Mater.* **2021,** 2105644.

343.   Chou, K. W.; Yan, B.; Li, R.; Li, E. Q.; Zhao, K.; Anjum, D. H.; Alvarez, S.; Gassaway, R.; Biocca, A.; Thoroddsen, S. T., et al., Spin-Cast Bulk Heterojunction Solar Cells: A Dynamical Investigation. *Adv. Mater.* **2013,** *25*, 1923-1929.

344.   Yang, D.; Grott, S.; Jiang, X.; Wienhold, K. S.; Schwartzkopf, M.; Roth, S. V.; Müller-Buschbaum, P., In Situ Studies of Solvent Additive Effects on the Morphology

Development During Printing of Bulk Heterojunction Films for Organic Solar Cells. *Small Methods* **2020,** *4*, 2000418.

345.   Wu, W.-R.; Jeng, U. S.; Su, C.-J.; Wei, K.-H.; Su, M.-S.; Chiu, M.-Y.; Chen, C.-Y.; Su, W.-B.; Su, C.-H.; Su, A.-C., Competition between Fullerene Aggregation and Poly(3-Hexylthiophene) Crystallization Upon Annealing of Bulk Heterojunction Solar Cells. *ACS Nano* **2011,** *5*, 6233-6243.

346.   Lee, K. H.; Zhang, Y. L.; Burn, P. L.; Gentle, I. R.; James, M.; Nelson, A.; Meredith, P., Correlation of Diffusion and Performance in Sequentially Processed P3HT/PCBM Heterojunction Films by Time-Resolved Neutron Reflectometry. *J. Mater. Chem. C* **2013,** *1*, 2593-2598.

347.   Collins, B. A.; Gann, E., Resonant Soft X-Ray Scattering in Polymer Science. *J. Polym. Sci.* **2021**.

348.   Liu, F.; Brady, M. A.; Wang, C., Resonant Soft X-Ray Scattering for Polymer Materials. *Eur. Polym. J.* **2016,** *81*, 555-568.

349.   Shpyrko, O. G.; Isaacs, E. D.; Logan, J. M.; Feng, Y.; Aeppli, G.; Jaramillo, R.; Kim, H. C.; Rosenbaum, T. F.; Zschack, P.; Sprung, M., et al., Direct Measurement of Antiferromagnetic Domain Fluctuations. *Nature* **2007,** *447*, 68-71.

350.   Johnson, K. J.; Wiegart, L.; Abbott, A. C.; Johnson, E. B.; Baur, J. W.; Koerner, H., In Operando Monitoring of Dynamic Recovery in 3d-Printed Thermoset Nanocomposites by Xpcs. *Langmuir* **2019,** *35*, 8758-8768.

351.   Madsen, A.; Seydel, T.; Tolan, M.; Grübel, G., Grazing-Incidence Scattering of Coherent X-Rays from a Liquid Surface. *Journal of Synchrotron Radiation* **2005,** *12*, 786-794.

352.   Lal, J.; Malkova, S.; Mukhopadhyay, M. K.; Narayanan, S.; Fluerasu, A.; Darling, S. B.; Lurio, L. B.; Sutton, M., Dewetting in Immiscible Polymer Bilayer Films. *Phys. Rev. Mater.* **2017,** *1*, 015601.

353.   Quah, S. P.; Zhang, Y. G.; Fluerasu, A.; Yu, X. X.; Zheng, B. Q.; Yin, X. C.; Liu, W. P.; Bhatia, S. R., Techniques to Characterize Dynamics in Biomaterials Microenvironments: Xpcs and Microrheology of Alginate/PEO-PPO-PEO Hydrogels. *Soft Matter* **2021,** *17*, 1685-1691.

354.   Hernández, R.; Criado, M.; Nogales, A.; Sprung, M.; Mijangos, C.; Ezquerra, T. A., Deswelling of Poly(N-Isopropylacrylamide) Derived Hydrogels and Their Nanocomposites with Iron Oxide Nanoparticles as Revealed by X-Ray Photon Correlation Spectroscopy. *Macromolecules* **2015,** *48*, 393-399.

355.   Torres Arango, M. A.; Zhang, Y.; Li, R.; Doerk, G.; Fluerasu, A.; Wiegart, L., In-Operando Study of Shape Retention and Microstructure Development in a Hydrolyzing Sol–Gel Ink During 3d-Printing. *ACS Appl. Mater. Interfaces* **2020,** *12*, 51044-51056.

356.   Ju, G.; Xu, D.; Highland, M. J.; Thompson, C.; Zhou, H.; Eastman, J. A.; Fuoss, P. H.; Zapol, P.; Kim, H.; Stephenson, G. B., Coherent X-Ray Spectroscopy Reveals the Persistence of Island Arrangements During Layer-by-Layer Growth. *Nat. Phys.* **2019,** *15*, 589-594.

357.   Slim, A. H.; Poling-Skutvik, R.; Conrad, J. C., Local Confinement Controls Diffusive Nanoparticle Dynamics in Semidilute Polyelectrolyte Solutions. *Langmuir* **2020,** *36*, 9153-9159.

358.   Torres Arango, M.; Zhang, Y.; Zhao, C.; Li, R.; Doerk, G.; Nykypanchuk, D.; Chen-Wiegart, Y. C. K.; Fluerasu, A.; Wiegart, L., Ink-Substrate Interactions During 3d Printing Revealed by Time-Resolved Coherent X-Ray Scattering. *Mater. Today Phys.* **2020,** *14*, 100220.

359.   Yavitt, B. M.; Salatto, D.; Huang, Z.; Koga, Y. T.; Endoh, M. K.; Wiegart, L.; Poeller, S.; Petrash, S.; Koga, T., Revealing Nanoscale Dynamics During an Epoxy Curing Reaction with X-Ray Photon Correlation Spectroscopy. *J. Appl. Phys.* **2020,** *127*, 114701.

360.   Yavitt, B. M.; Wiegart, L.; Salatto, D.; Huang, Z.; Endoh, M. K.; Poeller, S.; Petrash, S.; Koga, T., Structural Dynamics in UV Curable Resins Resolved by in Situ 3d Printing X-Ray Photon Correlation Spectroscopy. *ACS Appl. Polym. Mater.* **2020,** *2*, 4096-4108.

361.   Oparaji, O.; Narayanan, S.; Sandy, A.; Ramakrishnan, S.; Hallinan, D., Structural Dynamics of Strongly Segregated Block Copolymer Electrolytes. *Macromolecules* **2018,** *51*, 2591-2603.

362.   Aime, J. P.; Bargain, F.; Schott, M.; Eckhardt, H.; Miller, G. G.; Elsenbaumer, R. L., Structural Study of Doped and Undoped Polythiophene in Solution by Small-Angle Neutron Scattering. *Phys. Rev. Lett.* **1989,** *62*, 55-58.

363.   Newbloom, G. M.; Weigandt, K. M.; Pozzo, D. C., Structure and Property Development of Poly(3-Hexylthiophene) Organogels Probed with Combined Rheology, Conductivity and Small Angle Neutron Scattering. *Soft Matter* **2012,** *8*, 8854-8864.

364.   Murphy, R. J.; Weigandt, K. M.; Uhrig, D.; Alsayed, A.; Badre, C.; Hough, L.; Muthukumar, M., Scattering Studies on Poly(3,4-Ethylenedioxythiophene)–Polystyrenesulfonate in the Presence of Ionic Liquids. *Macromolecules* **2015,** *48*, 8989-8997.

365.   Etampawala, T.; Tehrani, M.; Nematollahi, A.; He, L.; Dadmun, M., The Impact of Solvent Doping on the Morphology and Performance of Spray-Coated PEDOT:dPSS: A Usans and Sans Study. *Org. Electron.* **2017,** *51*, 86-93.

366.   Hoffmann, I., Neutrons for the Study of Dynamics in Soft Matter Systems. *Colloid Polym. Sci.* **2014,** *292*, 2053-2069.

367.   Li, J.; Koshnick, C.; Diallo, S. O.; Ackling, S.; Huang, D. M.; Jacobs, I. E.; Harrelson, T. F.; Hong, K.; Zhang, G.; Beckett, J., et al., Quantitative Measurements of the Temperature-Dependent Microscopic and Macroscopic Dynamics of a Molecular Dopant in a Conjugated Polymer. *Macromolecules* **2017,** *50*, 5476-5489.

368.   Zhan, P.; Zhang, W.; Jacobs, I. E.; Nisson, D. M.; Xie, R.; Weissen, A. R.; Colby, R. H.; Moulé, A. J.; Milner, S. T.; Maranas, J. K., et al., Side Chain Length Affects Backbone Dynamics in Poly(3-Alkylthiophene)S. *J. Polym. Sci., Part B: Polym. Phys.* **2018,** *56*, 1193-1202.

369.   Guilbert, A. A. Y.; Urbina, A.; Abad, J.; Díaz-Paniagua, C.; Batallán, F.; Seydel, T.; Zbiri, M.; García-Sakai, V.; Nelson, J., Temperature-Dependent Dynamics of Polyalkylthiophene Conjugated Polymers: A Combined Neutron Scattering and Simulation Study. *Chem. Mater.* **2015,** *27*, 7652-7661.

370. Guilbert, A. A. Y.; Zbiri, M.; Finn, P. A.; Jenart, M.; Fouquet, P.; Cristiglio, V.; Frick, B.; Nelson, J.; Nielsen, C. B., Mapping Microstructural Dynamics up to the Nanosecond of the Conjugated Polymer P3HT in the Solid State. *Chem. Mater.* **2019,** *31*, 9635-9651.

371. Guilbert, A. A. Y.; Zbiri, M.; Dunbar, A. D. F.; Nelson, J., Quantitative Analysis of the Molecular Dynamics of P3HT:PCBM Bulk Heterojunction. *J. Phys. Chem. B* **2017,** *121*, 9073-9080.

372. Guilbert, A. A. Y.; Zbiri, M.; Jenart, M. V. C.; Nielsen, C. B.; Nelson, J., New Insights into the Molecular Dynamics of P3HT:PCBM Bulk Heterojunction: A Time-of-Flight Quasi-Elastic Neutron Scattering Study. *J. Phys. Chem. Lett.* **2016,** *7*, 2252-2257.

373. Higgins, J. S.; Benoit, H. C., Polymers and Neutron Scattering. Oxford (United Kingdom): 1994; pp 1-436.

374. Jobic, H.; Theodorou, D. N., Quasi-Elastic Neutron Scattering and Molecular Dynamics Simulation as Complementary Techniques for Studying Diffusion in Zeolites. *Microporous Mesoporous Mater.* **2007,** *102*, 21-50.

375. Arrighi, V.; Higgins, J. S., Local Effects of Ring Topology Observed in Polymer Conformation and Dynamics by Neutron Scattering—a Review. *Polymers* **2020,** *12*, 1884.

376. Triolo, A.; Arrighi, V.; Triolo, R.; Passerini, S.; Mastragostino, M.; Lechner, R. E.; Ferguson, R.; Borodin, O.; Smith, G. D., Dynamic Heterogeneity in Polymer Electrolytes. Comparison between Qens Data and Md Simulations. *Physica B* **2001,** *301*, 163-167.

377. Yasuda, Y.; Hidaka, Y.; Mayumi, K.; Yamada, T.; Fujimoto, K.; Okazaki, S.; Yokoyama, H.; Ito, K., Molecular Dynamics of Polyrotaxane in Solution Investigated by Quasi-Elastic Neutron Scattering and Molecular Dynamics Simulation: Sliding Motion of Rings on Polymer. *J. Am. Chem. Soc.* **2019,** *141*, 9655-9663.

378. Berberan-Santos, M. N.; Bodunov, E. N.; Valeur, B., Mathematical Functions for the Analysis of Luminescence Decays with Underlying Distributions 1. Kohlrausch Decay Function (Stretched Exponential). *Chem. Phys.* **2005,** *315*, 171-182.

379. Galuska, L. A.; Muckley, E. S.; Cao, Z.; Ehlenberg, D. F.; Qian, Z.; Zhang, S.; Rondeau-Gagné, S.; Phan, M. D.; Ankner, J. F.; Ivanov, I. N., et al., Smart Transfer Method to Directly Compare the Mechanical Response of Water-Supported and Free-Standing Ultrathin Polymeric Films. *Nat. Commun.* **2021,** *12*, 2347.

380. Easley, A. D.; Ma, T.; Eneh, C. I.; Yun, J.; Thakur, R. M.; Lutkenhaus, J. L., A Practical Guide to Quartz Crystal Microbalance with Dissipation Monitoring of Thin Polymer Films. *J. Polym. Sci.* **2021**.

381. Speller, N. C.; Siraj, N.; Regmi, B. P.; Marzoughi, H.; Neal, C.; Warner, I. M., Rational Design of QCM-D Virtual Sensor Arrays Based on Film Thickness, Viscoelasticity, and Harmonics for Vapor Discrimination. *Anal. Chem.* **2015,** *87*, 5156-5166.

382. Sadman, K.; Wiener, C. G.; Weiss, R.; White, C. C.; Shull, K. R.; Vogt, B. D., Quantitative Rheometry of Thin Soft Materials Using the Quartz Crystal Microbalance with Dissipation. *Anal. Chem.* **2018,** *90*, 4079-4088.

383.   Voinova, M. V.; Rodahl, M.; Jonson, M.; Kasemo, B., Viscoelastic Acoustic Response of Layered Polymer Films at Fluid-Solid Interfaces: Continuum Mechanics Approach. *Phys. Scr.* **1999,** *59*, 391-396.

384.   Rodahl, M.; Kasemo, B., On the Measurement of Thin Liquid Overlayers with the Quartz-Crystal Microbalance. *Sens. Actuat. A-Phys.* **1996,** *54*, 448-456.

385.   Shpigel, N.; Levi, M. D.; Aurbach, D., Eqcm-D Technique for Complex Mechanical Characterization of Energy Storage Electrodes: Background and Practical Guide. *Energy Storage Mater.* **2019,** *21*, 399-413.

386.   Cho, N.-J.; Kanazawa, K. K.; Glenn, J. S.; Frank, C. W., Employing Two Different Quartz Crystal Microbalance Models to Study Changes in Viscoelastic Behavior Upon Transformation of Lipid Vesicles to a Bilayer on a Gold Surface. *Anal. Chem.* **2007,** *79*, 7027-7035.

387.   Saftics, A.; Prósz, G. A.; Türk, B.; Peter, B.; Kurunczi, S.; Horvath, R., In Situ Viscoelastic Properties and Chain Conformations of Heavily Hydrated Carboxymethyl Dextran Layers: A Comparative Study Using Owls and QCM-I Chips Coated with Waveguide Material. *Sci. Rep.* **2018,** *8*, 11840.

388.   McNamara, T. P.; Blanford, C. F., A Sensitivity Metric and Software to Guide the Analysis of Soft Films Measured by a Quartz Crystal Microbalance. *The Analyst* **2016,** *141*, 2911-2919.

389.   Johannsmann, D., Viscoelastic, Mechanical, and Dielectric Measurements on Complex Samples with the Quartz Crystal Microbalance. *Phys. Chem. Chem. Phys.* **2008,** *10*, 4516.

390.   Martin, E. J.; Mathew, M. T.; Shull, K. R., Viscoelastic Properties of Electrochemically Deposited Protein/Metal Complexes. *Langmuir* **2015,** *31*, 4008-4017.

391.   Liao, S.; Ge, C.; Qiu, D.; Tang, J.; Tan, F.; Chen, C.; Xu, L., Bvd Model for QCM Loaded by Viscoelastic Film in Gas Phase Application. *AIP Advances* **2020,** *10*, 075119.

392.   Su, H.; Liu, H.-Y.; Pappa, A.-M.; Hidalgo, T. C.; Cavassin, P.; Inal, S.; Owens, R. M.; Daniel, S., Facile Generation of Biomimetic-Supported Lipid Bilayers on Conducting Polymer Surfaces for Membrane Biosensing. *ACS Appl. Mater. Interfaces* **2019,** *11*, 43799-43810.

393.   Krauss, G.; Meichsner, F.; Hochgesang, A.; Mohanraj, J.; Salehi, S.; Schmode, P.; Thelakkat, M., Polydiketopyrrolopyrroles Carrying Ethylene Glycol Substituents as Efficient Mixed Ion-Electron Conductors for Biocompatible Organic Electrochemical Transistors. *Adv. Funct. Mater.* **2021,** 2010048.

394.   Flagg, L. Q.; Bischak, C. G.; Quezada, R. J.; Onorato, J. W.; Luscombe, C. K.; Ginger, D. S., P-Type Electrochemical Doping Can Occur by Cation Expulsion in a High-Performing Polymer for Organic Electrochemical Transistors. *ACS Mater. Lett.* **2020,** *2*, 254-260.

395.   Matyba, P.; Maturova, K.; Kemerink, M.; Robinson, N. D.; Edman, L., The Dynamic Organic P–N Junction. *Nat. Mater.* **2009,** *8*, 672-676.

396.   Giridharagopal, R.; Flagg, L. Q.; Harrison, J. S.; Ziffer, M. E.; Onorato, J.; Luscombe, C. K.; D, Electrochemical Strain Microscopy Probes Morphology-Induced Variations in Ion Uptake and Performance in Organic Electrochemical transistors. *Nat. Mater.* **2017,** *16*, 737-742.

397.   Yang, R.; Garcia, A.; Korystov, D.; Mikhailovsky, A.; Bazan, G. C.; Nguyen, T.-Q., Control of Interchain Contacts, Solid-State Fluorescence Quantum Yield, and Charge Transport of Cationic Conjugated Polyelectrolytes by Choice of Anion. *J. Am. Chem. Soc.* **2006,** *128*, 16532-16539.

398.   Warren, S.; Munteanu, G.; Rathod, D.; McCormac, T.; Dempsey, E., Scanning Electrochemical Microscopy Imaging of Poly (3,4-Ethylendioxythiophene)/Thionine Electrodes for Lactate Detection via Nadh Electrocatalysis. *Biosens. Bioelectron.* **2019,** *137*, 15-24.

399.   Magonov, S. N.; Reneker, D. H., Characterization of Polymer Surfaces with Atomic Force Microscopy. *Annu. Rev. Mater. Sci.* **1997,** *27*, 175-222.

400.   Butt, H.-J.; Cappella, B.; Kappl, M., Force Measurements with the Atomic Force Microscope: Technique, Interpretation and Applications. *Surf. Sci. Rep.* **2005,** *59*, 1-152.

401.   Wang, D.; Russell, T. P., Advances in Atomic Force Microscopy for Probing Polymer Structure and Properties. *Macromolecules* **2018,** *51*, 3-24.

402.   Wang, D.; Liu, F.; Yagihashi, N.; Nakaya, M.; Ferdous, S.; Liang, X.; Muramatsu, A.; Nakajima, K.; Russell, T. P., New Insights into Morphology of High Performance BHJ Photovoltaics Revealed by High Resolution AFM. *Nano Lett.* **2014,** *14*, 5727-5732.

403.   Zhu, W.; Spencer, A. P.; Mukherjee, S.; Alzola, J. M.; Sangwan, V. K.; Amsterdam, S. H.; Swick, S. M.; Jones, L. O.; Heiber, M. C.; Herzing, A. A., et al., Crystallography, Morphology, Electronic Structure, and Transport in Non-Fullerene/Non-Indacenodithienothiophene Polymer:Y6 Solar Cells. *J. Am. Chem. Soc.* **2020,** *142*, 14532-14547.

404.   Paulo, Á. S.; García, R., Tip-Surface Forces, Amplitude, and Energy Dissipation in Amplitude-Modulation (Tapping Mode) Force Microscopy. *Phys. Rev. B* **2001,** *64*, 193411.

405.   Giridharagopal, R.; Cox, P. A.; Ginger, D. S., Functional Scanning Probe Imaging of Nanostructured Solar Energy Materials. *Acc. Chem. Res.* **2016,** *49*, 1769-1776.

406.   Morino, Y.; Yokota, Y.; Hara, H.; Bando, K.-I.; Ono, S.; Imanishi, A.; Okada, Y.; Matsui, H.; Uemura, T.; Takeya, J., et al., Rapid Improvements in Charge Carrier Mobility at Ionic Liquid/Pentacene Single Crystal Interfaces by Self-Cleaning. *Phys. Chem. Chem. Phys.* **2020,** *22*, 6131-6135.

407.   James, P., In Situ Rehydration of Perfluorosulphonate Ion-Exchange Membrane Studied by AFM. *Polymer* **2000,** *41*, 4223-4231.

408.   Arita, T.; Kanda, Y.; Higashitani, K., In Situ Observation of Single Polymers Adsorbed onto Mica Surfaces in Water. *J. Colloid Interface Sci.* **2004,** *273*, 102-105.

409.   Baba, A.; Knoll, W.; Advincula, R., Simultaneous in Situ Electrochemical, Surface Plasmon Optical, and Atomic Force Microscopy Measurements: Investigation of Conjugated Polymer Electropolymerization. *Rev. Sci. Instrum.* **2006,** *77*, 064101.

410.   Lo, M. K. F.; Dazzi, A.; Marcott, C. A.; Dillon, E.; Hu, Q.; Kjoller, K.; Prater, C. B.; King, S. W., Nanoscale Chemical-Mechanical Characterization of Nanoelectronic Low-Kdielectric/Cu Interconnects. *ECS J. Solid State Sci. Technol.* **2016,** *5*, P3018-P3024.

411.   Li, X.; Sun, M.; Shan, C.; Chen, Q.; Wei, X., Mechanical Properties of 2d Materials Studied by in Situ Microscopy Techniques. *Adv. Mater. Interfaces* **2018,** *5*, 1701246.

412.   Jiang, C. S.; Yin, Y.; Guthrey, H.; Park, K.; Lee, S. H.; Al-Jassim, M. M., Local Electrical Degradations of Solid-State Electrolyte by Nm-Scale Operando Imaging of Ionic and Electronic Transports. *J. Power Sources* **2021,** *481*, 229138.

413.   Tang, L.; Li, H.-T.; Du, H.-N.; Zhang, F.; Hu, X.-F.; Hu, H.-Y., Study of the Disassembly–Assembly Process of A-Synuclein Fibrils by in Situ Atomic Force Microscopy. *Micron* **2006,** *37*, 675-679.

414.   Nguyen-Tri, P.; Ghassemi, P.; Carriere, P.; Nanda, S.; Assadi, A. A.; Nguyen, D. D., Recent Applications of Advanced Atomic Force Microscopy in Polymer Science: A Review. *Polymers* **2020,** *12*, 1142.

415.   Wang, L.; Putnis, C. V., Dissolution and Precipitation Dynamics at Environmental Mineral Interfaces Imaged by in Situ Atomic Force Microscopy. *Acc. Chem. Res.* **2020,** *53*, 1196-1205.

416.   Boyle, C. J.; Upadhyaya, M.; Wang, P.; Renna, L. A.; Lu-Díaz, M.; Pyo Jeong, S.; Hight-Huf, N.; Korugic-Karasz, L.; Barnes, M. D.; Aksamija, Z., et al., Tuning Charge Transport Dynamics via Clustering of Doping in Organic Semiconductor Thin Films. *Nat. Commun.* **2019,** *10*, 2827.

417.   Yamagishi, Y.; Kobayashi, K.; Kimura, T.; Noda, K.; Yamada, H., Local Carrier Dynamics in Organic Thin Film Transistors Investigated by Time-Resolved Kelvin Probe Force Microscopy. *Org. Electron.* **2018,** *57*, 118-122.

418.   De Sio, A.; Madena, T.; Huber, R.; Parisi, J.; Neyshtadt, S.; Deschler, F.; Da Como, E.; Esposito, S.; Von Hauff, E., Solvent Additives for Tuning the Photovoltaic Properties of Polymer–Fullerene Solar Cells. *Sol. Energy Mater. Sol. Cells* **2011,** *95*, 3536-3542.

419.   Xu, X.; Xiao, T.; Gu, X.; Yang, X.; Kershaw, S. V.; Zhao, N.; Xu, J.; Miao, Q., Solution-Processed Ambipolar Organic Thin-Film Transistors by Blending P- and N-Type Semiconductors: Solid Solution Versus Microphase Separation. *ACS Appl. Mater. Interfaces* **2015,** *7*, 28019-28026.

420.   Melitz, W.; Shen, J.; Kummel, A. C.; Lee, S., Kelvin Probe Force Microscopy and its Application. *Surf. Sci. Rep.* **2011,** *66*, 1-27.

421.   Jakob, D. S.; Wang, H. M.; Xu, X. J. G., Pulsed Force Kelvin Probe Force Microscopy. *ACS Nano* **2020,** *14*, 4839-4848.

422.   Collins, L.; Kilpatrick, J. I.; Kalinin, S. V.; Rodriguez, B. J., Towards Nanoscale Electrical Measurements in Liquid by Advanced KPFM Techniques: A Review. *Rep. Prog. Phys.* **2018,** *81*, 086101.

423.   Slinker, J. D.; Defranco, J. A.; Jaquith, M. J.; Silveira, W. R.; Zhong, Y.-W.; Moran-Mirabal, J. M.; Craighead, H. G.; Abruña, H. D.; Marohn, J. A.; Malliaras, G. G., Direct

Measurement of the Electric-Field Distribution in a Light-Emitting Electrochemical Cell. *Nat. Mater.* **2007,** *6*, 894-899.

424.   Yamagishi, Y.; Kobayashi, K.; Noda, K.; Yamada, H., Visualization of Trapped Charges Being Ejected from Organic Thin-Film Transistor Channels by Kelvin-Probe Force Microscopy During Gate Voltage Sweeps. *Appl. Phys. Lett.* **2016,** *108*, 093302.

425.   Collins, L.; Ahmadi, M.; Wu, T.; Hu, B.; Kalinin, S. V.; Jesse, S., Breaking the Time Barrier in Kelvin Probe Force Microscopy: Fast Free Force Reconstruction Using the G-Mode Platform. *ACS Nano* **2017,** *11*, 8717-8729.

426.   Kelley, T. W.; Granstrom, E. L.; Frisbie, C. D., Conducting Probe Atomic Force Microscopy: A Characterization Tool for Molecular Electronics. *Adv. Mater.* **1999,** *11*, 261-+.

427.   Si, H.; Zhang, S.; Ma, S.; Xiong, Z.; Kausar, A.; Liao, Q.; Zhang, Z.; Sattar, A.; Kang, Z.; Zhang, Y., Emerging Conductive Atomic Force Microscopy for Metal Halide Perovskite Materials and Solar Cells. *Adv. Energy Mater.* **2020,** *10*, 1903922.

428.   Lanza, M., *Conductive Atomic Force Microscopy: Applications in Nanomaterials*. John Wiley & Sons: 2017.

429.   Lee, H. J.; Lee, J.; Park, S.-M., Electrochemistry of Conductive Polymers. 45. Nanoscale Conductivity of PEDOT and PEDOT:PSS Composite Films Studied by Current-Sensing AFM. *J. Phys. Chem. B* **2010,** *114*, 2660-2666.

430.   Maddali, H.; House, K. L.; Emge, T. J.; O'Carroll, D. M., Identification of the Local Electrical Properties of Crystalline and Amorphous Domains in Electrochemically Doped Conjugated Polymer Thin Films. *Rsc Advances* **2020,** *10*, 21454-21463.

431.   Wood, D.; Hancox, I.; Jones, T. S.; Wilson, N. R., Quantitative Nanoscale Mapping with Temperature Dependence of the Mechanical and Electrical Properties of Poly(3-Hexylthiophene) by Conductive Atomic Force Microscopy. *J. Phys. Chem. C* **2015,** *119*, 11459-11467.

432.   Wu, D.; Zhang, J.; Dong, W.; Chen, H.; Huang, X.; Sun, B.; Chen, L., Temperature Dependent Conductivity of Vapor-Phase Polymerized PEDOT Films. *Synth. Met.* **2013,** *176*, 86-91.

433.   Groves, C.; Reid, O. G.; Ginger, D. S., Heterogeneity in Polymer Solar Cells: Local Morphology and Performance in Organic Photovoltaics Studied with Scanning Probe Microscopy. *Acc. Chem. Res.* **2010,** *43*, 612-620.

434.   Douhéret, O.; Lutsen, L.; Swinnen, A.; Breselge, M.; Vandewal, K.; Goris, L.; Manca, J., Nanoscale Electrical Characterization of Organic Photovoltaic Blends by Conductive Atomic Force Microscopy. *Appl. Phys. Lett.* **2006,** *89*, 032107.

435.   Ramer, G.; Aksyuk, V. A.; Centrone, A., Quantitative Chemical Analysis at the Nanoscale Using the Photothermal Induced Resonance Technique. *Anal. Chem.* **2017,** *89*, 13524-13531.

436.   Jahng, J.; Fishman, D. A.; Park, S.; Nowak, D. B.; Morrison, W. A.; Wickramasinghe, H. K.; Potma, E. O., Linear and Nonlinear Optical Spectroscopy at the Nanoscale with Photoinduced Force Microscopy. *Acc. Chem. Res.* **2015,** *48*, 2671-2679.

437.   Amenabar, I.; Poly, S.; Goikoetxea, M.; Nuansing, W.; Lasch, P.; Hillenbrand, R., Hyperspectral Infrared Nanoimaging of Organic Samples Based on Fourier Transform Infrared Nanospectroscopy. *Nat. Commun.* **2017,** *8*, 14402.

438.   Xue, L.; Yang, Y.; Xu, J.; Zhang, C.; Bin, H.; Zhang, Z.-G.; Qiu, B.; Li, X.; Sun, C.; Gao, L., et al., Side Chain Engineering on Medium Bandgap Copolymers to Suppress Triplet Formation for High-Efficiency Polymer Solar Cells. *Adv. Mater.* **2017,** *29*, 1703344.

439.   Harrison, J. S.; Waldow, D. A.; Cox, P. A.; Giridharagopal, R.; Adams, M.; Richmond, V.; Modahl, S.; Longstaff, M.; Zhuravlev, R.; Ginger, D. S., Noncontact Imaging of Ion Dynamics in Polymer Electrolytes with Time-Resolved Electrostatic Force Microscopy. *ACS Nano* **2019,** *13*, 536-543.

440.   Nowak, D.; Morrison, W.; Wickramasinghe, H. K.; Jahng, J.; Potma, E.; Wan, L.; Ruiz, R.; Albrecht, T. R.; Schmidt, K.; Frommer, J., et al., Nanoscale Chemical Imaging by Photoinduced Force Microscopy. *Sci. Adv.* **2016,** *2*, e1501571.

441.   Mathurin, J.; Pancani, E.; Deniset-Besseau, A.; Kjoller, K.; Prater, C. B.; Gref, R.; Dazzi, A., How to Unravel the Chemical Structure and Component Localization of Individual Drug-Loaded Polymeric Nanoparticles by Using Tapping AFM-IR. *Analyst* **2018,** *143*, 5940-5949.

442.   Dazzi, A.; Prater, C. B., AFM-IR: Technology and Applications in Nanoscale Infrared Spectroscopy and Chemical Imaging. *Chem. Rev.* **2017,** *117*, 5146-5173.

443.   Morsch, S.; Lyon, S.; Smith, S. D.; Gibbon, S. R., Mapping Water Uptake in an Epoxy-Phenolic Coating. *Prog. Org. Coat.* **2015,** *86*, 173-180.

444.   Awatani, T.; Midorikawa, H.; Kojima, N.; Ye, J.; Marcott, C., Morphology of Water Transport Channels and Hydrophobic Clusters in Nafion from High Spatial Resolution AFM-IR Spectroscopy and Imaging. *Electrochem. Commun.* **2013,** *30*, 5-8.

445.   Balke, N.; Jesse, S.; Kim, Y.; Adamczyk, L.; Tselev, A.; Ivanov, I. N.; Dudney, N. J.; Kalinin, S. V., Real Space Mapping of Li-Ion Transport in Amorphous Si Anodes with Nanometer Resolution. *Nano Lett.* **2010,** *10*, 3420-3425.

446.   Kim, S.; No, K.; Hong, S., Visualization of Ion Transport in Nafion Using Electrochemical Strain Microscopy. *Chem. Commun. (Cambridge, U. K.)* **2016,** *52*, 831-834.

447.   Morozovska, A. N.; Eliseev, E. A.; Balke, N.; Kalinin, S. V., Local Probing of Ionic Diffusion by Electrochemical Strain Microscopy: Spatial Resolution and Signal Formation Mechanisms. *J. Appl. Phys.* **2010,** *108*, 053712.

448.   Kim, Y.; Jang, J. H.; Park, S. J.; Jesse, S.; Donovan, L.; Borisevich, A. Y.; Lee, W.; Kalinin, S. V., Local Probing of Electrochemically Induced Negative Differential Resistance in Tio2 Memristive Materials. *Nanotechnology* **2013,** *24*, 085702.

449.   Alikin, D. O.; Romanyuk, K. N.; Slautin, B. N.; Rosato, D.; Shur, V. Y.; Kholkin, A. L., Quantitative Characterization of the Ionic Mobility and Concentration in Li-Battery Cathodes via Low Frequency Electrochemical Strain Microscopy. *Nanoscale* **2018,** *10*, 2503-2511.

450.   Polcari, D.; Dauphin-Ducharme, P.; Mauzeroll, J., Scanning Electrochemical Microscopy: A Comprehensive Review of Experimental Parameters from 1989 to 2015. *Chem. Rev.* **2016,** *116*, 13234-13278.

451.   Csóka, B.; Nagy, G., Determination of Diffusion Coefficient in Gel and in Aqueous Solutions Using Scanning Electrochemical Microscopy. *J. Biochem. Biophys. Methods* **2004,** *61*, 57-67.

452.   Ruiz, V.; Liljeroth, P.; Quinn, B. M.; Kontturi, K., Probing Conductivity of Polyelectrolyte/Nanoparticle Composite Films by Scanning Electrochemical Microscopy. *Nano Lett.* **2003,** *3*, 1459-1462.

453.   Ling, H.; Liu, L.; Lee, P. S.; Mandler, D.; Lu, X., Layer-by-Layer Assembly of PEDOT:PSS and Wo3 Nanoparticles: Enhanced Electrochromic Coloration Efficiency and Mechanism Studies by Scanning Electrochemical Microscopy. *Electrochim. Acta* **2015,** *174*, 57-65.

454.   Burchardt, M.; Wittstock, G., Kinetic Studies of Glucose Oxidase in Polyelectrolyte Multilayer Films by Means of Scanning Electrochemical Microscopy (SECM). *Bioelectrochemistry* **2008,** *72*, 66-76.

455.   De Jonge, N.; Ross, F. M., Electron Microscopy of Specimens in Liquid. *Nat. Nanotechnol.* **2011,** *6*, 695-704.

456.   Parent, L. R.; Gnanasekaran, K.; Korpanty, J.; Gianneschi, N. C., 100th Anniversary of Macromolecular Science Viewpoint: Polymeric Materials by in Situ Liquid-Phase Transmission Electron Microscopy. *ACS Macro Lett.* **2021,** *10*, 14-38.

457.   Wu, F.; Yao, N., Advances in Sealed Liquid Cells for in-Situ TEM Electrochemial Investigation of Lithium-Ion Battery. *Nano Energy* **2015,** *11*, 196-210.

458.   He, K.; Shokuhfar, T.; Shahbazian-Yassar, R., Imaging of Soft Materials Using in Situ Liquid-Cell Transmission Electron Microscopy. *J. Phys.: Condens. Matter* **2019,** *31*, 103001.

459.   Liu, J.; Wei, B.; Sloppy, J. D.; Ouyang, L.; Ni, C.; Martin, D. C., Direct Imaging of the Electrochemical Deposition of Poly(3,4-Ethylenedioxythiophene) by Transmission Electron Microscopy. *ACS Macro Lett.* **2015,** *4*, 897-900.

460.   Kelly, D. J.; Zhou, M.; Clark, N.; Hamer, M. J.; Lewis, E. A.; Rakowski, A. M.; Haigh, S. J.; Gorbachev, R. V., Nanometer Resolution Elemental Mapping in Graphene-Based TEM Liquid Cells. *Nano Lett.* **2018,** *18*, 1168-1174.

461.   Yuk, J. M.; Park, J.; Ercius, P.; Kim, K.; Hellebusch, D. J.; Crommie, M. F.; Lee, J. Y.; Zettl, A.; Alivisatos, A. P., High-Resolution EM of Colloidal Nanocrystal Growth Using Graphene Liquid Cells. *Science* **2012,** *336*, 61-64.

462.   De Jonge, N., Theory of the Spatial Resolution of (Scanning) Transmission Electron Microscopy in Liquid Water or Ice Layers. *Ultramicroscopy* **2018,** *187*, 113-125.

463.   Xin, W. B.; De Rosa, I. M.; Ye, P. Y.; Zheng, L.; Cao, Y.; Cao, C. Z.; Carlson, L.; Yang, J. M., Simplified Fabrication Strategy of Graphene Liquid Cells for the in Situ Transmission Electron Microscopy Study of Au Nanoparticles. *J. Phys. Chem. C* **2019,** *123*, 4523-4530.

464. Schneider, N. M.; Norton, M. M.; Mendel, B. J.; Grogan, J. M.; Ross, F. M.; Bau, H. H., Electron–Water Interactions and Implications for Liquid Cell Electron Microscopy. *J. Phys. Chem. C* **2014,** *118*, 22373-22382.

465. Newbury, D. E.; Ritchie, N. W. M., Elemental Mapping of Microstructures by Scanning Electron Microscopy-Energy Dispersive X-Ray Spectrometry (SEM-EDS): Extraordinary Advances with the Silicon Drift Detector (SDD). *J. Anal. At. Spectrom.* **2013,** *28*, 973-988.

466. Goldstein, J. I.; Newbury, D. E.; Michael, J. R.; Ritchie, N. W.; Scott, J. H. J.; Joy, D. C., *Scanning Electron Microscopy and X-Ray Microanalysis*. Springer: 2017.

467. Liang, J.; Xiao, X. X.; Chou, T. M.; Libera, M., Analytical Cryo-Scanning Electron Microscopy of Hydrated Polymers and Microgels. *Acc. Chem. Res.* **2021,** *54*, 2386-2396.

468. Arnoult, C.; Di Martino, J.; Khouchaf, L.; Toniazzo, V.; Ruch, D., Pressure and Scattering Regime Influence on the EDS Profile Resolution at a Composite Interface in Environmental SEM. *Micron* **2011,** *42*, 877-883.

469. Zoukel, A.; Khouchaf, L.; Arnoult, C.; Di Martino, J.; Ruch, D., A New Approach to Reach the Best Resolution of X-Ray Microanalysis in the Variable Pressure SEM. *Micron* **2013,** *46*, 12-21.

470. De Pablo, J. J.; Jackson, N. E.; Webb, M. A.; Chen, L.-Q.; Moore, J. E.; Morgan, D.; Jacobs, R.; Pollock, T.; Schlom, D. G.; Toberer, E. S., et al., New Frontiers for the Materials Genome Initiative. *Npj Comput. Mater.* **2019,** *5*, 41.

471. Clegg, P. S., Characterising Soft Matter Using Machine Learning. *Soft Matter* **2021,** *17*, 3991-4005.

472. He, B.; Chi, S.; Ye, A.; Mi, P.; Zhang, L.; Pu, B.; Zou, Z.; Ran, Y.; Zhao, Q.; Wang, D., et al., High-Throughput Screening Platform for Solid Electrolytes Combining Hierarchical Ion-Transport Prediction Algorithms. *Sci. Data* **2020,** *7*, 151.

473. Liu, Y.; Hu, Z.; Suo, Z.; Hu, L.; Feng, L.; Gong, X.; Liu, Y.; Zhang, J., High-Throughput Experiments Facilitate Materials Innovation: A Review. *Sci. China Technol. Sci.* **2019,** *62*, 521-545.

474. De Nicola, A.; Correa, A.; Giunchi, A.; Muccioli, L.; D'Avino, G.; Kido, J.; Milano, G., Bidimensional H-Bond Network Promotes Structural Order and Electron Transport in Bpympms Molecular Semiconductor. *Adv. Theory Simul.* **2021,** *4*, 2000302.

475. Bässler, H., Charge Transport in Disordered Organic Photoconductors a Monte Carlo Simulation Study. *physica status solidi (b)* **1993,** *175*, 15-56.

476. Heiber, M., Excimontec V1.0: An Open-Source Software Tool for Kinetic Monte Carlo Simulations of Organic Electronic Devices. *J. Open Source Softw.* **2020,** *5*, 2307.

477. Graf, P.; Nitzan, A.; Kurnikova, M. G.; Coalson, R. D., A Dynamic Lattice Monte Carlo Model of Ion Transport in Inhomogeneous Dielectric Environments: Method and Implementation. *J. Phys. Chem. B* **2000,** *104*, 12324-12338.

478. Lugli, P., Monte Carlo Simulation of Charge Transport in Semiconductor Devices. *Microelectron. Eng.* **1992,** *19*, 275-282.

479.   Houili, H.; Tutiš, E.; Lütjens, H.; Bussac, M. N.; Zuppiroli, L., Moled: Simulation of Multilayer Organic Light Emitting Diodes. *Comput. Phys. Commun.* **2003,** *156*, 108-122.

480.   Coehoorn, R.; Van Mensfoort, S. L. M., Effects of Disorder on the Current Density and Recombination Profile in Organic Light-Emitting Diodes. *Phys. Rev. B* **2009,** *80*, 085302.

481.   Knapp, E.; Häusermann, R.; Schwarzenbach, H. U.; Ruhstaller, B., Numerical Simulation of Charge Transport in Disordered Organic Semiconductor Devices. *J. Appl. Phys.* **2010,** *108*, 054504.

482.   Stavrinidou, E.; Leleux, P.; Rajaona, H.; Fiocchi, M.; Sanaur, S.; Malliaras, G. G., A Simple Model for Ion Injection and Transport in Conducting Polymers. *J. Appl. Phys.* **2013,** *113*, 244501.

483.   Zojer, K., Simulation of Charge Carriers in Organic Electronic Devices: Methods with Their Fundamentals and Applications. *Adv. Opt. Mater.* **2021,** 2100219.

484.   Tu, D.; Herlogsson, L.; Kergoat, L.; Crispin, X.; Berggren, M.; Forchheimer, R., A Static Model for Electrolyte-Gated Organic Field-Effect Transistors. *IEEE Trans. Electron Devices* **2011,** *58*, 3574-3582.

485.   Friedlein, J. T.; McLeod, R. R.; Rivnay, J., Device Physics of Organic Electrochemical Transistors. *Org. Electron.* **2018,** *63*, 398-414.

486.   Koch, W.; Holthausen, M. C., A Chemist's Guide to Density Functional Theory. Wiley: 2001; pp 1-313.

487.   Cramer, C. J., *Essentials of Computational Chemistry, Theories and Models*. Wiley: Chichester, England: 2002; p 562.

488.   Perdew, J. P.; Schmidt, K. In *Jacob's Ladder of Density Functional Approximations for the Exchange-Correlation Energy*, Density Functional Theory and Its Application to Materials, 2001; pp 1-20.

489.   Maurer, R. J.; Freysoldt, C.; Reilly, A. M.; Brandenburg, J. G.; Hofmann, O. T.; Bjorkman, T.; Lebegue, S.; Tkatchenko, A., Advances in Density-Functional Calculations for Materials Modeling. *Annual Review of Materials Research, Vol 49* **2019,** *49*, 1-30.

490.   Migliore, A., How to Extract Quantitative Information on Electronic Transitions from the Density Functional Theory "Black Box". *J. Chem. Theory Comput.* **2019,** *15*, 4915-4923.

491.   Nam, S.; Cho, E.; Sim, E.; Burke, K., Explaining and Fixing DFT Failures for Torsional Barriers. *J. Phys. Chem. Lett.* **2021,** *12*, 2796-2804.

492.   Cohen, A. J.; Mori-Sanchez, P.; Yang, W. T., Challenges for Density Functional Theory. *Chem. Rev.* **2012,** *112*, 289-320.

493.   Flait, D.; Head-Gordon, M., Delocalization Errors in Density Functional Theory Are Essentially Quadratic in Fractional Occupation Number. *J. Phys. Chem. Lett.* **2018,** *9*, 6280-6288.

494.   Bremond, E.; Perez-Jimenez, A. J.; Sancho-Garcia, J. C.; Adamo, C., Range-Separated Hybrid Density Functionals Made Simple. *J. Chem. Phys.* **2019,** *150*, 201102.

495.   Antony, J.; Sure, R.; Grimme, S., Using Dispersion-Corrected Density Functional Theory to Understand Supramolecular Binding Thermodynamics. *Chem. Commun. (Cambridge, U. K.)* **2015,** *51*, 1764-1774.

496.   Christensen, A. S.; Kubař, T.; Cui, Q.; Elstner, M., Semiempirical Quantum Mechanical Methods for Noncovalent Interactions for Chemical and Biochemical Applications. *Chem. Rev.* **2016,** *116*, 5301-5337.

497.   Levine, I. N.; Busch, D. H.; Shull, H., *Quantum Chemistry*. Pearson Prentice Hall Upper Saddle River, NJ: 2009; Vol. 6.

498.   Becke, A. D., Perspective: Fifty Years of Density-Functional Theory in Chemical Physics. *J. Chem. Phys.* **2014,** *140*, 18A301.

499.   Grimme, S., Density Functional Theory with London Dispersion Corrections. *WIREs Computational Molecular Science* **2011,** *1*, 211-228.

500.   Singh, S. K.; Crispin, X.; Zozoulenko, I. V., Oxygen Reduction Reaction in Conducting Polymer PEDOT: Density Functional Theory Study. *J. Phys. Chem. C* **2017,** *121*, 12270-12277.

501.   Cappai, A.; Antidormi, A.; Bosin, A.; Galliani, D.; Narducci, D.; Melis, C., Interplay between Synthetic Conditions and Micromorphology in Poly(3,4-Ethylenedioxythiophene):Tosylate (PEDOT:Tos): An Atomistic Investigation. *Phys. Chem. Chem. Phys.* **2019,** *21*, 8580-8586.

502.   Pinna, A.; Casula, M. F.; Pilia, L.; Cappai, A.; Melis, C.; Ricci, P. C.; Carbonaro, C. M., Driving the Polymerization of PEDOT:PSS by Means of a Nanoporous Template: Effects on the Structure. *Polymer* **2019,** *185*, 121941.

503.   Kim, D.; Zozoulenko, I., Why Is Pristine PEDOT Oxidized to 33%? A Density Functional Theory Study of Oxidative Polymerization Mechanism. *J. Phys. Chem. B* **2019,** *123*, 5160-5167.

504.   Gueskine, V.; Singh, A.; Vagin, M.; Crispin, X.; Zozoulenko, I., Molecular Oxygen Activation at a Conducting Polymer: Electrochemical Oxygen Reduction Reaction at PEDOT Revisited, a Theoretical Study. *J. Phys. Chem. C* **2020,** *124*, 13263-13272.

505.   Poater, J.; Casanovas, J.; Solà, M.; AlemáN, C., Examining the Planarity of Poly(3,4-Ethylenedioxythiophene): Consideration of Self-Rigidification, Electronic, and Geometric Effects. *J. Phys. Chem. A* **2010,** *114*, 1023-1028.

506.   Zade, S. S.; Bendikov, M., Twisting of Conjugated Oligomers and Polymers: Case Study of Oligo- and Polythiophene. *Chem. Eur. J* **2007,** *13*, 3688-3700.

507.   Lenz, A.; Kariis, H.; Pohl, A.; Persson, P.; Ojamäe, L., The Electronic Structure and Reflectivity of PEDOT:PSS from Density Functional Theory. *Chem. Phys.* **2011,** *384*, 44-51.

508.   McCormick, T. M.; Bridges, C. R.; Carrera, E. I.; Dicarmine, P. M.; Gibson, G. L.; Hollinger, J.; Kozycz, L. M.; Seferos, D. S., Conjugated Polymers: Evaluating DFT Methods for More Accurate Orbital Energy Modeling. *Macromolecules* **2013,** *46*, 3879-3886.

509.   Abutaha, A.; Kumar, P.; Yildirim, E.; Shi, W.; Yang, S.-W.; Wu, G.; Hippalgaonkar, K., Correlating Charge and Thermoelectric Transport to Paracrystallinity in Conducting Polymers. *Nat. Commun.* **2020,** *11*, 1737.

510. Liu, W.; Müller, L.; Ma, S.; Barlow, S.; Marder, S. R.; Kowalsky, W.; Köhn, A.; Lovrincic, R., Origin of the π–π Spacing Change Upon Doping of Semiconducting Polymers. *J. Phys. Chem. C* **2018,** *122*, 27983-27990.

511. Kim, E.-G.; BréDas, J.-L., Electronic Evolution of Poly(3,4-Ethylenedioxythiophene) (PEDOT): From the Isolated Chain to the Pristine and Heavily Doped Crystals. *J. Am. Chem. Soc.* **2008,** *130*, 16880-16889.

512. Wang, S.; Sun, H.; Ail, U.; Vagin, M.; Persson, P. O. Å.; Andreasen, J. W.; Thiel, W.; Berggren, M.; Crispin, X.; Fazzi, D., et al., Thermoelectric Properties of Solution-Processed N-Doped Ladder-Type Conducting Polymers. *Adv. Mater.* **2016,** *28*, 10764-10771.

513. Pingel, P.; Zhu, L.; Park, K. S.; Vogel, J.-O.; Janietz, S.; Kim, E.-G.; Rabe, J. P.; Brédas, J.-L.; Koch, N., Charge-Transfer Localization in Molecularly Doped Thiophene-Based Donor Polymers. *J. Phys. Chem. Lett.* **2010,** *1*, 2037-2041.

514. Shi, W.; Zhao, T.; Xi, J.; Wang, D.; Shuai, Z., Unravelling Doping Effects on PEDOT at the Molecular Level: From Geometry to Thermoelectric Transport Properties. *J. Am. Chem. Soc.* **2015,** *137*, 12929-12938.

515. Sahalianov, I.; Hynynen, J.; Barlow, S.; Marder, S. R.; Müller, C.; Zozoulenko, I., UV-to-IR Absorption of Molecularly P-Doped Polythiophenes with Alkyl and Oligoether Side Chains: Experiment and Interpretation Based on Density Functional Theory. *J. Phys. Chem. B* **2020,** *124*, 11280-11293.

516. Wheeler, D. L.; Rainwater, L. E.; Green, A. R.; Tomlinson, A. L., Modeling Electrochromic Poly-Dioxythiophene-Containing Materials through TDDFT. *Phys. Chem. Chem. Phys.* **2017,** *19*, 20251-20258.

517. Sainbileg, B.; Lan, Y.-B.; Wang, J.-K.; Hayashi, M., Deciphering Anomalous Raman Features of Regioregular Poly(3-Hexylthiophene) in Ordered Aggregation Form. *J. Phys. Chem. C* **2018,** *122*, 4224-4231.

518. Farouil, L.; Alary, F.; Bedel-Pereira, E.; Heully, J.-L., Revisiting the Vibrational and Optical Properties of P3HT: A Combined Experimental and Theoretical Study. *J. Phys. Chem. A* **2018,** *122*, 6532-6545.

519. Fazzi, D.; Negri, F., Addressing the Elusive Polaronic Nature of Multiple Redox States in a π-Conjugated Ladder-Type Polymer. *Adv. Electron. Mater.* **2021,** *7*, 2000786.

520. Barone, V.; Biczysko, M.; Bloino, J., Fully Anharmonic IR and Raman Spectra of Medium-Size Molecular Systems: Accuracy and Interpretation. *Phys. Chem. Chem. Phys.* **2014,** *16*, 1759-1787.

521. Donohoo-Vallett, P. J.; Bragg, A. E., π-Delocalization and the Vibrational Spectroscopy of Conjugated Materials: Computational Insights on Raman Frequency Dispersion in Thiophene, Furan, and Pyrrole Oligomers. *J. Phys. Chem. B* **2015,** *119*, 3583-3594.

522. Milani, A.; Brambilla, L.; Del Zoppo, M.; Zerbi, G., Raman Dispersion and Intermolecular Interactions in Unsubstituted Thiophene Oligomers. *J. Phys. Chem. B* **2007,** *111*, 1271-1276.

523.   Bedoya-Martínez, N.; Schrode, B.; Jones, A. O. F.; Salzillo, T.; Ruzié, C.; Demitri, N.; Geerts, Y. H.; Venuti, E.; Della Valle, R. G.; Zojer, E., et al., DFT-Assisted Polymorph Identification from Lattice Raman Fingerprinting. *J. Phys. Chem. Lett.* **2017,** *8*, 3690-3695.

524.   Erba, A.; Maul, J.; Ferrabone, M.; Dovesi, R.; Rérat, M.; Carbonnière, P., Anharmonic Vibrational States of Solids from DFT Calculations. Part Ii: Implementation of the Vscf and Vci Methods. *J. Chem. Theory Comput.* **2019,** *15*, 3766-3777.

525.   Lin, C. Y.; Gilbert, A. T. B.; Gill, P. M. W., Calculating Molecular Vibrational Spectra Beyond the Harmonic Approximation. *Theor. Chem. Acc.* **2008,** *120*, 23-35.

526.   Yang, Q.; Mendolicchio, M.; Barone, V.; Bloino, J., Accuracy and Reliability in the Simulation of Vibrational Spectra: A Comprehensive Benchmark of Energies and Intensities Issuing from Generalized Vibrational Perturbation Theory to Second Order (GVPT2). *Frontiers in Astronomy and Space Sciences* **2021,** *8*, 77.

527.   Huff, G. S.; Gallaher, J. K.; Hodgkiss, J. M.; Gordon, K. C., No Single DFT Method Can Predict Raman Cross-Sections, Frequencies and Electronic Absorption Maxima of Oligothiophenes. *Synth. Met.* **2017,** *231*, 1-6.

528.   Yildirim, E.; Wu, G.; Yong, X.; Tan, T. L.; Zhu, Q.; Xu, J.; Ouyang, J.; Wang, J.-S.; Yang, S.-W., A Theoretical Mechanistic Study on Electrical Conductivity Enhancement of Dmso Treated PEDOT:PSS. *J. Mater. Chem. C* **2018,** *6*, 5122-5131.

529.   Sahalianov, I.; Singh, S. K.; Tybrandt, K.; Berggren, M.; Zozoulenko, I., The Intrinsic Volumetric Capacitance of Conducting Polymers: Pseudo-Capacitors or Double-Layer Supercapacitors? *RSC Advances* **2019,** *9*, 42498-42508.

530.   Williams, C. D.; Dix, J.; Troisi, A.; Carbone, P., Effective Polarization in Pairwise Potentials at the Graphene–Electrolyte Interface. *J. Phys. Chem. Lett.* **2017,** *8*, 703-708.

531.   Mosconi, E.; Salvatori, P.; Saba, M. I.; Mattoni, A.; Bellani, S.; Bruni, F.; Santiago Gonzalez, B.; Antognazza, M. R.; Brovelli, S.; Lanzani, G., et al., Surface Polarization Drives Photoinduced Charge Separation at the P3HT/Water Interface. *ACS Energy Letters* **2016,** *1*, 454-463.

532.   Misra, R. P.; Blankschtein, D., Insights on the Role of Many-Body Polarization Effects in the Wetting of Graphitic Surfaces by Water. *J. Phys. Chem. C* **2017,** *121*, 28166-28179.

533.   Noriega, R.; Salleo, A.; Spakowitz, A. J., Chain Conformations Dictate Multiscale Charge Transport Phenomena in Disordered Semiconducting Polymers. *Proc. Natl. Acad. Sci.* **2013,** *110*, 16315-16320.

534.   Rolland, N.; Franco-Gonzalez, J. F.; Volpi, R.; Linares, M.; Zozoulenko, I. V., Understanding Morphology-Mobility Dependence in PEDOT:Tos. *Phys. Rev. Mater.* **2018,** *2*, 045605.

535.   Chung, J.; Khot, A.; Savoie, B. M.; Boudouris, B. W., 100th Anniversary of Macromolecular Science Viewpoint: Recent Advances and Opportunities for Mixed Ion and Charge Conducting Polymers. *ACS Macro Lett.* **2020,** *9*, 646-655.

536. Warshel, A.; Karplus, M., Calculation of Ground and Excited State Potential Surfaces of Conjugated Molecules. I. Formulation and Parametrization. *J. Am. Chem. Soc.* **1972,** *94*, 5612-5625.

537. Thompson, M. A.; Glendening, E. D.; Feller, D., The Nature of K+/Crown Ether Interactions: A Hybrid Quantum Mechanical-Molecular Mechanical Study. *J. Phys. Chem.* **1994,** *98*, 10465-10476.

538. Watanabe, H. C.; Cui, Q., Quantitative Analysis of QM/MM Boundary Artifacts and Correction in Adaptive QM/MM Simulations. *J. Chem. Theory Comput.* **2019,** *15*, 3917-3928.

539. Karelina, M.; Kulik, H. J., Systematic Quantum Mechanical Region Determination in QM/MM Simulation. *J. Chem. Theory Comput.* **2017,** *13*, 563-576.

540. Pezeshki, S.; Lin, H., Adaptive-Partitioning QM/MM for Molecular Dynamics Simulations: 4. Proton Hopping in Bulk Water. *J. Chem. Theory Comput.* **2015,** *11*, 2398-2411.

541. Zheng, M.; Kuriappan, J. A.; Waller, M. P., Toward More Efficient Density-Based Adaptive QM/MM Methods. *Int. J. Quantum Chem.* **2017,** *117*, e25336.

542. Watanabe, H. C.; Kubař, T.; Elstner, M., Size-Consistent Multipartitioning QM/MM: A Stable and Efficient Adaptive QM/MM Method. *J. Chem. Theory Comput.* **2014,** *10*, 4242-4252.

543. Groenhof, G., Introduction to QM/MM Simulations. Humana Press: 2013; pp 43-66.

544. Senn, H. M.; Thiel, W., QM/MM Methods for Biomolecular Systems. *Angew. Chem. Int. Ed.* **2009,** *48*, 1198-1229.

545. Boulanger, E.; Harvey, J. N., QM/MM Methods for Free Energies and Photochemistry. *Curr. Opin. Struct. Biol.* **2018,** *49*, 72-76.

546. Morzan, U. N.; Alonso De Armiño, D. J.; Foglia, N. O.; Ramírez, F.; González Lebrero, M. C.; Scherlis, D. A.; Estrin, D. A., Spectroscopy in Complex Environments from QM–MM Simulations. *Chem. Rev.* **2018,** *118*, 4071-4113.

547. Sokol, A. A.; Bromley, S. T.; French, S. A.; Catlow, C. R. A.; Sherwood, P., Hybrid QM/MM Embedding Approach for the Treatment of Localized Surface States in Ionic Materials. *Int. J. Quantum Chem.* **2004,** *99*, 695-712.

548. Kaneko, Y.; Park, J.; Yokotsuji, H.; Odawara, M.; Takase, H.; Ue, M.; Lee, M.-E., Cathode Solid Electrolyte Interface's Function Originated from Salt Type Additives in Lithium Ion Batteries. *Electrochim. Acta* **2016,** *222*, 271-279.

549. Zuo, G.; Linares, M.; Upreti, T.; Kemerink, M., General Rule for the Energy of Water-Induced Traps in Organic Semiconductors. *Nat. Mater.* **2019,** *18*, 588-593.

550. Sjöqvist, J.; Linares, M.; Mikkelsen, K. V.; Norman, P., QM/MM-Md Simulations of Conjugated Polyelectrolytes: A Study of Luminescent Conjugated Oligothiophenes for Use as Biophysical Probes. *J. Phys. Chem. A* **2014,** *118*, 3419-3428.

551. Canales, M.; Torras, J.; Fabregat, G.; Meneguzzi, A.; Alemán, C., Polyaniline Emeraldine Salt in the Amorphous Solid State: Polaron Versus Bipolaron. *J. Phys. Chem. B* **2014,** *118*, 11552-11562.

552.	Loco, D.; Lagardère, L.; Caprasecca, S.; Lipparini, F.; Mennucci, B.; Piquemal, J.-P., Hybrid QM/MM Molecular Dynamics with AMOEBA Polarizable Embedding. *J. Chem. Theory Comput.* **2017,** *13*, 4025-4033.

553.	Lev, B.; Roux, B.; Noskov, S. Y., Relative Free Energies for Hydration of Monovalent Ions from QM and QM/MM Simulations. *J. Chem. Theory Comput.* **2013,** *9*, 4165-4175.

554.	Elliott, J. D.; Troisi, A.; Carbone, P., A QM/Md Coupling Method to Model the Ion-Induced Polarization of Graphene. *J. Chem. Theory Comput.* **2020,** *16*, 5253-5263.

555.	Dohm, S.; Spohr, E.; Korth, M., Developing Adaptive QM/MM Computer Simulations for Electrochemistry. *J. Comput. Chem.* **2017,** *38*, 51-58.

556.	Smith, G. D.; Bedrov, D.; Li, L.; Byutner, O., A Molecular Dynamics Simulation Study of the Viscoelastic Properties of Polymer Nanocomposites. *J. Chem. Phys.* **2002,** *117*, 9478-9489.

557.	Bosko, J. T.; Todd, B. D.; Sadus, R. J., Viscoelastic Properties of Dendrimers in the Melt from Nonequlibrium Molecular Dynamics. *J. Chem. Phys.* **2004,** *121*, 12050-12059.

558.	Borodin, O.; Bedrov, D.; Smith, G. D.; Nairn, J.; Bardenhagen, S., Multiscale Modeling of Viscoelastic Properties of Polymer Nanocomposites. *J. Polym. Sci., Part B: Polym. Phys.* **2005,** *43*, 1005-1013.

559.	Nouri, N.; Ziaei-Rad, S., A Molecular Dynamics Investigation on Mechanical Properties of Cross-Linked Polymer Networks. *Macromolecules* **2011,** *44*, 5481-5489.

560.	Shi, W.; Shuai, Z.; Wang, D., Tuning Thermal Transport in Chain-Oriented Conducting Polymers for Enhanced Thermoelectric Efficiency: A Computational Study. *Adv. Funct. Mater.* **2017,** *27*, 1702847.

561.	Li, C.; Ma, H.; Tian, Z., Thermoelectric Properties of Crystalline and Amorphous Polypyrrole: A Computational Study. *Applied Thermal Engineering* **2017,** *111*, 1441-1447.

562.	De Oliveira Neto, P. H.; Da Silva Filho, D. A.; Roncaratti, L. F.; Acioli, P. H.; E Silva, G. M., Low-Temperature Seebeck Coefficients for Polaron-Driven Thermoelectric Effect in Organic Polymers. *J. Phys. Chem. A* **2016,** *120*, 4923-4927.

563.	Andrew, R. L., *Molecular Modeling Principles and Applications*. 2001.

564.	Allen, M. P.; Tildesley, D. J., *Computer Simulation of Liquids*. Oxford university press: 2017.

565.	Frenkel, D.; Smit, B., *Understanding Molecular Simulation: From Algorithms to Applications*. Elsevier: 2001; Vol. 1.

566.	Dkhissi, A.; Beljonne, D.; Lazzaroni, R.; Louwet, F.; Groenendaal, B., Modeling of the Solid-State Packing of Charged Chains (PEDOT) in the Presence of the Counterions (TSA) and the Solvent (DEG). *Theor. Chem. Acc.* **2008,** *119*, 305-312.

567.	Preat, J.; Zanuy, D.; PerpèTe, E. A.; AlemáN, C., Binding of Cationic Conjugated Polymers to DNA: Atomistic Simulations of Adducts Involving the Dickerson's Dodecamer. *Biomacromolecules* **2011,** *12*, 1298-1304.

568.   Teixeira-Dias, B.; Zanuy, D.; Del Valle, L. J.; Estrany, F.; Armelin, E.; Alemán, C., Influence of the Doping Level on the Interactions between Poly(3,4-Ethylenedioxythiophene) and Plasmid DNA. *Macromol. Chem. Phys.* **2010,** *211*, 1117-1126.

569.   Zanuy, D.; Alemán, C., Resolving the Subnanometric Structure of Ultrathin Films of Poly(3,4-Ethylenedioxythiophene) on Steel Surfaces: A Molecular Modeling Approach. *Soft Matter* **2013,** *9*, 11634.

570.   Bhowmik, R.; Berry, R. J.; Varshney, V.; Durstock, M. F.; Leever, B. J., Molecular Modeling of Interfaces between Hole Transport and Active Layers in Flexible Organic Electronic Devices. *J. Phys. Chem. C* **2015,** *119*, 27909-27918.

571.   Franco-Gonzalez, J. F.; Rolland, N.; Zozoulenko, I. V., Substrate-Dependent Morphology and Its Effect on Electrical Mobility of Doped Poly(3,4-Ethylenedioxythiophene) (PEDOT) Thin Films. *ACS Appl. Mater. Interfaces* **2018,** *10*, 29115-29126.

572.   De Izarra, A.; Choi, C.; Jang, Y. H.; Lansac, Y., Ionic Liquid for PEDOT:PSS Treatment. Ion Binding Free Energy in Water Revealing the Importance of Anion Hydrophobicity. *J. Phys. Chem. B* **2021,** *125*, 1916-1923.

573.   Friederich, P.; León, S.; Perea, J. D.; Roch, L. M.; Aspuru-Guzik, A., The Influence of Sorbitol Doping on Aggregation and Electronic Properties of PEDOT: PSS: A Theoretical Study. *Mach. Learn.: Sci. Technol.* **2020,** *2*, 01LT01.

574.   Franco-Gonzalez, J. F.; Zozoulenko, I. V., Molecular Dynamics Study of Morphology of Doped PEDOT: From Solution to Dry Phase. *J. Phys. Chem. B* **2017,** *121*, 4299-4307.

575.   Matta, M.; Wu, R.; Paulsen, B. D.; Petty, A. J.; Sheelamanthula, R.; McCulloch, I.; Schatz, G. C.; Rivnay, J., Ion Coordination and Chelation in a Glycolated Polymer Semiconductor: Molecular Dynamics and X-Ray Fluorescence Study. *Chem. Mater.* **2020,** *32*, 7301-7308.

576.   Dong, B. X.; Nowak, C.; Onorato, J. W.; Ma, T.; Niklas, J.; Poluektov, O. G.; Grocke, G.; Ditusa, M. F.; Escobedo, F. A.; Luscombe, C. K., et al., Complex Relationship between Side-Chain Polarity, Conductivity, and Thermal Stability in Molecularly Doped Conjugated Polymers. *Chem. Mater.* **2021,** *33*, 741-753.

577.   Dong, B. X.; Liu, Z.; Misra, M.; Strzalka, J.; Niklas, J.; Poluektov, O. G.; Escobedo, F. A.; Ober, C. K.; Nealey, P. F.; Patel, S. N., Structure Control of a π-Conjugated Oligothiophene-Based Liquid Crystal for Enhanced Mixed Ion/Electron Transport Characteristics. *ACS Nano* **2019,** *13*, 7665-7675.

578.   Misra, M.; Liu, Z.; Dong, B. X.; Patel, S. N.; Nealey, P. F.; Ober, C. K.; Escobedo, F. A., Thermal Stability of π-Conjugated N-Ethylene-Glycol-Terminated Quaterthiophene Oligomers: A Computational and Experimental Study. *ACS Macro Lett.* **2020,** *9*, 295-300.

579.   Moser, M.; Savagian, L. R.; Savva, A.; Matta, M.; Ponder, J. F.; Hidalgo, T. C.; Ohayon, D.; Hallani, R.; Reisjalali, M.; Troisi, A., et al., Ethylene Glycol-Based Side Chain Length Engineering in Polythiophenes and its Impact on Organic Electrochemical Transistor Performance. *Chem. Mater.* **2020,** *32*, 6618-6628.

580. Ghosh, S.; Zozoulenko, I., Effect of Substrate on Structural Phase Transition in a Conducting Polymer During Ion Injection and Water Intake: A View from a Computational Microscope. *ACS Appl. Electron. Mater.* **2020,** *2*, 4034-4041.

581. Gkeka, P.; Stoltz, G.; Farimani, A. B.; Belkacemi, Z.; Ceriotti, M.; Chodera, J. D.; Dinner, A. R.; Ferguson, A. L.; Maillet, J. B.; Minoux, H., et al., Machine Learning Force Fields and Coarse-Grained Variables in Molecular Dynamics: Application to Materials and Biological Systems. *J. Chem. Theory Comput.* **2020,** *16*, 4757-4775.

582. Morawietz, T.; Artrith, N., Machine Learning-Accelerated Quantum Mechanics-Based Atomistic Simulations for Industrial Applications. *Journal of Computer-Aided Molecular Design* **2021,** *35*, 557-586.

583. Smith, J. S.; Zubatyuk, R.; Nebgen, B.; Lubbers, N.; Barros, K.; Roitberg, A. E.; Isayev, O.; Tretiak, S., The Ani-1ccx and Ani-1x Data Sets, Coupled-Cluster and Density Functional Theory Properties for Molecules. *Sci. Data* **2020,** *7*, 134.

584. Mueller, T.; Hernandez, A.; Wang, C., Machine Learning for Interatomic Potential Models. *J. Chem. Phys.* **2020,** *152*, 050902.

585. Ko, T. W.; Finkler, J. A.; Goedecker, S.; Behler, J., A Fourth-Generation High-Dimensional Neural Network Potential with Accurate Electrostatics Including Non-Local Charge Transfer. *Nat. Commun.* **2021,** *12*, 398.

586. Böselt, L.; Thürlemann, M.; Riniker, S., Machine Learning in QM/MM Molecular Dynamics Simulations of Condensed-Phase Systems. *J. Chem. Theory Comput.* **2021,** *17*, 2641-2658.

587. Yue, S.; Muniz, M. C.; Calegari Andrade, M. F.; Zhang, L.; Car, R.; Panagiotopoulos, A. Z., When Do Short-Range Atomistic Machine-Learning Models Fall Short? *J. Chem. Phys.* **2021,** *154*, 034111.

588. Grisafi, A.; Ceriotti, M., Incorporating Long-Range Physics in Atomic-Scale Machine Learning. *J. Chem. Phys.* **2019,** *151*, 204105.

589. Bedrov, D.; Piquemal, J.-P.; Borodin, O.; Mackerell, A. D.; Roux, B.; Schröder, C., Molecular Dynamics Simulations of Ionic Liquids and Electrolytes Using Polarizable Force Fields. *Chem. Rev.* **2019,** *119*, 7940-7995.

590. Borodin, O., Polarizable Force Field Development and Molecular Dynamics Simulations of Ionic Liquids. *J. Phys. Chem. B* **2009,** *113*, 11463-11478.

591. Goloviznina, K.; Canongia Lopes, J. N.; Costa Gomes, M.; Pádua, A. A. H., Transferable, Polarizable Force Field for Ionic Liquids. *J. Chem. Theory Comput.* **2019,** *15*, 5858-5871.

592. Chen, J.; Martínez, T. J., Qtpie: Charge Transfer with Polarization Current Equalization. A Fluctuating Charge Model with Correct Asymptotics. *Chem. Phys. Lett.* **2007,** *438*, 315-320.

593. Rick, S. W.; Stuart, S. J., Potentials and Algorithms for Incorporating Polarizability in Computer Simulations. *Rev. Comput. Chem.* **2002,** *18*, 89-146.

594.   Harger, M.; Li, D.; Wang, Z.; Dalby, K.; Lagardère, L.; Piquemal, J. P.; Ponder, J.; Ren, P., Tinker-OpenMM: Absolute and Relative Alchemical Free Energies Using AMOEBA on GPUs. *J. Comput. Chem.* **2017,** *38*, 2047-2055.

595.   Corrigan, R. A.; Qi, G.; Thiel, A. C.; Lynn, J. R.; Walker, B. D.; Casavant, T. L.; Lagardere, L.; Piquemal, J.-P.; Ponder, J. W.; Ren, P., et al., Implicit Solvents for the Polarizable Atomic Multipole AMOEBA Force Field. *J. Chem. Theory Comput.* **2021,** *17*, 2323-2341.

596.   Adjoua, O.; Lagardère, L.; Jolly, L.-H.; Durocher, A.; Very, T.; Dupays, I.; Wang, Z.; Inizan, T. J.; Célerse, F.; Ren, P., et al., Tinker-Hp: Accelerating Molecular Dynamics Simulations of Large Complex Systems with Advanced Point Dipole Polarizable Force Fields Using GPUs and Multi-Gpu Systems. *J. Chem. Theory Comput.* **2021,** *17*, 2034-2053.

597.   Jiang, W.; Hardy, D. J.; Phillips, J. C.; Mackerell, A. D.; Schulten, K.; Roux, B., High-Performance Scalable Molecular Dynamics Simulations of a Polarizable Force Field Based on Classical Drude Oscillators in Namd. *J. Phys. Chem. Lett.* **2011,** *2*, 87-92.

598.   Jing, Z.; Liu, C.; Cheng, S. Y.; Qi, R.; Walker, B. D.; Piquemal, J.-P.; Ren, P., Polarizable Force Fields for Biomolecular Simulations: Recent Advances and Applications. *Annual Review of Biophysics* **2019,** *48*, 371-394.

599.   Zhang, H.; Chen, F.; Carrasco, J., Nanoscale Modelling of Polymer Electrolytes for Rechargeable Batteries. *Energy Storage Mater.* **2021,** *36*, 77-90.

600.   Grest, G. S.; Lacasse, M. D.; Kremer, K.; Gupta, A. M., Efficient Continuum Model for Simulating Polymer Blends and Copolymers. *J. Chem. Phys.* **1996,** *105*, 10583-10594.

601.   Bello, L.; Sing, C. E., Mechanisms of Diffusive Charge Transport in Redox-Active Polymer Solutions. *Macromolecules* **2020,** *53*, 7658-7671.

602.   Shen, K.-H.; Fan, M.; Hall, L. M., Molecular Dynamics Simulations of Ion-Containing Polymers Using Generic Coarse-Grained Models. *Macromolecules* **2021,** *54*, 2031-2052.

603.   Klein, M. L.; Shinoda, W., Large-Scale Molecular Dynamics Simulations of Self-Assembling Systems. *Science* **2008,** *321*, 798-800.

604.   Khot, A.; Savoie, B. M., Top–Down Coarse-Grained Framework for Characterizing Mixed Conducting Polymers. *Macromolecules* **2021,** 4889–4901.

605.   Modarresi, M.; Franco-Gonzalez, J. F.; Zozoulenko, I., Morphology and Ion Diffusion in PEDOT:Tos. A Coarse Grained Molecular Dynamics Simulation. *Phys. Chem. Chem. Phys.* **2018,** *20*, 17188-17198.

606.   Rühle, V.; Junghans, C.; Lukyanov, A.; Kremer, K.; Andrienko, D., Versatile Object-Oriented Toolkit for Coarse-Graining Applications. *J. Chem. Theory Comput.* **2009,** *5*, 3211-3223.

607.   Reith, D.; Pütz, M.; Müller-Plathe, F., Deriving Effective Mesoscale Potentials from Atomistic Simulations. *J. Comput. Chem.* **2003,** *24*, 1624-1636.

608.   Marrink, S. J.; Risselada, H. J.; Yefimov, S.; Tieleman, D. P.; De Vries, A. H., The Martini Force Field: Coarse Grained Model for Biomolecular Simulations. *J. Phys. Chem. B* **2007,** *111*, 7812-7824.

609.   Izvekov, S.; Parrinello, M.; Burnham, C. J.; Voth, G. A., Effective Force Fields for Condensed Phase Systems from Ab Initio Molecular Dynamics Simulation: A New Method for Force-Matching. *J. Chem. Phys.* **2004,** *120*, 10896-10913.

610.   Brini, E.; Algaer, E. A.; Ganguly, P.; Li, C.; Rodríguez-Ropero, F.; Van Der Vegt, N. F. A., Systematic Coarse-Graining Methods for Soft Matter Simulations – a Review. *Soft Matter* **2013,** *9*, 2108-2119.

611.   Scherer, C.; Andrienko, D., Comparison of Systematic Coarse-Graining Strategies for Soluble Conjugated Polymers. *Eur. Phys. J. Spec. Top.* **2016,** *225*, 1441-1461.

612.   Wang, W.; Gómez-Bombarelli, R., Coarse-Graining Auto-Encoders for Molecular Dynamics. *Npj Comput. Mater.* **2019,** *5*, 125.

613.   Mashayak, S. Y.; Jochum, M. N.; Koschke, K.; Aluru, N. R.; Rühle, V.; Junghans, C., Relative Entropy and Optimization-Driven Coarse-Graining Methods in Votca. *PLoS ONE* **2015,** *10*, e0131754.

614.   De Jong, D. H.; Singh, G.; Bennett, W. F. D.; Arnarez, C.; Wassenaar, T. A.; Schäfer, L. V.; Periole, X.; Tieleman, D. P.; Marrink, S. J., Improved Parameters for the Martini Coarse-Grained Protein Force Field. *J. Chem. Theory Comput.* **2013,** *9*, 687-697.

615.   Izvekov, S.; Voth, G. A., Multiscale Coarse Graining of Liquid-State Systems. *J. Chem. Phys.* **2005,** *123*, 134105.

616.   Ingólfsson, H. I.; Lopez, C. A.; Uusitalo, J. J.; De Jong, D. H.; Gopal, S. M.; Periole, X.; Marrink, S. J., The Power of Coarse Graining in Biomolecular Simulations. *Wiley Interdiscip. Rev. Comput. Mol. Sci.* **2014,** *4*, 225-248.

617.   Rolland, N.; Modarresi, M.; Franco-Gonzalez, J. F.; Zozoulenko, I., Large Scale Mobility Calculations in PEDOT (Poly(3,4-Ethylenedioxythiophene)): Backmapping the Coarse-Grained Martini Morphology. *Comput. Mater. Sci.* **2020,** *179*, 109678.

618.   Modarresi, M.; Franco-Gonzalez, J. F.; Zozoulenko, I., Computational Microscopy Study of the Granular Structure and Ph Dependence of PEDOT:PSS. *Phys. Chem. Chem. Phys.* **2019,** *21*, 6699-6711.

619.   Modarresi, M.; Mehandzhiyski, A.; Fahlman, M.; Tybrandt, K.; Zozoulenko, I., Microscopic Understanding of the Granular Structure and the Swelling of PEDOT:PSS. *Macromolecules* **2020,** *53*, 6267-6278.

620.   Jayaraman, A., 100th Anniversary of Macromolecular Science Viewpoint: Modeling and Simulation of Macromolecules with Hydrogen Bonds: Challenges, Successes, and Opportunities. *ACS Macro Lett.* **2020,** *9*, 656-665.

621.   Fraaije, J. G. E. M.; Van Male, J.; Becherer, P.; Serral Gracià, R., Calculation of Diffusion Coefficients through Coarse-Grained Simulations Using the Automated-Fragmentation-Parametrization Method and the Recovery of Wilke–Chang Statistical Correlation. *J. Chem. Theory Comput.* **2018,** *14*, 479-485.

622.   Jackson, N. E.; Bowen, A. S.; Antony, L. W.; Webb, M. A.; Vishwanath, V.; De Pablo, J. J., Electronic Structure at Coarse-Grained Resolutions from Supervised Machine Learning. *Sci. Adv.* **2019,** *5*, eaav1190.

623. Craig, B.; Skylaris, C.-K.; Schoetz, T.; De León, C. P., A Computational Chemistry Approach to Modelling Conducting Polymers in Ionic Liquids for Next Generation Batteries. *Energy Rep.* **2020,** *6*, 198-208.

624. Solt, I.; Kulhánek, P.; Simon, I.; Winfield, S.; Payne, M. C.; Csányi, G.; Fuxreiter, M., Evaluating Boundary Dependent Errors in QM/MM Simulations. *J. Phys. Chem. B* **2009,** *113*, 5728-5735.

625. Kulik, H. J.; Zhang, J.; Klinman, J. P.; Martínez, T. J., How Large Should the QM Region Be in QM/MM Calculations? The Case of Catechol O-Methyltransferase. *J. Phys. Chem. B* **2016,** *120*, 11381-11394.

626. Yang, Y. I.; Shao, Q.; Zhang, J.; Yang, L. J.; Gao, Y. Q., Enhanced Sampling in Molecular Dynamics. *J. Chem. Phys.* **2019,** *151*, 070902.

627. Berggren, M.; Malliaras, G. G., How Conducting Polymer Electrodes Operate. *Science* **2019,** *364*, 233-234.